

DEPOSITION OF ELECTROACTIVE POLYMERS ONTO POLYMER NANOFIBERS FOR
NERVE REGENERATION

by

Marvin D. Santiago, B.S.

A thesis submitted to the Graduate Council of
Texas State University in partial fulfillment
of the requirements for the degree of
Master of Science
with a Major in Chemistry
August 2022

Committee Members:

Jennifer Irvin, Chair

Tania Betancourt

Nathaniel Lynd

COPYRIGHT

by

Marvin D. Santiago

2022

FAIR USE AND AUTHOR'S PERMISSION STATEMENT

Fair Use

This work is protected by the Copyright Laws of the United States (Public Law 94-553, section 107). Consistent with fair use as defined in the Copyright Laws, brief quotations from this material are allowed with proper acknowledgement. Use of this material for financial gain without the author's express written permission is not allowed.

Duplication permission

As the copyright holder of this work I, Marvin D. Santiago, authorize duplication of this work, in whole or in part, for educational or scholarly purposes only.

DEDICATION

To the scientists and freedom fighters of my home, the Philippines.

*Aling pag-ibig pa ang hihigit kaya sa pagkadalisay at pagkadakila gaya ng pag-ibig sa
tinubuang lupa?*

Aling pag-ibig pa? Wala na nga, wala.

ACKNOWLEDGEMENTS

I would like to thank the following for their valuable help:

Dr. Jennifer Irvin, for being a patient and effective mentor,

Dr. Gabriela Romero-Uribe, for supplying us with MNPs and providing help in biological studies,

Dr. Nicolas Muzzio for doing the cell adhesion experiments for my composites,

Dr. Tania Betancourt for providing technical advice on experiments,

Dr. Casey Smith for training me in the use of the SEM and providing advice for better use of the SEM,

Dr. Christopher Rhodes and Dr. Craig Damin for training me and providing advice in ATR-IR analysis,

The Graduate College at Texas State University, for providing me with the Graduate Thesis Support Fellowship,

The Irvin Group members especially Adelyne Towne, Mariana Ocampo, and Dr. Dami Runsewe, for their help in experimentation,

My friends, for their valuable support, and

My family.

+amdg

TABLE OF CONTENTS

	Page
ACKNOWLEDGEMENTS	v
LIST OF TABLES	x
LIST OF FIGURES	xi
LIST OF EQUATIONS	xv
LIST OF SCHEMES	xvi
LIST OF ABBREVIATIONS	xvii
ABSTRACT.....	xx
CHAPTER	
1 INTRODUCTION	1
1.1 Nerve Regeneration and Neural Scaffolds.....	1
1.2 Polypyrrole and Inherently Conducting Polymers (ICPs)	6
1.3 Polymer Nanofibers and Electrospinning	9
1.4 ICP Nanofibers.....	11
1.5 Scope and Objectives of This Study	14
2 ELECTROSPINNING	17
2.1 Introduction	17
2.1.1 Electrospinning theory	17
2.1.2 The electrospinning apparatus	19
2.1.3 Process parameters in electrospinning	20
2.1.4 Solution parameters in electrospinning.....	22
2.1.5 Electrospinnable polymers	24
2.1.6 Fiber alignment in electrospinning	26
2.1.7 Electrospun polymer applications and bioengineering	26
2.1.8 Scope and limitations of this study	27
2.2 Materials and Methods.....	28
2.2.1 Materials	28

2.2.2 Instrumentation	28
2.2.3 Preparation and electrospinning.....	29
2.2.4 Rastering experiment	30
2.2.5 Collector speed experiment.....	31
2.2.6 SEM and SEM-EDX analysis	31
2.2.7 ATR-IR analysis	31
2.3 Results and Discussion	32
2.3.1 Electrospun polymers.....	32
2.3.2 Effect of rastering	45
2.3.3 Effect of collector speed	46
2.4 Conclusions and Future Work	48
3 COATING ELECTROSPUN POLYMERS WITH INHERENTLY CONDUCTING POLYMERS	49
3.1 Introduction	49
3.1.1 Inherently Conducting Polymers	49
3.1.2 Properties and applications of ICPs in biomedicine	56
3.1.3 ICP nanofibers	57
3.1.4 Applications of nanofibrous ICPs	60
3.1.5 Scope and limitations of this Study	62
3.2 Materials and Methods.....	62
3.2.1 Materials	62
3.2.2 Instrumentation	63
3.2.3 Polypyrrole coating on electrospun PCL without pre-treatment	63
3.2.4 Polypyrrole coating on electrospun PCL with pre-treatment	64
3.2.5 Tape test	65
3.2.6 ATR-IR analysis	65
3.2.7 SEM-EDX analysis	65
3.3 Results and Discussion	65
3.3.1 No pre-treatment	67
3.3.2 With oxidant pre-treatment	69
3.3.3 With monomer pre-treatment.....	73
3.3.4 Tape test	75
3.4 Conclusions and Future Work	76

4 PCL-MNP-PPy FOR NERVE REGENERATION	78
4.1 Introduction	78
4.1.1 Nerve regeneration and strategies for enhancement	78
4.1.2 Nerve scaffolds and use of polycaprolactone as material	81
4.1.3 Magnetic nanoparticles for nerve regeneration	84
4.1.4 Scope and limitations of the study	87
4.2 Materials and Methods	87
4.2.1 Materials	87
4.2.2 Instrumentation	88
4.2.3 Electrospinning of PCL-MNPs	89
4.2.4 Effect of MNP concentration	89
4.2.5 Polypyrrole coating	89
4.2.6 ATR-IR analysis	89
4.2.7 SEM-EDX analysis	90
4.2.8 Cell adhesion tests.....	90
4.3 Results and Discussion	91
4.3.1 PCL-MNP	91
4.3.2 Effect of MNP concentration	94
4.3.3 PCL-MNP-PPy	96
4.3.4 Cell adhesion test results (Courtesy of Dr. Nicolas Muzzio, UTSA).....	98
4.4 Conclusions and Future Work	103
5 CHEMICAL MODIFICATION OF POLYMER NANOFIBERS	104
5.1 Introduction	104
5.1.1 Stability of electrospun composites and graft copolymerization.....	104
5.1.2 Graft copolymerization considerations and electrospun polymer-ICP graft copolymers	107
5.1.3 Scope and limitations of the study	111
5.2 Materials and Methods.....	111
5.2.1 Materials	111
5.2.2 Instrumentation	112
5.2.3 Synthesis of modified EDOTs	112
5.2.3.1 Synthesis of 2-(Bromomethyl)-2,3- dihydrothieno[3,4-b][1,4]dioxine (EDOT-MeBr)	113
5.2.3.2 Synthesis of 2-(Chloromethyl)-2,3- dihydrothieno[3,4-b][1,4]dioxine (EDOT-MeCl).....	113

5.2.3.3 Synthesis of 2-(Azidomethyl)-2,3-dihydrothieno[3,4-b][1,4]dioxine (EDOT-MeN ₃)	114
5.2.3.4 Synthesis of 2-(Aminomethyl)-2,3-dihydrothieno[3,4-b][1,4]dioxine (EDOT-MeNH ₂)	115
5.2.3.5 Synthesis of 2-(Hydroxymethyl)-2,3-dihydrothieno[3,4-b][1,4]dioxine (EDOT-MeOH).....	116
5.2.4 Polymer modification.....	118
5.2.4.1 PAN modification	118
5.2.4.1.1 PAN modification via hydrolysis and EDC/NHS coupling	118
5.2.4.1.2 PAN modification via hydrolysis and Fischer esterification	119
5.2.4.1.3 PAN modification via direct reaction ...	120
5.2.4.2 PMMA modification	121
5.3 Results and Discussion	122
5.3.1 Modified EDOTs	122
5.3.2 Polymer modification.....	133
5.3.2.1 Surface PAN modification via hydrolysis and esterification.....	133
5.3.2.2 PAN modification via hydrolysis and amidation.....	139
5.3.2.3 PAN modification via direct reaction with EDOT-MeNH ₂	145
5.3.2.4 Surface PMMA modification.....	149
5.4 Conclusions and Future Work	153
6 CONCLUSIONS AND FUTURE WORK	155
REFERENCES	158

LIST OF TABLES

Table	Page
1. Optimal process and solution parameters used in the electrospinning of polymers	30
2. Samples tested for cell adhesion at UTSA.....	90

LIST OF FIGURES

Figure	Page
1. Structure of a neuron, showing important organelles.....	2
2. (A) SEM micrograph of the human neural and spinal ECM.....	5
3. Polycaprolactone (PCL).....	5
4. (Top) Polypyrrole (PPy) (bottom) hexameric PPy	6
5. Poly(3,4-ethylenedioxythiophene) (PEDOT)	8
6. Electrospinning setup.....	9
7. Polyacrylonitrile (left) and poly(methyl methacrylate) (right)	10
8. Nanofibers of PCL-based polymers coated with PPy, showing distinct regions of PCL and PPy.	12
9. PPy film microstructure.....	13
10. PCL-MNP-PPy composite fabrication.....	15
11. Scheme for the chemical modification of electrospun nanofibers with ICPs.....	15
12. Looping and thinning of polymer jet in electrospinning due to instability.....	18
13. Electrospinning apparatus	19
14. Electrospun PCL	32
15. EDX mapping of electrospun PCL.....	33
16. ATR-IR spectrum of electrospun PCL	33
17. Electrospun PAN	34
18. EDX mapping of electrospun PAN.....	35
19. ATR-IR of electrospun PAN	36

20. Electrospun PVC.....	37
21. EDX analysis of electrospun PVC.....	38
22. ATR-IR spectrum of electrospun PVC	38
23. Electrospun PMMA	39
24. EDX analysis of electrospun PMMA.	40
25. ATR-IR spectrum of electrospun PMMA.....	40
26. Electrospun HPAN.....	41
27. EDX analysis of HPAN.	42
28. ATR-IR spectrum of electrospun HPAN	42
29. Electrospun PCL without rastering	46
30. Electrospun PCL with rastering	46
31. Electrospun PCL with rotating drum collector set to 80 rpm	47
32. Electrospun PCL with rotating drum collector set to 4000 rpm	47
33. Inherently conducting polymers.	50
34. Neutral, polaron, and bipolaron forms of polythiophene.....	52
35. Coating of PPy on PCL without pre-treatment	63
36. Coating of PCL with PPy with pre-treatment.	64
37. PCL-PPy with no pre-treatment.....	67
38. EDX analysis of PCL-PPy with no pre-treatment.	68
39. ATR-IR spectrum of PCL-PPy with no pre-treatment	69
40. PCL-PPy with oxidant pre-treatment.....	69
41. EDX analysis of PPy-coated PCL with oxidant pre-treatment.....	70

42. ATR-IR spectrum of PCL-PPy with oxidant pre-treatment	71
43. PAN-PEDOT, courtesy of Mariana Ocampo.....	72
44. PCL-PPy with monomer pre-treatment	73
45. EDX analysis of PCL-PPy with monomer pre-treatment.....	74
46. ATR-IR spectrum of PCL-PPy with monomer pre-treatment	75
47. (Left) 1 in x 1 in electrospun PCL coated with PPy.	76
48. The process of nerve regeneration and consequence of failed regeneration.	79
49. Structure of a nerve conduit for in vivo use.....	81
50. TEM of Core 40 MNPs, courtesy of Dr. Romero-Uribe's group	87
51. EDX of Core 40 MNPs, courtesy of Dr. Romero-Uribe's group	88
52. PCL-MNP	91
53. EDX analysis of PCL-MNP.....	92
54. ATR-IR spectrum of PCL-MNP	93
55. (Top to bottom) PCL electrospun at 4000 rpm with 0, 2.5, and 25 µg/mL MNPs....	95
56. PCL-MNP-PPy	96
57. EDX analysis of PCL-MNP-PPy.....	97
58. ATR-IR spectrum of PCL-MNP-PPy	97
59. Confocal images of C2C12 cells seeded on composites (blue: DAPI stain; green: phalloidin stain)	99
60. Confocal images of ND7/23 cells seeded on PCL (blue: DAPI stain; green: phalloidin stain).....	101
61. Confocal image of ND7/23 cells seeded on electrospinning samples (blue: DAPI stain; green: phalloidin stain).....	102
62. The three methods of graft copolymerization.....	106

63. ^1H NMR of synthesized EDOT-MeBr	123
64. ^1H NMR of synthesized EDOT-MeCl	124
65. ^1H NMR of synthesized EDOT-MeN ₃	127
66. ^1H NMR of synthesized EDOT-MeOH	129
67. ^1H NMR of synthesized EDOT-MeNH ₂	131
68. ATR-IR spectrum of PAN (grey) and base-hydrolyzed PAN (pink)	134
69. ATR-IR spectra of (teal): PAN-co-PAA.....	138
70. PAN ^1H NMR spectrum in DMF-d ₇	140
71. ^1H NMR of PAN-co-PAA-graft-EDOT-MeNH ₂ in DMF-d ₇	142
72. ^1H NMR spectrum of EDOT-MeNH ₂ in DMF-d ₇	143
73. (Top) ^1H NMR of PAN-co-PAA-graft-EDOT-MeNH ₂ in DMF-d ₇ ; (middle) ^1H NMR of EDOT-MeNH ₂ in DMF-d ₇ ; (bottom) ^1H NMR of PAN-co-PAA	144
74. ^1H NMR of PAN-graft-EDOT-MeNH ₂ in DMF-d ₇	147
75. (Top) ^1H NMR of PAN-graft-EDOT-MeNH ₂ in DMF-d ₇ ; (middle) ^1H NMR of EDOT-MeNH ₂ in DMF-d ₇ ; (bottom) ^1H NMR of PAN in DMF-d ₇	148
76. ATR-IR spectra of PMMA (red) and PMMA-graft-EDOT-MeNH ₂ (gold)	150
77. ^1H NMR spectrum of PMMA in CDCl ₃	151
78. 1H NMR spectrum of PMMA-graft-EDOT-MeNH ₂ in CDCl ₃	152
79. (Top) ^1H NMR of PMMA-graft-EDOT-MeNH ₂ in CDCl ₃ ; (middle) ^1H NMR of EDOT-MeNH ₂ in CDCl ₃ ; (bottom) ^1H NMR of PMMA in CDCl ₃	153

LIST OF EQUATIONS

Equation	Page
1. Mark-Houwink equation ⁵⁶	22
2. Formula for calculating M_N , the number-average molecular weight of a polymer	23
3. Formula for calculating M_W , the weight-average molecular weight of a polymer	23
4. PAN alkaline hydrolysis	28
5. Grafting of ethanolamine to PAN	44
6. Chemical oxidative polymerization of pyrrole	62
7. Synthesis of halomethyl EDOTs.....	112
8. Synthesis of EDOT-MeN ₃ from EDOT-Cl	114
9. Synthesis of EDOT-MeNH ₂ from EDOT-MeN ₃	115
10. Synthesis of EDOT-MeOH from EDOT-MeBr.....	116
11. Reaction of EDOT-MeNH ₂ with HPAN via EDC/NHS coupling.....	118
12. Reaction of EDOT-MeOH with HePAN via Fischer esterification.....	119
13. Direct reaction of PAN with EDOT-MeNH ₂	120
14. Amidolysis of PMMA with EDOT-MeNH ₂	121

LIST OF SCHEMES

Scheme	Page
1. Proposed mechanism for the alkaline hydrolysis of PAN	43
2. Proposed mechanism for the chemical oxidative polymerization of pyrrole.	54
3. Synthesis of Py-modified PEG and subsequent oxidative polymerization.....	109
4. Proposed mechanism of acid-catalyzed transesterification of 3,4-dimethoxythiophene with 3-halo-1,2-propanediols	125
5. Proposed EDOT-MeN ₃ synthesis mechanism	127
6. Proposed EDOT-MeOH synthesis mechanism.....	130
7. Proposed mechanism for the reduction of EDOT-MeN ₃ into EDOT-MeNH ₂	132
8. Proposed mechanism for the reaction of PAA with EDOT-MeOH	136
9. Proposed mechanism for the reaction of EDOT-MeNH ₂ and PAA via EDC/NHS coupling.....	139
10. Proposed mechanism for the direct grafting of EDOT-MeNH ₂ on PAN	146
11. PMMA amidolysis mechanism.....	149

LIST OF ABBREVIATIONS

Abbreviation	Description
ATR-IR	Attenuated total reflectance – infrared radiation spectroscopy
CNS	Central Nervous System
DMF	<i>N,N</i> -dimethylformamide
DMSO	Dimethylsulfoxide
ECM	Extracellular matrix
EDC	<i>N</i> -ethyl- <i>N'</i> -(3-(dimethylamino)-propyl)carbodiimide
EDOT	3,4-ethylenedioxythiophene
EDOT-MeBr	Bromomethyl EDOT
EDOT-MeCl	Chloromethyl EDOT
EDOT-MeN ₃	Azidomethyl EDOT
EDOT-MeNH ₂	Aminomethyl EDOT
EDOT-MeOAc	Acetomethyl EDOT
EDOT-MeOH	Hydroxymethyl EDOT
EDX	Energy dispersive x-ray spectroscopy
EtOAc	Ethyl acetate
EtOH	Ethanol

FTIR	Fourier transform infrared radiation spectroscopy
HePAN	Base-hydrolyzed electrospun PAN
HPAN	Base-hydrolyzed PAN
ICP	Inherently conducting polymer
ITO	Indium tin oxide
MNPs	Magnetic nanoparticles
NHS	<i>N</i> -hydroxysuccinimide
NMR	Nuclear magnetic resonance spectroscopy
PAA	Poly(acrylic acid)
PAN	Polyacrylonitrile
PANI	Polyaniline
PCL	Polycaprolactone
PCL-PPy	Polycaprolactone coated with polypyrrole
PCL-MNP	Electrospun polycaprolactone/magnetic nanoparticle blend
PCL-MNP-PPy	Electrospun polycaprolactone/magnetic nanoparticle blend coated with polypyrrole
PEDOT	Polyethylenedioxythiophene

PMMA	Poly(methyl methacrylate)
PNS	Peripheral Nervous System
PPV	Poly(phenylene vinylene)
PPy	Polypyrrole
PS	Polystyrene
PSS	Poly(styrene sulfonate)
PT	Polythiophene
PVC	Poly(vinyl chloride)
Py	Pyrrole
SEM	Scanning electron microscopy
TEM	Transmission electron microscopy
THF	Tetrahydrofuran

ABSTRACT

Although peripheral nerves can regenerate after an injury through the Wallerian degeneration process, the degree of regeneration is often not efficient enough to achieve full return of functionality. To overcome the disadvantages of current nerve repair approaches, peripheral nerve tissue engineering strategies have been proposed by developing synthetic graft alternatives for long-gap nerve injuries. Nerve tissue engineering approach relies on mimicking the microenvironment of nerve tissue.

This study reports the successful fabrication of an alternative for nerve tissue engineering. Electrospinning of the biocompatible polymer polycaprolactone (PCL) is used to produce porous and ordered nanofibers that resemble the structure and organization of the extracellular matrix, providing a suitable environment to promote the adhesion and directional growth of nerves. These oriented nanofibers are conformally coated with the inherently conducting polymer (ICP) polypyrrole (PPy) to provide an electrically conductive medium enabling the application of external stimuli to enhance cellular growth and connectivity. Furthermore, the scaffold is engineered with magnetic nanoparticles (MNPs) to provide a remote-controlled option for the delivery of electrical inputs through the generation of eddy currents when exposed to alternating magnetic fields.

The biocompatibility of the fabricated composite has been proven using C2C12 and ND7/23 mouse cells. The growth of these cells has been shown to coincide with the alignment of the nanofibers. On highly aligned composites, there is evidence of neuroblastoma differentiation.

While adhesion of the PPy coating onto the electrospun polymer has been demonstrated to be strong by tape test, it can potentially be enhanced by the formation of covalent bonds between the electrospun substrate and the modifier ICP. This study also preliminarily reports the success of reacting modified monomers of poly(3,4-ethylenedioxythiophene) (PEDOT) onto polyacrylonitrile (PAN) and poly(methyl methacrylate) (PMMA). Aminomethyl EDOT (EDOT-MeNH₂) was potentially successfully grafted onto PAN, alkaline hydrolyzed PAN , and PMMA. Hydroxymethyl EDOT (EDOT-MeOH) was also potentially successfully grafted onto alkaline hydrolyzed PAN. These would then be polymerized on the electrospun substrates, forming graft copolymers.

The results of this study not only provide the foundations for a device for enhanced nerve regeneration, but also would be an enabling technology for the fabrication of improved composites of electrospun polymers and ICPs with applications in biomedical engineering and, potentially, energy storage, water purification, sensors, and wearable electronics.

1 INTRODUCTION

1.1 Nerve Regeneration and Neural Scaffolds

The nervous system is responsible for the phenomenon of sensing, cognition, and response. The nervous system is divided into the Central Nervous System (CNS) which is composed of the nerves making up the brain and the spinal cord, and the Peripheral Nervous System (PNS), which is composed of the nerves making up sensory and efferent organs. The main component of the nervous system is neurons, or nerve cells, which is responsible for the transmission of signals from one part of the body to another. There are three types of nerve cells. Sensory or afferent neurons relay signals from sensory receptors to the CNS. Motor or efferent neurons relay signals from the CNS to effector/target organs. Interneurons link sensory and motor neurons.

Signals from either external stimuli or other nerves are received by dendrites. These stimuli are collected in the soma or nerve cell body, which then converts the stimuli into a frequency of action potentials. These action potentials travel along the axon as changes in the cell membrane potential. In the CNS, these axons are either bare or sheathed by oligodendrocytes. In the PNS, these axons are sheathed by Schwann cells, which form a myelin sheath around them. This myelin sheath insulates the axon and increases the speed of conduction of action potentials. These signals eventually reach the terminals of the axon, called the synapse, and cause the release of neurotransmitters. These induce the desired effect in the target cells they are attached to, or the further conduction of the signal in another nerve¹. Figure 1 shows the structure of a neuron, showing these organelles².

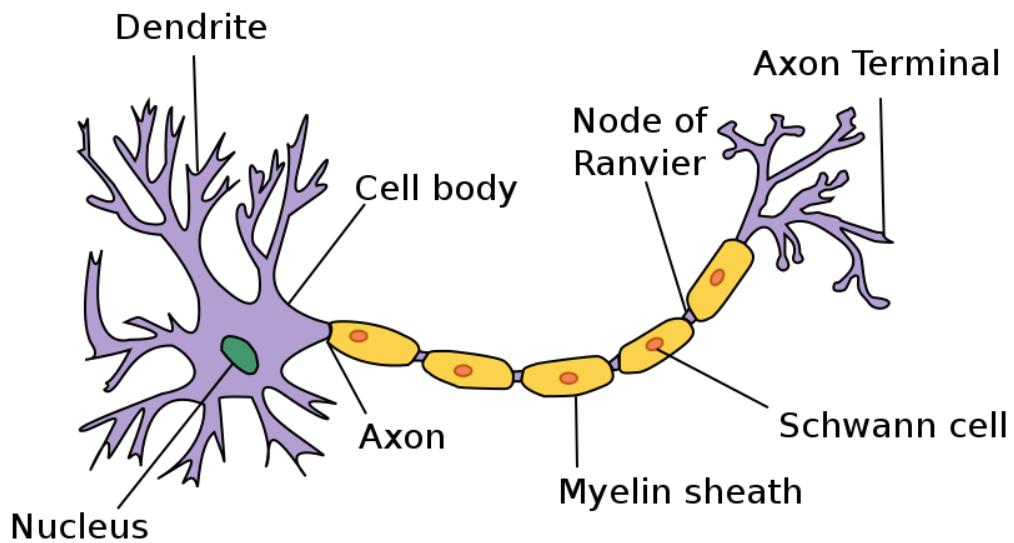


Figure 1. Structure of a neuron, showing important organelles. From ref 2. CC BY-SA 3.0.

Damage in the PNS is common because of physical activity. The body naturally repairs this damage through a series of cellular and molecular events called Wallerian degeneration³. The damaged sections of nerves are broken down and expelled by a collection of Schwann cells, macrophages, and small molecules in the body, allowing for their replacement by neurotrophic factors and new nerve cells. Proteins then reattach axons to each other and to Schwann cells, and growth factors promote the regeneration of axons⁴.

The process of nerve regeneration has been studied extensively in rats. This process, however, is slower and less successful in humans than in rats due to the length of the nerve segments that need to be regrown. This problem is aggravated when the injury results in a complete disconnection in the nerve trunk, as this results in a marked decrease in the quality of life on patients.

To remedy this, several strategies have been employed. The current treatment of choice is grafting healthy nerves from the same patient onto the injured nerve⁵, although this is a surgical process that sacrifices a healthy nerve, which then necessitates nerve regeneration in that area. Other strategies include the intake of growth factors and small molecules which induce Wallerian degeneration. However, the side effects of ingesting these remains to be seen, and the amount, timing, and dosage of growth factors that need to be taken should be carefully considered to prevent harmful effects from happening.

Two promising areas of treatment that do not involve either grafting or the use of drugs with unexplored side effects are the use of magnetic nanoparticles (MNPs) and neural scaffolds.

MNPs used in nerve regeneration applications are made up of iron oxide and can be functionalized with drugs and growth factors in order to make them interact favorably with the body⁶. MNPs offer the advantage of being able to be activated remotely by an external magnetic field for targeted treatment. The mechanical tension offered by the introduction of MNPs manipulated by external magnetic fields onto sites of nerve injury has been shown to induce stretch growth in axons. Importantly, MNPs have also been observed to generate heat locally when exposed to a low frequency electromagnetic field, a phenomenon called hysteretic heating. The research group of Dr. Gabriela Romero-Uribe at the University of Texas at San Antonio has developed a biocompatible MNP composed of Fe and Zn for use in nerve regeneration applications^{7,8}. These MNPs were observed to stimulate the heat-dependent functions of transmembrane ion channels in rat hippocampal neurons and neurons containing capsaicin receptors TRPV1 when subjected to an external alternating magnetic field. Hysteretic heating was also observed to

accomplish the delivery of a thermally-labile molecule functionalized on the surface of the MNP onto target cells⁹. MNPs thus offer a method for enhanced, remote-controlled nerve regeneration.

Neural scaffolds are polymers, either natural or synthetic, that are processed into nanofibrous structures and implanted into the site of injury. Neural scaffolds address the cell attachment and growth phase of nerve regeneration by mimicking the extracellular matrix (ECM). The ECM is a fibrous structure consisting of polysaccharides and structural proteins which influence cell growth by providing sites for growing cells to attach, and influence cell function with the use of both physical and chemical cues¹⁰. Scaffolds should thus provide many sites for cell attachment and directional nerve growth, mechanical support for growing nerves, and allow for the delivery of growth factors and proteins necessary for nerve function. The nanofibrous, aligned structure of scaffolds, which gives them high surface-to-volume ratios and porosity, matches these criteria. The large surface area allows for many sites of cell attachment, growth, and even potential modification with drugs and growth factors which enhance nerve growth. The alignment allows for directional nerve growth and mechanical support for growing nerves. The porosity allows for the efficient delivery of proteins and growth factors from the body to the site of healing. Figure 2 below shows the structures of the ECM of nerve tissue and its similarity with the structure of a nanofibrous polymer.

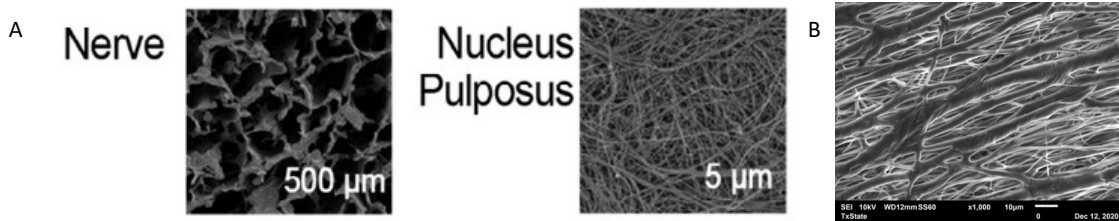


Figure 2. (A) SEM micrograph of the human neural and spinal ECM. Adapted with permission from ref. 10. Copyright 2006 Elsevier. (B) SEM micrograph of nanofibrous polycaprolactone

Additionally, neural scaffolds should be biocompatible, have a controlled biodegradability matching the rate of nerve regeneration, and a high surface area for cell attachment and growth¹¹. In this regard, biocompatible and biodegradable polymers, both natural and synthetic, such as collagen and polycaprolactone (PCL), Figure 3, can be fabricated into nanofibrous scaffolds which have a similar structure to the ECM of various tissues. PCL, being a polyester, can be slowly degraded by hydrolysis into smaller molecules that can be easily resorbed or expelled by the body. PCL can be dissolved by many organic solvents including tetrahydrofuran (THF) and *N,N*-Dimethylformamide (DMF) but not water. This property enhances its processability and ensures PCL maintains its structure in aqueous environments, both of which make it a good candidate material for neural scaffolds¹².

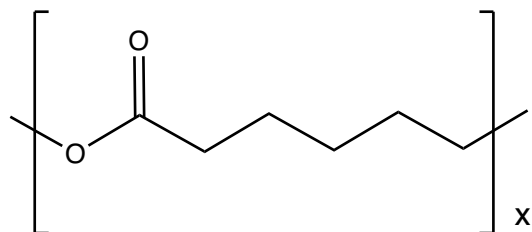


Figure 3. Polycaprolactone (PCL)

Aligned nanofibrous PCL has been used in nerve regeneration because of its biocompatibility, biodegradability, good mechanical properties, and modifiability. Because of its high surface-to-volume ratio, nanofibrous PCL has been modified with attachments of gelatin¹³, collagen¹⁴, the cytokine interleukin-10¹⁵, and gold nanoparticles¹⁶ to promote the attachment of cells necessary for Wallerian degeneration, enhance the adhesion of cells to the scaffold, and enhance nerve growth. The alignment of these scaffolds also enables the directional growth of neurons¹⁷, which is important in the retention of their function of transmission of impulses.

1.2 Polypyrrole and Inherently Conducting Polymers (ICPs)

The inherently conducting polymer (ICP) polypyrrole (PPy) has also been used in nerve regeneration applications. Polypyrrole (Figure 4) is composed of a chain of 5-membered aromatic heterocycles, each containing one nitrogen.

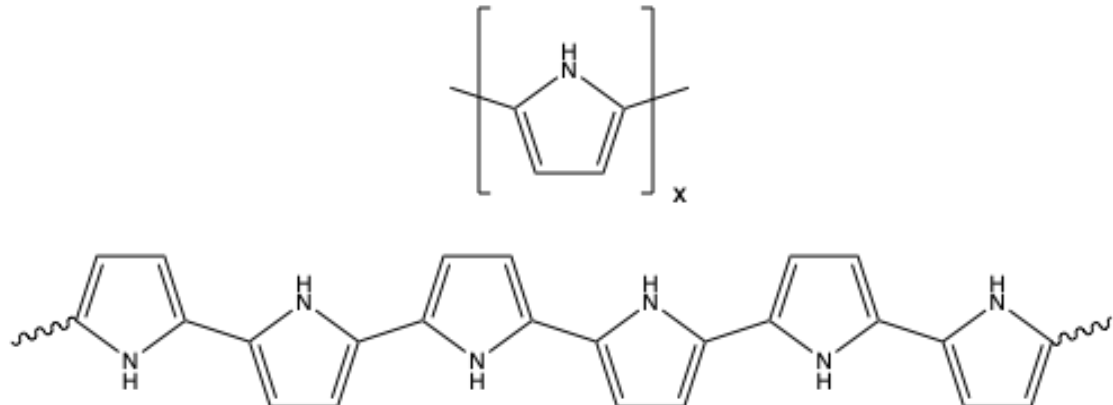


Figure 4. (Top) Polypyrrole (PPy) (bottom) hexameric PPy

PPy-coated onto PCL nanoyarns has been shown to enhance the attachment and proliferation of Schwann Cells onto these tissue scaffolds¹⁸. The resultant structure of regenerated nerves was observed to resemble the structure of native axons. Membranes of poly(D,L-lactide-co-ε-caprolactone) coated with PPy have been shown to have a good

affinity for model rat nerve PC12 cells. When these scaffolds were stimulated with moderate intensity direct current in the presence of nerve growth factors, neurite growth was observed¹⁹. Neurites grown from PC12 cells were further observed to undergo differentiation on films of PPy²⁰. ECM proteins were also observed to efficiently adsorb onto films of PPy, which promoted the attachment of endothelial cells²¹. The authors of this preceding study theorized that PPy, a biocompatible conductive polymer, can play a role in axonal growth and nerve regeneration. PPy-coated substrates have the advantage of providing an electrically conductive biocompatible platform which is conducive for nerve growth, as it allows for cell-cell and cell-scaffold communication. The electrical stimulation mimics the electrophysiological environment of native nerve cells and promotes their growth and proliferation²².

As can be seen in Figure 4, PPy, like all ICPs, has conjugation along its backbone, with pi-electrons delocalized. This property accounts for the small band gap of these materials. For example, the conductivity of PPy can range from 10^{-11} S/cm to 200 S/cm, depending on the conditions of its polymerization and the presence of doping²³. ICPs have tunable electrical and optical properties, dependent on oxidation state. Because of this, ICPs have been used in a wide range of applications. ICP-based biomedical materials have been fabricated for the photothermal ablation of cancer²⁴, sensing of biochemical analytes²⁵, simulated sensing of tastes and odors²⁶ and even simulated beating of cardiac tissue²⁷. Energy conversion and storage devices have also been fabricated that are based on ICPs²⁸. These properties may be enhanced when ICPs are processed to produce an overall ordered nanofibrous, porous structure. This kind of structure would result in ICPs with high surface-to-volume ratios, the ability to be

modified with nanoparticles for various applications, and enhanced crystallinity and conductivity due to orientation of the processed fibers²⁹.

PPy can be synthesized in many ways, including chemical oxidative polymerization in aqueous medium. Many oxidizing agents have been used for this reaction, including peroxides such as ammonium peroxydisulfate, and salts of iron, copper, or cerium³⁰. It has been observed that the use of FeCl₃ as oxidant has yielded PPy with the highest conductivity³¹.

Another aromatic heterocycle-based ICP is poly(3,4-ethylenedioxythiophene) (PEDOT, Figure 5). The alkoxy substituents on the thiophene ring donate electron density to the thiophene, decreasing the oxidation potential of the polymer.

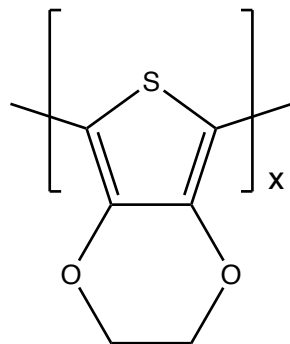


Figure 5. Poly(3,4-ethylenedioxythiophene) (PEDOT)

PEDOT has seen applications in cardiac and muscle tissue engineering³², supercapacitors³³, gas sensors for aromatic volatile organic compounds³⁴, biosensors for cancer detection³⁵, wearable flex sensors³⁶, and water purification³⁷. The ethylenedioxy substituent has also been further functionalized with substituents such as azides³⁸ and amines³⁹ that either enable their reaction with small molecules or better adhesion to hydrophilic surfaces.

1.3 Polymer Nanofibers and Electrospinning

Processing polymers into nanofibrous structures lends them interesting properties such as high surface-to-volume ratio and porosity⁴⁰. These properties allow the modification of polymer nanofiber surfaces with coatings and/or nanoparticles that can be held onto the substrate by primary/covalent interactions, or secondary/non-covalent interactions. These give them applications in the fields of tissue engineering and medicine, but also separations, sensing, and energy storage.

Electrospinning is a process that can be used to produce polymer nanofibers. It involves the subjection of a polymer in the liquid phase to an electric field, where it is stretched and elongated to generate fibers⁴¹. Figure 6 below shows a simple electrospinning setup where the collector is a simple metal sheet.

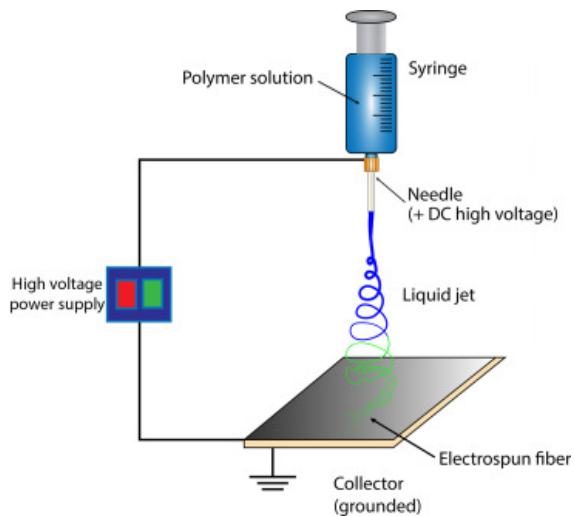


Figure 6. Electrospinning setup. Reprinted with permission from ref. 42. Copyright 2019 Elsevier.

A polymer that can be electrospun is first dissolved in a good solvent and then placed in a syringe connected to a high-voltage power supply. The accumulation of positive charges on the tip of the needle where the polymer solution is discharged from causes electrostatic repulsions resulting in the formation of a Taylor cone and propels the

solution to the collector⁴². The solvent evaporates as the solution travels to the grounded collector, leaving behind polymer nanofibers. The collector can be a simple metal sheet, but it can also be a rotating drum, which provides the added advantage of having a degree of control over the orientation of the nanofibers. This is due to the increase in the stretching force experienced by the polymer fibers⁴³. The alignment of polymer nanofibers is desirable in the fields of biomedical engineering, device fabrication, and composite reinforcement. Highly-aligned polymer nanofibers have been of particular interest in the field of tissue engineering, especially in the design of scaffolds for tissues which depend on a well-aligned organization for function, such as muscles, bone, and nerves⁴⁴.

Polymers that can be electrospun must satisfy two criteria: they must have a sufficiently high molecular weight for polymer chain entanglement, and they must be soluble in a suitable solvent⁴¹. Aside from PCL, a wide variety of polymers can be electrospun, including polyacrylonitrile (PAN) and poly(methyl methacrylate) (PMMA) (Figure 7).

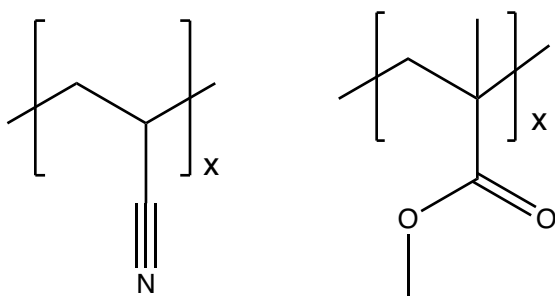


Figure 7. Polyacrylonitrile (left) and poly(methyl methacrylate) (right)

1.4 ICP Nanofibers

ICPs are very difficult to electrospin directly into nanofibers. ICPs are low-molecular weight, rigid polymers due to the extent of conjugation along their polymer backbones⁴⁵. They thus do not have sufficient polymer chain entanglement to form solutions of adequate viscosity for nanofiber formation during electrospinning⁴⁶. Furthermore, many ICPs such as PPy and PEDOT are insoluble in any solvent²³, which is a requirement for electrospinning them. Thus, ICPs are typically incorporated into electrospun polymers in various ways. As has been described above, one way of doing this is by coating electrospun polymers with ICPs. The previous studies mentioned which used PCL-PPy scaffolds for nerve regeneration were able to incorporate PPy via *in situ* chemical oxidative polymerization of pyrrole (Py) onto the surface of electrospun PCL. However, the microstructures of the resultant composites indicate that while the coating may be even, it is not conformal, as shown in Figure 8. Shown on the left is electrospun poly(L-lactic acid-co-ε-caprolactone) coated with PPy⁴⁷ and on the right is electrospun PCL coated with PPy¹⁸. It can be observed that while the substrate electrospun PCL-based polymer is still intact, there are distinct regions within the microstructure consisting of grey fibers, which is the PCL-based polymer, and clusters of white material, which is the PPy coating. The conductivity of the material on the left was measured to be 6.72×10^{-5} S/cm⁴⁷, within the range of conductivity values expected from PPy synthesized via chemical oxidative polymerization. For comparison, the conductivity of the PPy film shown in Figure 9 is at 0.302 S/cm²².

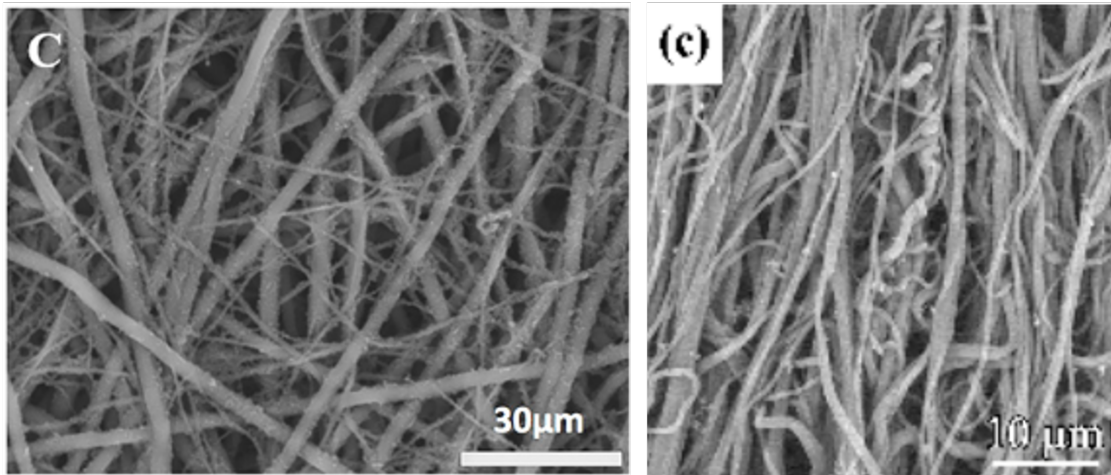


Figure 8. Nanofibers of PCL-based polymers coated with PPy, showing distinct regions of PCL and PPy. Adapted with permission from refs. 47 and 18. CC BY 4.0 and Copyright 2019 Elsevier, respectively.

These values make sense, given that conductivity depends on the mobility of electrons and that the microstructure of the PPy film shown in Figure 9 shows an uninterrupted path of conductive PPy material for electrons to travel in while the PPy-coated nanofibers shown in Figure 8 can be interpreted to show regions of conductive PPy interrupted by regions of insulating PCL-based polymer. As per percolation theory, reduced connections between conductive elements result in reduced overall conductivity of a composite, since moving electrons will need to have a certain energy to hop across a gap in conductive material⁴⁸. Because of this theory, it is also reasonable to hypothesize that processing ICPs into nanofibrous structures would avoid discontinuities between conductive ICPs and insulating material. Furthermore, the high surface-to-volume ratio of nanofibers would also provide the advantage of offering more conduction paths for electrons. These two effects would result in the enhancement of conductivity of ICPs. One condition that therefore must be met in coating electrospun polymers with ICPs is that, for the conductivity of ICPs (and thus their function) to be retained and possibly enhanced, there must be an even, conformal coating of ICPs on the surface of fibers.

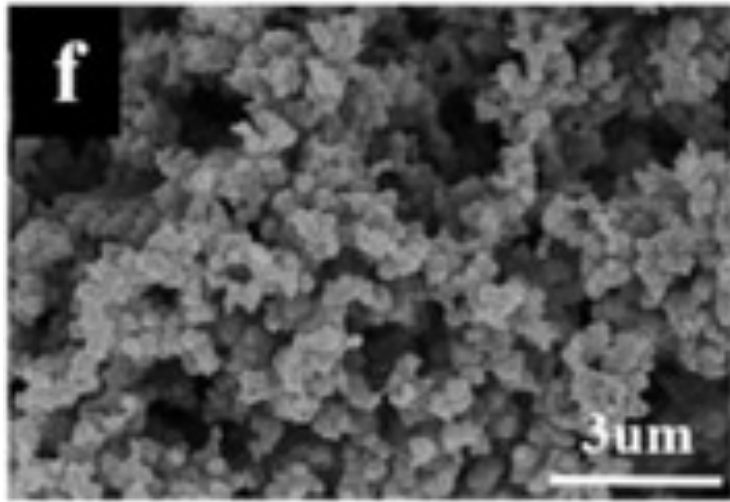


Figure 9. PPy film microstructure. Adapted with permission from ref. 22. Copyright 2018 Elsevier.

The aforementioned composites of insulating substrate electrospun polymer and ICPs are held together by non-covalent interactions. The studies cited above¹⁸⁻²² which used PCL-PPy composites for nerve regeneration did not include experiments to explore the stability of the PPy coating. However, non-covalent interactions often have problems with delamination. For example, electrochemically-polymerized PPy coated on indium tin oxide (ITO) glass electrodes were observed to delaminate easily with the use of Scotch tape⁴⁹. Electrochemically-polymerized PEDOT coated onto ITO glass slides were also observed to delaminate after ultrasonication³⁹. Therefore, to ensure a robust coating of ICPs onto electrospun substrate polymers, strong interactions are needed between them, which can come in the form of reacting the substrate electrospun polymer with ICPs to form covalent bonds.

A variety of strategies have been proposed to successfully functionalize electrospun polymers. Click chemistry has been used to tag electrospun poly(γ -benzyl-L-glutamate) end-capped with the alkyne-containing 4-dibenzocyclooctynol with an azide-containing stain⁵⁰. A Diels-Alder reaction has been used to tag a furan-functionalized

electrospun poly(lactic acid) with a maleimide-containing biotin⁵¹. Azlactone-functionalized electrospun PMMA was successfully reacted with an amine-containing compound in a “click-like” reaction⁵². Therefore, it is reasonable to hypothesize that these same strategies can be used to functionalize electrospun polymers with electroactive monomers and then polymerize these on the surface to fabricate the same substrate electrospun polymer-coated ICP composite, with the added advantage of having the ICP have a covalent tether to the substrate electrospun polymer.

1.5 Scope and Objectives of This Study

This study focuses on the coating of electrospun polymers with ICPs for nerve regeneration applications. It is hypothesized that combining the current strategies for nerve regeneration, namely: MNPs, biocompatible and biodegradable synthetic aligned nanofibrous scaffolds, and the use of ICPs such as PPy, would yield a composite that has an enhanced capability for nerve regeneration. The enhanced porosity of nanofibrous scaffolds fabricated through electrospinning would enhance the adhesion not only of neurites, proteins, and growth factors, but also of MNPs which promote the stretch growth of neurons, deliver drugs, and locally stimulate heat-dependent cellular functions. The high surface-to-volume ratio property of nanofibrous scaffolds also not only increases the surface available for cells to adhere to, but also increases the surface available for PPy to adhere to. A conformal coating of PPy on this surface would lend a nanofibrous morphology to the ICP, which circumvents the limitation of difficulty in electrospinning ICPs while potentially providing enhanced conductivity. Thus, firstly, this study focuses on the fabrication of the PCL-MNP-PPy composite (Figure 10).

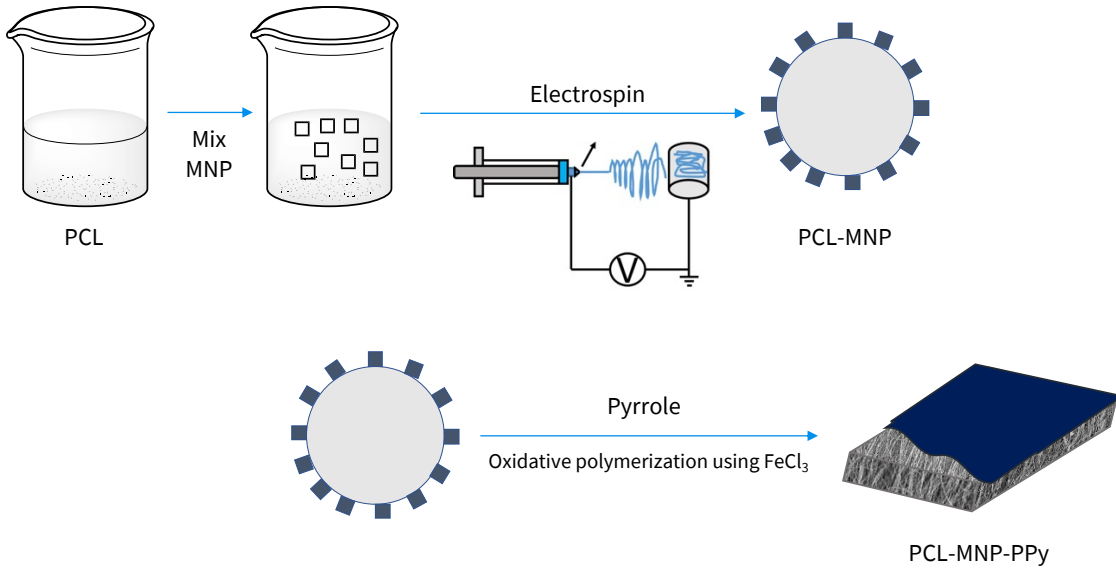


Figure 10. PCL-MNP-PPy composite fabrication

Second, this study performs a preliminary exploration of methods of chemically attaching ICPs onto electrospun polymers to potentially enhance the adhesion of ICP coatings. PAN and PMMA are electrospun, and the nitrile and ester functionality in their pendant groups is reacted with functionalized 3,4-ethylenedioxothiophene (EDOT) monomers. The EDOT pendant groups are then used as initiation sites to graft PEDOT chains to the modified PAN and PMMA surfaces (Figure 11).

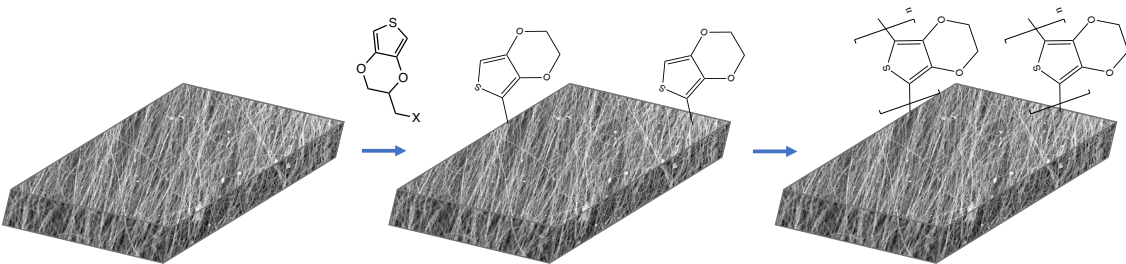


Figure 11. Scheme for the chemical modification of electrospun nanofibers with ICPs. While a wide variety of nanofiber functionalities could be used, efforts to modify PAN and PMMA will be presented in this study.

The findings from this study may not only enable the fabrication of a nanocomposite for enhanced nerve regeneration but may also be an enabling technology for many other applications, including other types of tissue engineering, energy storage, purification, and sensing. It is hypothesized that the same advantages that have been hypothesized for nanofibrous PPy and ICPs apply to nanofibrous PEDOT as well.

2 ELECTROSPINNING

2.1 Introduction

2.1.1 *Electrospinning theory*

Electrospinning is a method of processing polymer melts, solutions, or suspensions into continuous fibers with diameters in the nano- to micrometer range. As has been mentioned in Section 1.3, in an electrospinning setup, a polymer in the liquid phase is transferred to a syringe, which is connected to a high-voltage power supply and a grounded collector. This chapter focuses on solution electrospinning, although the discussion of the theory behind electrospinning can be generalized to apply to melt electrospinning as well. Where necessary, the phase of the polymer being electrospun is indicated.

The high-voltage power supply supplies positive charges to the polymer liquid. The positive charge buildup at the surface of the polymer liquid causes electrostatic repulsions which compete with the surface tension of the liquid and causes the formation of a cone shape, called a Taylor cone. This is because, while the surface tension in a droplet favors the formation of a sphere to lower surface free energy, the presence of electrostatic repulsions increases its surface area⁴¹. Above a certain critical voltage, the electrostatic repulsions overcome this surface tension, and liquid is ejected as a jet from the tip of the cone⁴².

This jet then travels to the collector, influenced by the electric field created from the positively charged tip of the polymer solution to the grounded collector. As it travels, the charges on the polymer jet are unevenly distributed throughout its length, which causes it to experience instabilities in the electric field⁵³. In the region near the Taylor

cone, the polymer jet travels in a straight path. The length of this straight path segment can be shortened by a slow flow rate of the polymer liquid. It first encounters Rayleigh instability. At this point, if the polymer liquid's viscoelastic properties such as surface tension are insufficient, or if the accelerating voltage of the setup is too low to suppress this instability, the jet breaks into droplets. Next, as the jet travels to the collector, surface tension and viscoelastic forces act against it, slowing it down. The dominant force in the polymer jet becomes the electrostatic repulsions present in it, and it experiences more Rayleigh instability, axisymmetric instability, and bending instability which bends and elongates the polymer jet, causing it to expand into loops and thin out (Figure 12)⁵⁴. The magnitude of the whipping and bending forces on the jet is crucial in the thinning of the polymer fibers down to the nanoscale. These draw the polymer jet in a matter of microseconds. Eventually, the solvent evaporates, leaving behind thin, continuous fibers on the collector, which can either be a plate or a rotating drum. If the collector is a rotating drum, an added variable that can be controlled is the rotation speed, which can induce alignment of the nanofibers that form.



Figure 12. Looping and thinning of polymer jet in electrospinning due to instability.
Adapted with permission from ref. 54. Copyright 2014 Elsevier.

2.1.2 The electrospinning apparatus

An electrospinning apparatus is shown in Figure 13 below. It has the following components: a syringe pump (1), a high voltage power supply (2), the electrospinning instrument proper (3) which controls the rasterable spray head (3a) and the grounded rotating drum collector (3b), and the positioning stand (4).

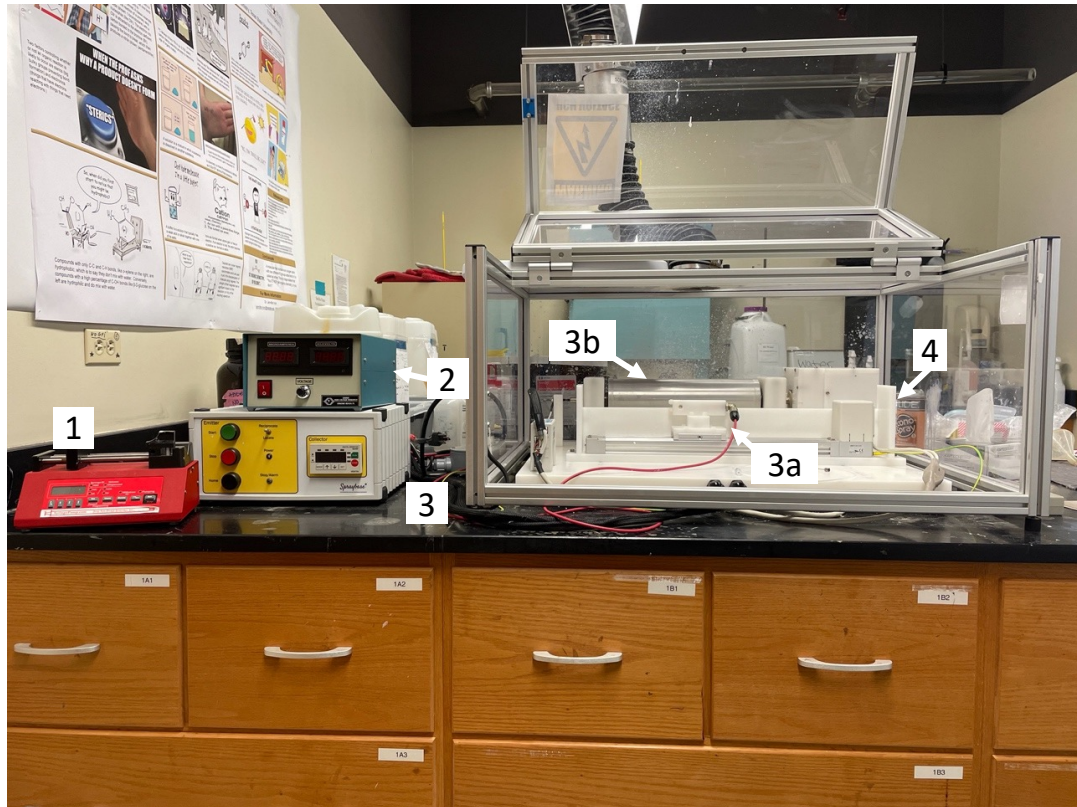


Figure 13. Electrospinning apparatus

To electrospin a polymer, it must be in the liquid phase, which can be accomplished by either melting the polymer or dissolving it in a suitable solvent. This polymer liquid is then placed in a syringe, which is then placed in a syringe pump and delivered to the electrospinner. The flow rate of the polymer liquid can be controlled from this end. At the end of this syringe pump is a metallic blunt tip needle. This is nestled in the rasterable spray head (3a) which is connected in series between a high

voltage power supply, and a grounded collector (3b). The high voltage power supply provides the charge necessary to deliver the polymer from the syringe to the collector. Figure 13 shows a setup wherein the grounded collector is a rotating drum (3b), and the rotation speed of this drum can be controlled by (3). The rasterable spray head is nestled on a removable positioning stand (4) which allows for the manipulation of the working distance between the area where the polymer liquid is discharged and the grounded collector. (3) also allows for the latitudinal motion of this component. Because solvent evaporation also occurs in the process of solution electrospinning, it is advantageous to house the electrospinnner under a hood or a snorkel, as shown here.

2.1.3 Process parameters in electrospinning

The variables that can be controlled in an electrospinning setup can be classified into three: process parameters, which refer to the variables that can be altered by manipulating the electrospinner; solution parameters, which refer to the variables directly related to the composition of the polymer being electrospun; and environmental conditions.

The process parameters for electrospinning are the applied voltage, working distance, flow rate, and nozzle speed⁴².

The applied voltage of an electrospinning setup refers to the voltage setting of the power supply connected to it. The applied voltage should be sufficient to overcome the surface tension of the liquid and cause the formation of a jet ejected from the Taylor cone. Increasing the applied voltage typically results in a reduction in the diameter of the electrospun fibers due to more stretching as observed in polystyrene (PS)⁵⁴, as more charges are present for instabilities to act on. At even higher applied voltages, this results

in the formation of polymer networks composed of closed loops stacked on top of each other, as observed in PS⁵⁵, possibly due to the “freezing-in” of the looping seen in Figure 12. It is, however, difficult to draw a direct relationship between applied voltage and fiber diameter because there are a host of variables operational in electrospinning, as has been mentioned, and that these observations can be quite polymer- or even polymer and solvent-specific.

The working distance refers to the distance between the nozzle from which the polymer liquid is expelled to the grounded collector. This working distance is directly related to the critical voltage required by a polymer liquid for electrospinning⁴¹. Manipulating this parameter allows for controlling the amount and duration of instability experienced by the polymer liquid jet and thus the width and dryness of the deposited fibers. Elongating this distance causes the polymer jet to experience more instability and become more extended and thinned. This is borne out by experimental observation: in the electrospinning of PS, increasing the working distance decreases the diameter of the nanofibers until a threshold distance was reached where no fiber formation was observed. The existence of this threshold distance probably results from elongation of the polymer jet competing with evaporation of the polymer solvent or solidification of the polymer. When the distance is decreased, down below another threshold distance, no fiber formation is also observed, with the fibers also being still wet with solvent⁴².

The flow rate refers to the rate at which polymer liquid is injected into the electrospinning setup. Flow rate controls the rate of deposition of the polymer onto the collector. As more polymer liquid is injected onto the electrospinner, more and more of the solvent needs to be evaporated, or more polymer needs to be solidified; thus, at high

flow rates, the diameter of the polymer fibers increases⁴¹, and the morphology of the polymer deposited tends to become less and less fibrous⁴², even forming beads⁵⁴.

From the discussion of these process parameters, it should be apparent that not one of them singularly determines the diameter or morphology of the polymer fibers being electrospun. These process parameters are highly specific to polymer choice and desired morphology of the product. In fact, in literature, the process parameters for electrospinning are specified for each polymer.

2.1.4 Solution parameters in electrospinning

The solution parameters for electrospinning are the concentration, viscosity, and conductivity of the polymer liquid or solution.

The concentration of a polymer in solution directly determines its viscosity, together with its molecular weight, as per the Mark-Houwink equation (Equation 1).

$$[\eta] = KM_r^a$$

Equation 1. Mark-Houwink equation⁵⁶

Where $[\eta]$ is the intrinsic viscosity of the polymer, M_r is the polymer relative molecular weight, and K and a are constants depending on the identity of the polymer and its conformation in the solvent system. M_r can either take the value of the number-average molecular weight M_N or the weight-average molecular weight M_W . Except for biopolymers such as proteins, and polymers synthesized through controlled polymerization, polymers exist as molecules of covalently bound repeat units of varying lengths. Because of this, it is not possible to calculate a single uniform molecular weight for a polymer, and averages of the molecular weight of the polymer chains are reported⁵⁷. The number-average molecular weight (M_N) of a polymer can be calculated by getting the

sum of all the products of the mole fraction n_i of species i in a sample with the same polymer chain length multiplied by their molecular weight M_i (Equation 2).

$$M_N = \sum_i n_i M_i$$

Equation 2. Formula for calculating M_N , the number-average molecular weight of a polymer

Meanwhile, the weight-average molecular weight (M_W) of a polymer can be calculated by getting the sum of all the products of the weight fraction w_i of species i in a sample with the same polymer chain length multiplied by their molecular weight M_i (Equation 3).

$$M_W = \sum_i w_i M_i$$

Equation 3. Formula for calculating M_W , the weight-average molecular weight of a polymer

The greater the viscosity of the polymer liquid, the greater is its resistance to the instabilities it encounters in the electric field generated by electrospinning⁴². The viscosity is also directly related to the degree of polymer entanglements which should occur for the formation of fibers. The effect of this is an elongation of the straight path segment of the polymer liquid, as mentioned in the previous section, and results in a smaller area for deposition of the polymer on the collector. Conversely, if the viscosity of the polymer solution is low, the polymer jet breaks into droplets, and particles are deposited on the collector instead of fibers. This process is called electrospraying⁵⁵. Another property that is affected by the polymer concentration is the diameter of the deposited fibers: the square root of the concentration of the polymer solution is directly related to the diameter of the fibers formed, and indirectly related to the final diameter of

the polymer jet⁵⁸. This final diameter of the polymer jet is itself directly related to the surface tension of the liquid and the flow rate of the electrospinning setup, and indirectly related to the electric current generated in electrospinning.

Because the initiation of electrospinning requires the accumulation of positive charges on the tip of the syringe from which the polymer liquid enters the electrospinning setup, the conductivity of the liquid is an important factor in electrospinning. A polymer liquid for electrospinning has to be able to conduct the right amount of positive charge from the bulk of the solution to the surface: too low, and charges will not accumulate, and too high, and there would be lessened electrostatic repulsions because of delocalization of charge⁴¹. The net result of these two would be the inability of the polymer liquid to form a Taylor cone and thus electrospin.

2.1.5 Electrospinnable polymers

Not all polymers can be electrospun, and there are specific conditions polymers must meet to be processed into nanofibers through this process. Firstly, polymers to be electrospun must either be soluble in a suitable solvent or able to be melted without degradation. Second, they have to have a sufficiently high molecular weight⁴¹.

This solvent must have a suitable vapor pressure and volatility: if the solvent is too volatile, then it will evaporate too quickly and not let the polymer undergo the whipping and bending forces which draw it out to form nanofibers, and if the solvent is not sufficiently volatile, then the polymer being deposited onto the collector would still be wet with solvent⁵⁵.

The molecular weight of a polymer must be sufficiently high for it to have favorable rheological properties in solution. This is because higher molecular weight polymers have a high degree of chain entanglement to stabilize the jet of polymer liquid formed in electrospinning and resist the instabilities acting on them⁴¹. Chain entanglement in polymers refers to the interlocking of polymer chains due to overlap. As the length of the polymer chain increases with increasing molecular weight, there are more and more sites of entanglement. As the solvent in the polymer jet evaporates, the concentration of the polymer solution increases, and chain entanglements commence. At this point, the polymer jet either breaks into droplets and accomplishes electrospraying (deposition of polymer powder on the grounded collector) or stays intact and accomplishes electrospinning (deposition of polymer fiber on the grounded collector).

The crucial factor for electrospinning to occur is the formation of long-range entanglement networks⁵⁹. There exists an entanglement molecular weight for each polymer, which refers to the average molecular weight between sites of entanglement. These values are a function of secondary interactions in the polymer as determined by the chemical structure of the repeat unit; the values are determined experimentally for each polymer and are reported in the literature. This effect also explains the requirement of sufficient concentration and/or viscosity for a polymer to be electrospun: when more polymer chains are present in a given volume, there are more chain entanglements in that volume, and the better the electrospinning process would be for that polymer.

There are many polymers that have been electrospun, including PAN, PMMA, and PCL. The molecular weights necessary for electrospinning solutions of each of these polymers are given in literature and are in the order of magnitude of 10^3 g/mol⁶⁰⁻⁶².

2.1.6 Fiber alignment in electrospinning

The polymer nanofibers produced from electrospinning are oriented randomly. It is possible to align these polymer nanofibers via several methods. One method involves the controlling of the electric field in the electrospinning experiment⁴². An easier method is the incorporation of a rotating drum mandrel as the grounded collector in the electrospinning setup⁵⁴. This accomplishes alignment of nanofibers by applying a mechanical stretching force to align the nanofibers along the axis of rotation⁴¹. The degree of alignment is dependent on the rotation speed of the mandrel: the faster rotation results in increased nanofiber alignment. However, at very high speeds, the turbulent air flow around the vicinity of the collector and the strong mechanical stretching forces fracture the fibers, leading to a decrease in fiber alignment⁴³. Fiber alignment is important in applications requiring anisotropic properties, such as in the directional growth of cells in nerve regeneration, device fabrication, and composite reinforcement.

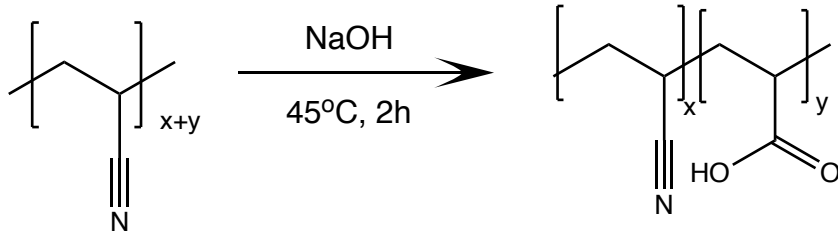
2.1.7 Electrospun polymer applications and bioengineering

Electrospinning polymers into nanofibrous structures lends them many favorable properties, such as a high surface to volume ratio, porosity, tailorabile morphology with control of process and solution parameters, and non-woven fibrous structure. This allows them to have applications in fields needing a high degree of surface adhesion and sustained and controlled release of materials adhered onto their surfaces⁵³.

Electrospun polymers have seen applications in the field of bioengineering. Biocompatible polymers can be electrospun into tissue scaffolds that have the advantage of mimicking the ECM, which is the natural environment cells face *in vivo*, a phenomenon called biomimesis. These tissue scaffolds can have the effect of replacing damaged tissue by providing a medium for the growth of cells. The high porosity and surface area of electrospun tissue scaffolds are conducive for the survival, attachment, and proliferation of cells¹⁷. The controllability of nanofiber alignment during electrospinning broadens this application into tissues which have unique anisotropic structures⁶³, such as musculoskeletal, cardiac, and neural tissue. This is because tissue scaffolds based on aligned nanofibers have the additional properties of modulating cell shape, migration, differentiation, and even ECM assembly⁴³. Aside from being biocompatible, these tissue scaffolds must have controlled biodegradability *in vivo* which should accomplish degradation at a rate that is slower than the growth of cells on the tissue scaffold, and the requisite mechanical properties mimicking the mechanical properties of native tissue. Fortunately, both criteria can be met by controlling parameters such as polymer choice, fiber alignment, and fiber diameter, all of which are easily modified during electrospinning.

2.1.8 Scope and limitations of this study

This study focuses on the attempts to electrospin the polymers PAN, PMMA, PCL, and poly(vinyl chloride) (PVC). PAN powder is also hydrolyzed to form PAN-co-poly(acrylic acid) (PAA), following a method described in literature, as shown in Equation 4⁶⁴, and this copolymer is also attempted to be electrospun, in order to test the suitability of modified electrospinnable polymers to be electrospun.



Equation 4. PAN alkaline hydrolysis

This study also examines the morphology and elemental composition of the electrospun polymers. It does not delve into the optimal conditions for the electrospinning of each of these polymers, nor the effects of altering differing parameters in the morphology of the resultant nanofibrous polymer

2.2 Materials and Methods

2.2.1 Materials

PCL ($M_N=80,000$ g/mol), PAN ($M_w=150,000$ g/mol), and PVC ($M_N=99,000$ g/mol, $M_w=233,000$ g/mol) were obtained from Sigma-Aldrich. PMMA ($M_w=550,000$ g/mol) was obtained from Alfa Aesar. DMF and THF were obtained from EMD Millipore. For electrospinning, 10 mL BD Luer-LokTM syringes were used.

2.2.2 Instrumentation

An electrospinning setup composed of a New Era Pump Systems syringe pump, Gamma High Voltage Research high voltage power supply, and Spraybase electrospinning rotating drum collector were used. For material characterization, analysis was done using a JEOL JSM-6010 PLUS/LA Scanning Electron Microscope in the Shared Research Operations facility at the Texas State University. Attenuated Total Reflectance – Infrared (ATR-IR) spectroscopic analysis was done using a Bruker Tensor II Fourier Transform – Infrared (FT-IR) Spectrometer with a Harrick SplitPeaTM

Attenuated Total Reflectance accessory in the Department of Chemistry and Biochemistry at Texas State University.

2.2.3 Preparation and electrospinning

Polymers were dissolved in optimal solvent systems as shown in Table 1 and stirred for 24-48 hours at room temperature before electrospinning. PAN was also hydrolyzed before electrospinning as per a literature procedure⁶⁴: PAN powder (1 g) was added to a 100 mL aqueous solution of 1.5M NaOH, and heated with stirring at 45 °C for 2 h. The hydrolyzed PAN (HPAN) powder was then collected by vacuum filtration and washed with deionized water until the washings were neutral. HPAN was allowed to air dry for a day. The product is a yellowish solid (1 g) which was then dissolved in 10 mL of DMF.

The process and solution parameters for the electrospun polymers are optimized for formation of a Taylor cone during the ejection of the polymer solution, and/or to achieve a drip-free polymer flow, as shown in Table 1. All polymers were electrospun using a stationary needle (“rastering off”); PCL was also electrospun using a moving needle (“rastering on”), as described in the following section.

Table 1. Optimal process and solution parameters used in the electrospinning of polymers

Polymer	Solvent system and polymer concentration (w/v)	Applied voltage	Working distance	Flow rate
PCL	15% in THF:DMF (1:1 v:v)	17.0 kV	130 mm	0.05 mL/min
PAN	10% in DMF	15.0 kV	110 mm	0.05 mL/min
PVC	10% in THF:DMF (1:1 v:v)	15.0 kV	150 mm	3 mL/hr
PMMA	15% in DMF	15.0 kV	110 mm	1 mL/hr
HPAN (hydrolyzed PAN)	10% in DMF	25.0 kV	110 mm	0.05 mL/min
Ethanolamine-modified PAN	12% in DMF	14.0 kV	150 mm	1.30 mL/hr

2.2.4 Rastering experiment

A 10 mL solution of 15% PCL in THF:DMF (1:1 v/v) was prepared and electrospun following the procedure and parameters outlined above. The first 5 mL of polymer solution was electrospun without rastering of the emitter. The electrospinning setup was then stopped, and the electrospun PCL was removed from the collector and stored until further use. The remaining 5 mL solution was then electrospun with emitter rastering at 0.20 m/s across 10 cm. This was also removed from the collector afterwards and stored until further use.

2.2.5 *Collector speed experiment*

Two 10 mL solutions of 15% PCL in THF:DMF (1:1 v/v) were prepared and electrospun following the procedure and parameters outlined above. One solution was electrospun with the rotating drum collector set to 80 rotations per minute (rpm), and the other solution was electrospun at 4000 rpm. The electrospun polymers were removed from the collector and stored until further use.

2.2.6 *SEM and SEM-EDX analysis*

The electrospun polymers were cut into 1x1 cm squares and then analyzed without further modification under low vacuum in an SEM. Fiber diameter analysis was accomplished using visual inspection of SEM images using ImageJ 1.52v. Random fibers and features of interest in each of the SEM images of the electrospun polymers were picked. The pixel length was first calibrated using the provided dimension measures in each of the images. Afterwards, lines were drawn transverse each of the fibers and features selected, and the length of these lines measured.

2.2.7 *ATR-IR analysis*

1 x 1 cm squares of electrospun polymer were cut from the middle of the fiber mat and subjected to ATR-IR analysis without further modification.

2.3 Results and Discussion

2.3.1 *Electrospun polymers*

PCL has been electrospun, resulting in a microstructure composed of fibers with diameters from 0.83-12.86 μm (Figure 14).

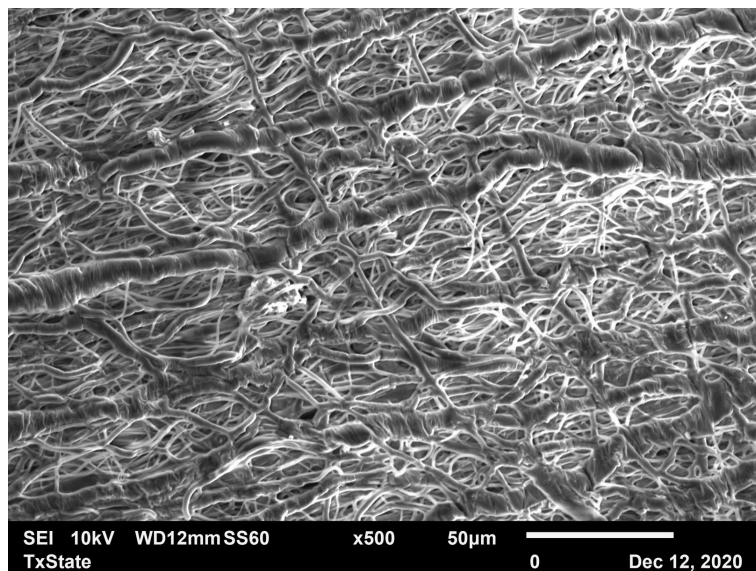


Figure 14. Electrospun PCL

EDX analysis shows the presence of C and O atoms in this microstructure (Figure 15), and ATR-IR analysis shows a characteristic carbonyl C=O stretch at 1724 cm^{-1} , and a strong C-O ester stretch at 1171 cm^{-1} (Figure 16), indicating the presence of the respective functionalities on the electrospun polymer, which corresponds to the structure of PCL as shown in Figure 3.

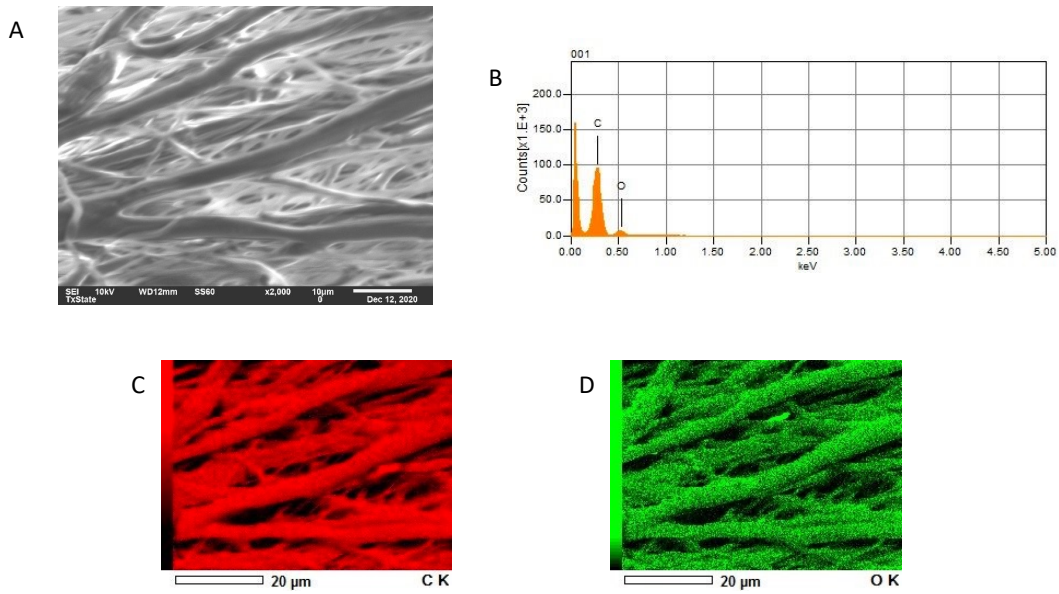


Figure 15. EDX mapping of electrospun PCL. (A) SEM micrograph of area where elemental mapping was done (B) Graph of detected atoms in A and their relative abundance (C) Map showing the areas in A where C was detected (D) Map showing the areas in A where O was detected

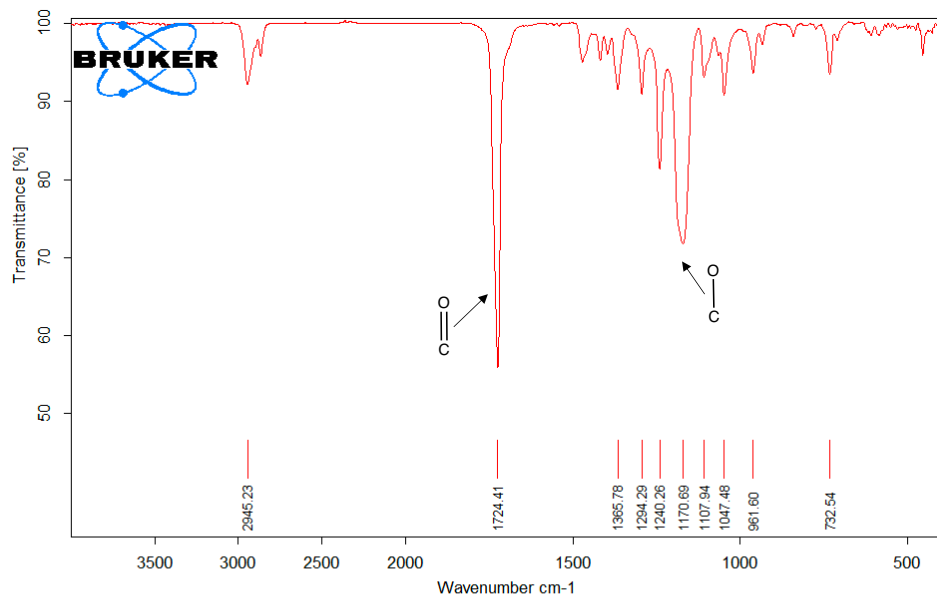


Figure 16. ATR-IR spectrum of electrospun PCL

Overall, these indicate that PCL has been successfully electrospun into nanofibers with its ester functional groups unaffected by the electrospinning process.

PAN has been electrospun, resulting in a microstructure composed of fibers with diameters from 0.23-2.05 μm (Figure 17). Interestingly, beads with diameters from 4-18.36 μm can also be observed. This is an undesirable byproduct of electrospinning, as it reduces the degree of porosity of the nanofiber structure and the surface area, although beaded structures have applications in drug delivery and membrane filtration⁶⁵. To remedy this, either or both the viscosity of the PAN solution and the applied voltage must be optimized⁶⁶.

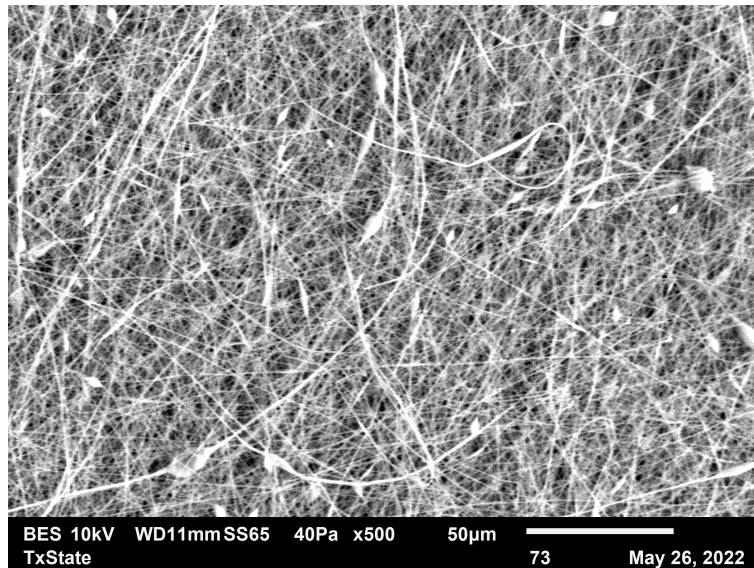


Figure 17. Electrospun PAN

EDX analysis shows the presence of C and N atoms in this microstructure, but also O and Si atoms (Figure 18). Meanwhile, ATR-IR analysis (Figure 19) reveals that not only does the electrospun polymer have a characteristic nitrile C≡N stretch at 2244 cm^{-1} , as to be expected in polyacrylonitrile, the structure of which is shown in Figure 7, but also a carbonyl C=O stretch at 1664 cm^{-1} , a C=N imine stretch at 1627 cm^{-1} , a broad

N-H stretch at 3620 cm^{-1} , a possible weak broad carboxylic acid OH stretch centered at 2921 cm^{-1} , and a carboxylic acid OH bend at 1453 cm^{-1} . These may indicate that the sample has undergone hydrolysis, as these are characteristic products of PAN hydrolysis⁶⁰. In any case, these peaks are also reported in literature for untreated PAN nanofibers, which have also been attributed to traces of poly(methyl acrylate) in commercially-available PAN⁶⁷ or traces of unevaporated DMF⁶⁸. The latter explanation seems to be unlikely, as PCL was also electrospun with DMF, and these peaks do not appear in the ATR-IR spectrum of electrospun PCL.

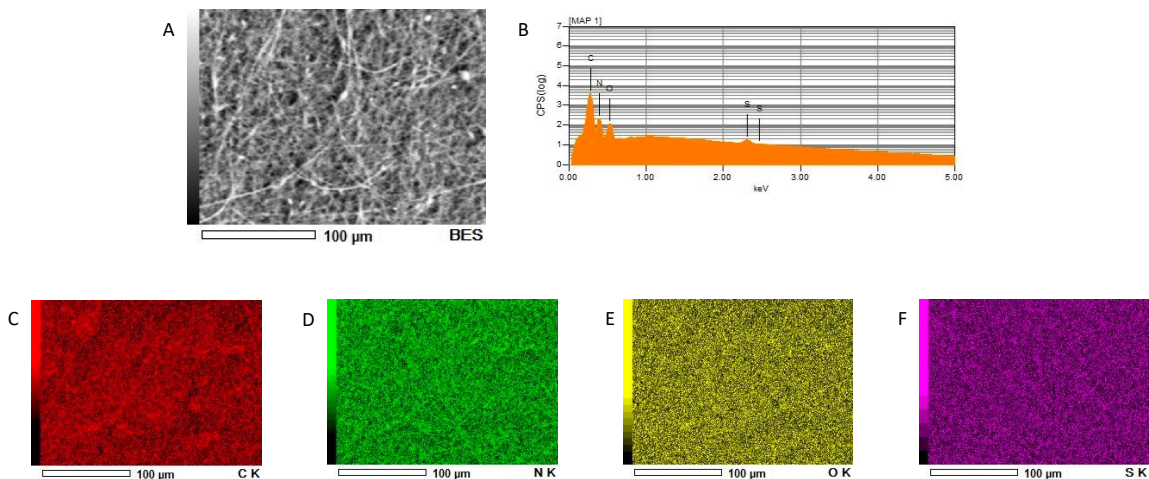


Figure 18. EDX mapping of electrospun PAN. (A) SEM micrograph of area where elemental mapping was done (B) Graph of detected atoms in A and their relative abundance (C) Map showing the areas in A where C was detected (D) Map showing the areas in A where N was detected (E) Map showing the areas where O was detected (F) Map showing the areas where S was detected

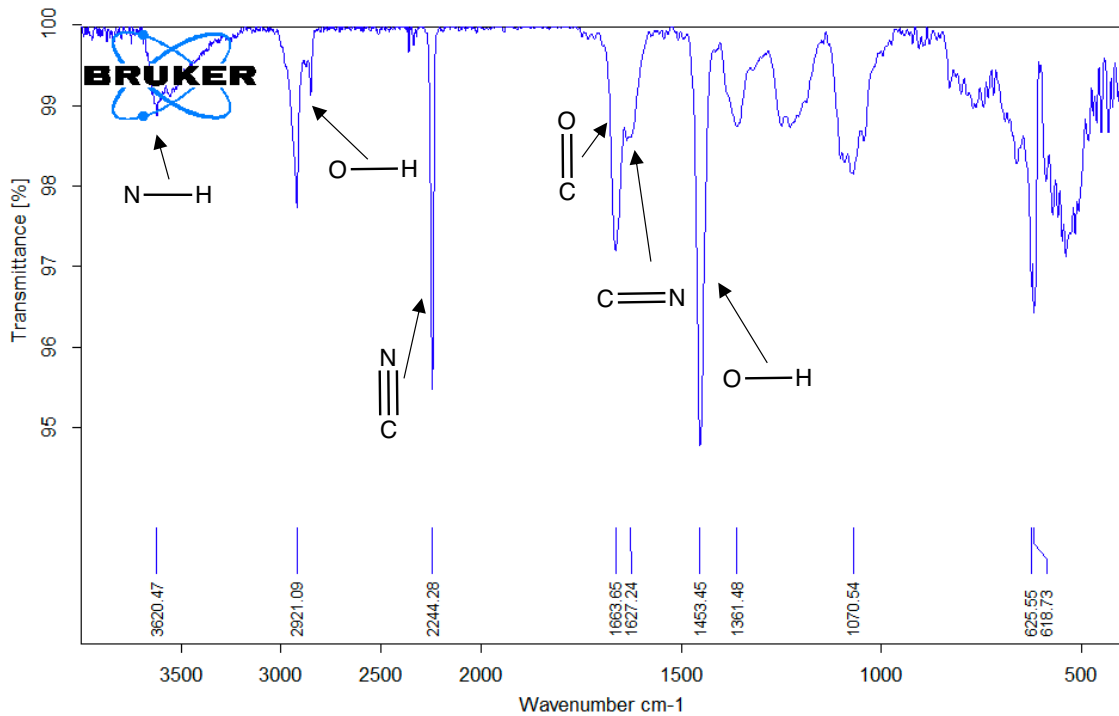


Figure 19. ATR-IR of electrospun PAN

Overall, these indicate that the electrospinning of PAN must be further optimized to result in nanofibers, but the important nitrile functional groups survive the electrospinning process.

PVC has been electrospun, resulting in a microstructure composed of fibers with diameters from 0.64-6.71 μm . Notably, wide bands of polymer with diameters of about 58 μm can also be observed (Figure 20). This can be attributed to solvent not evaporating between the emitter and the collector in the electrospinner but drying off on the surface of the collector. This means that the parameters used may not have been optimal, and the applied voltage and the working distance must be increased to result in the formation of nanofibers.

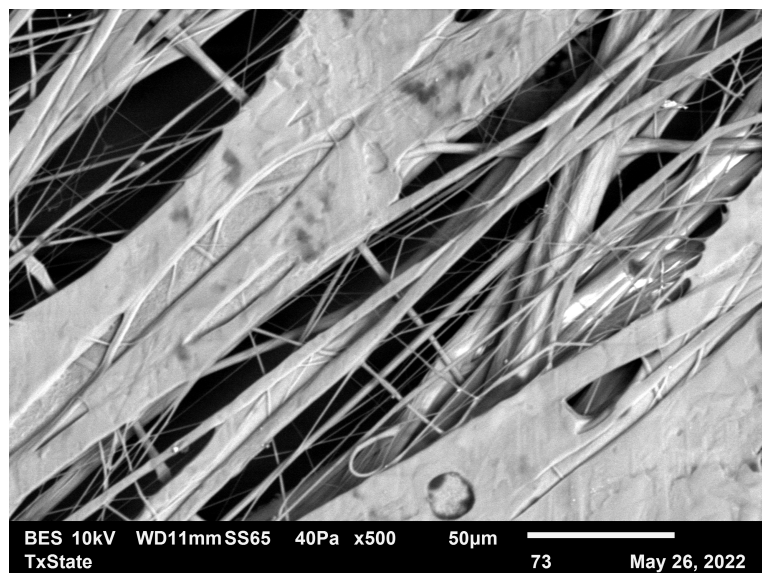


Figure 20. Electrospun PVC

EDX analysis shows the presence of C and Cl atoms in this microstructure (Figure 21). The ATR-IR spectrum of electrospun PVC shows a characteristic strong C-Cl stretch at 613 cm^{-1} (Figure 22).

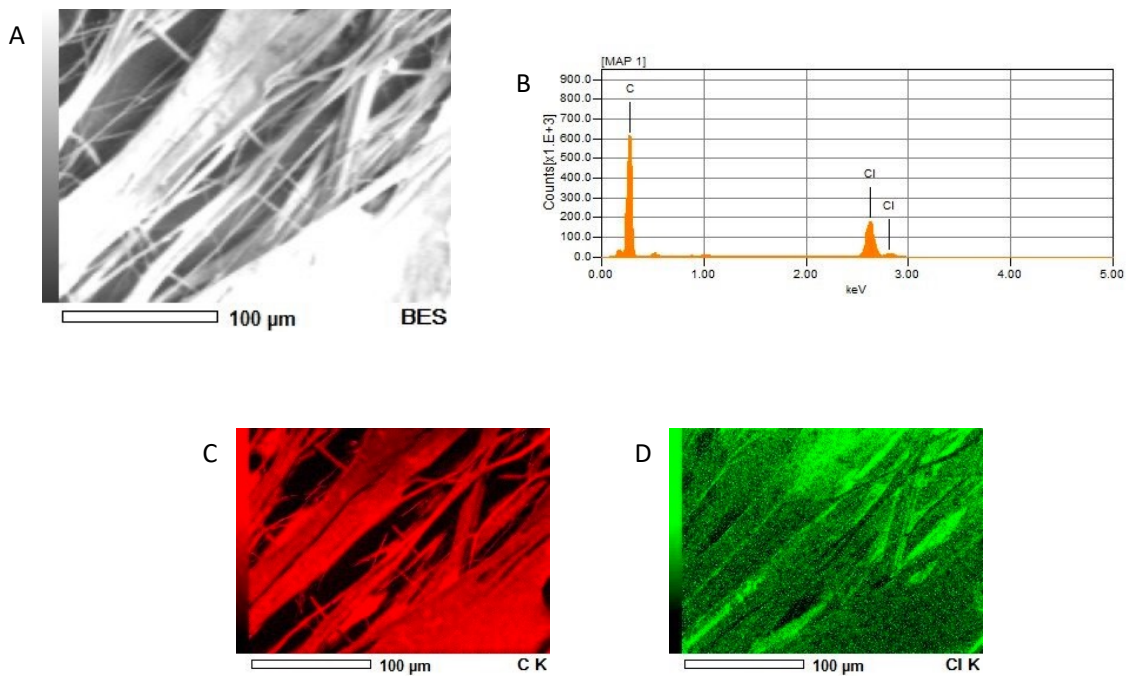


Figure 21. EDX analysis of electrospun PVC. (A) SEM micrograph of area where elemental mapping was done (B) Graph of detected atoms in A and their relative abundance (C) Map showing the areas in A where C was detected (D) Map showing the areas in A where Cl was detected

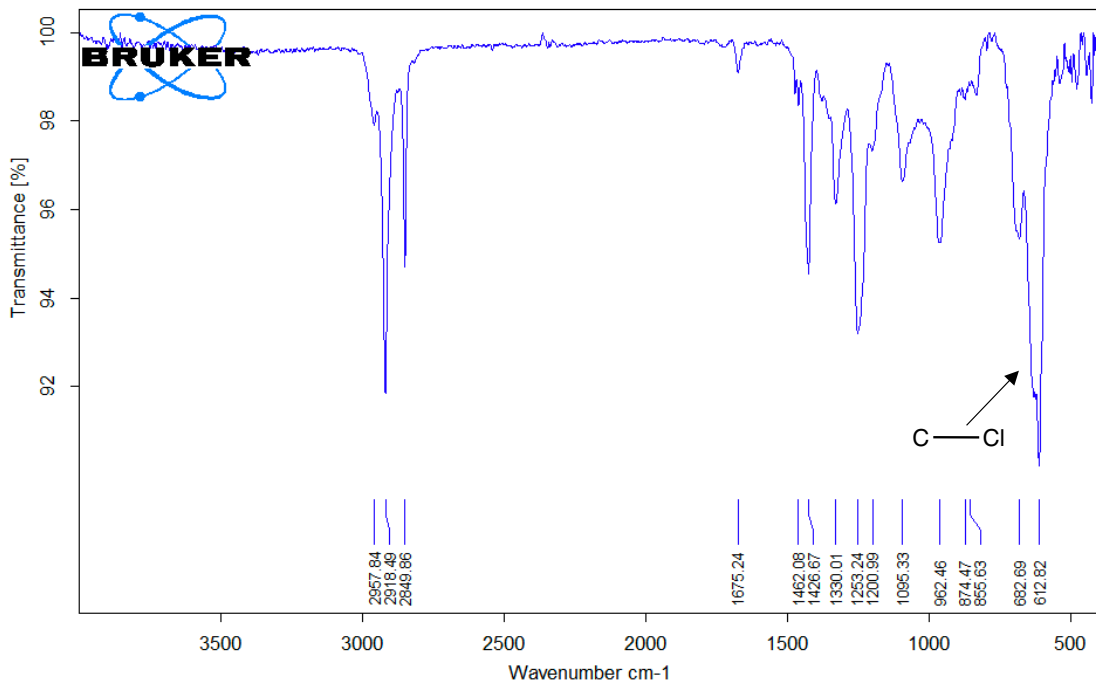


Figure 22. ATR-IR spectrum of electrospun PVC

Overall, these indicate that optimization must be done in the process parameters in electrospinning PVC, but that the alkyl chloride functional groups survive the electrospinning process.

PMMA has been electrospun, resulting in a microstructure composed of fibers with diameters from 0.96-5.53 μm (Figure 23).

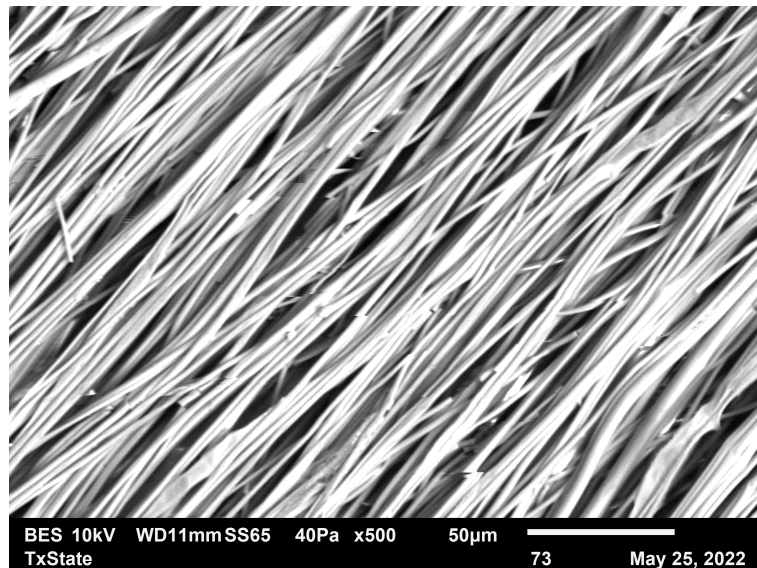


Figure 23. Electrospun PMMA

EDX analysis shows the presence of C and O on the fibers (Figure 24). ATR-IR analysis shows the presence of a strong carbonyl C=O stretch at 1726 cm^{-1} and a strong ester C-O stretch at 1147 cm^{-1} (Figure 25).

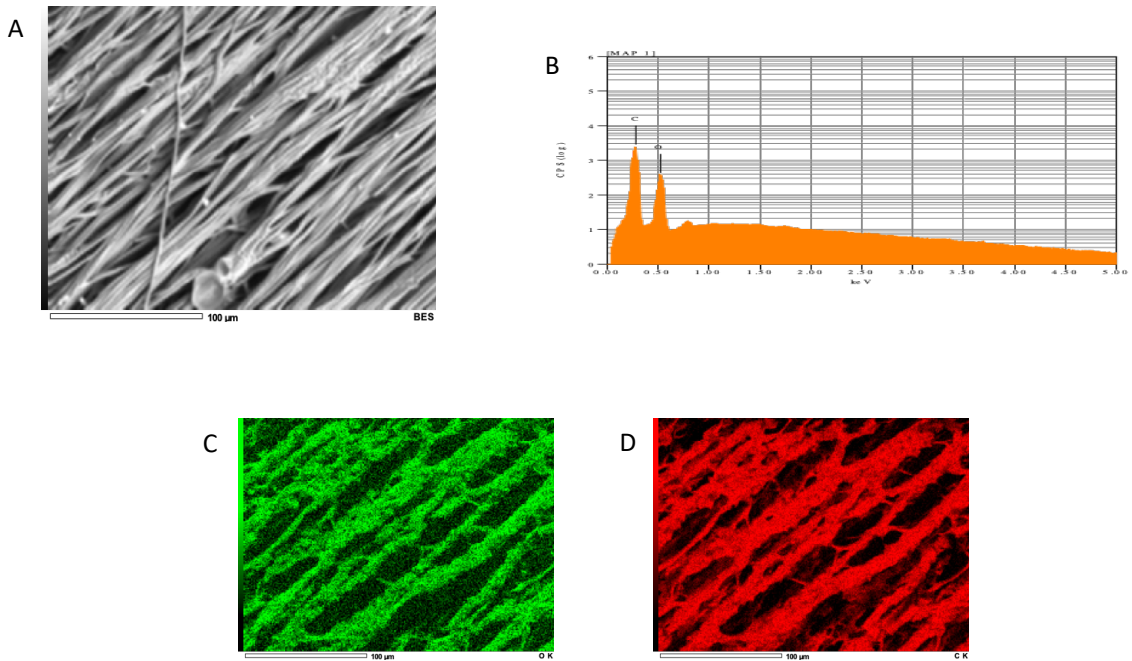


Figure 24. EDX analysis of electrospun PMMA. (A) SEM micrograph of area where elemental mapping was done (B) Graph of detected atoms in A and their relative abundance (C) Map showing the areas in A where C was detected (D) Map showing the areas in A where O was detected

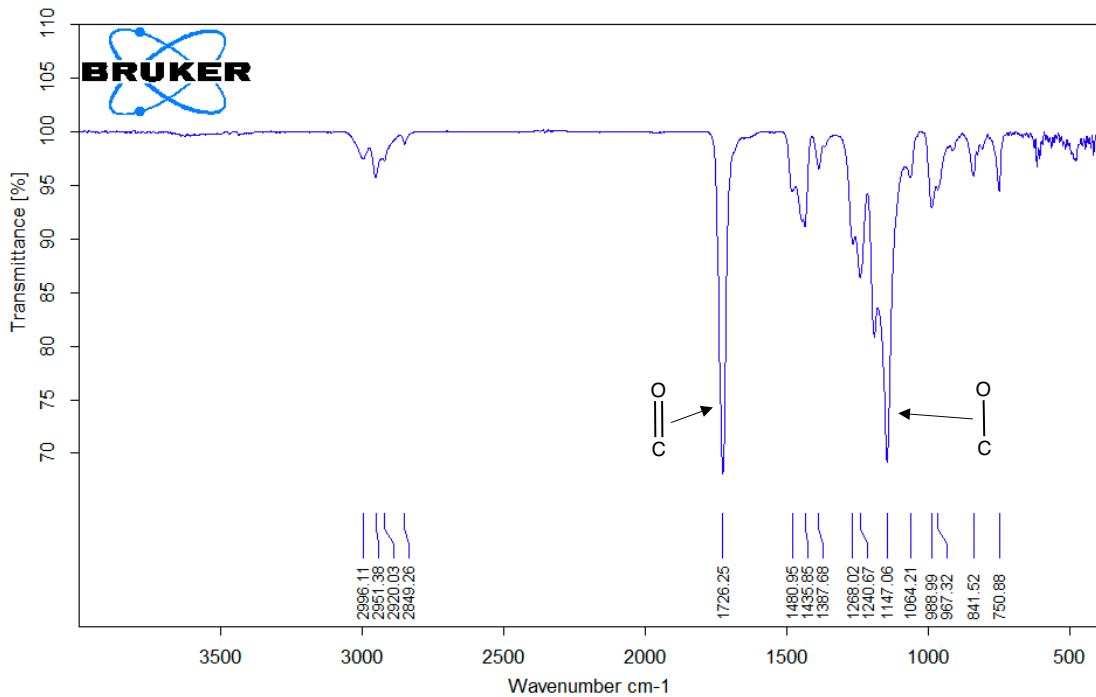


Figure 25. ATR-IR spectrum of electrospun PMMA

Overall, these indicate that the solution and process parameters for electrospinning have been successfully optimized for PMMA, with its ester functional groups surviving the electrospinning process.

In the electrospinning of HPAN, an interesting microstructure can be seen in Figure 26 which is composed of fibers with diameters from 0.64-2.32 μm , beads with diameters from 3.64-19.14 μm , and film extending 143.41 μm across.

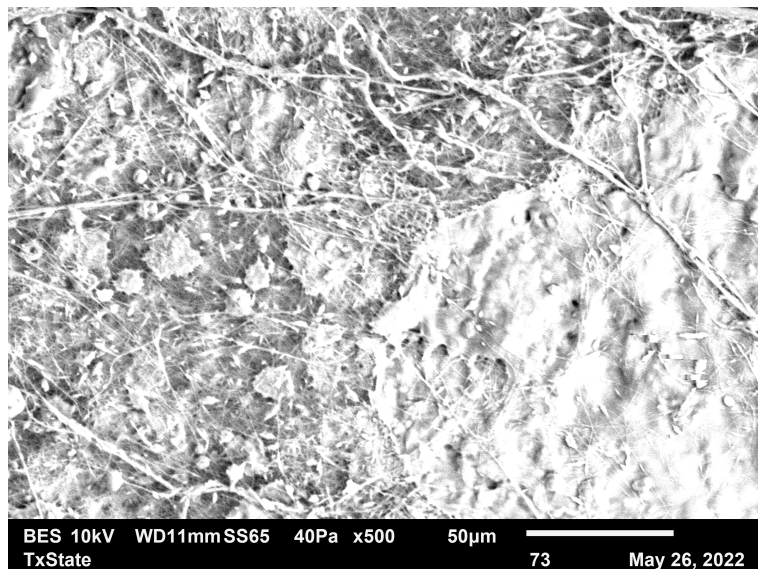


Figure 26. Electrospun HPAN

EDX analysis indicates the presence of C, N, Na, and O on the electrospun fibers (Figure 27). ATR-IR analysis indicates the presence of an absorption at 3420 cm^{-1} which can be attributed to either carboxylic acid O-H or amine N-H stretching, a possible weak broad carboxylic acid O-H stretch at 2956 cm^{-1} , a nitrile C≡N stretch at 2244 cm^{-1} , an absorption at 1664 cm^{-1} which can be attributed to either carboxylic acid C=O or imine C=N stretching, an N-H bend at 1572 cm^{-1} , a carboxylic acid O-H bend at 1454 cm^{-1} , and amine C-N stretches at 1252 cm^{-1} , and 1096 cm^{-1} (Figure 28).

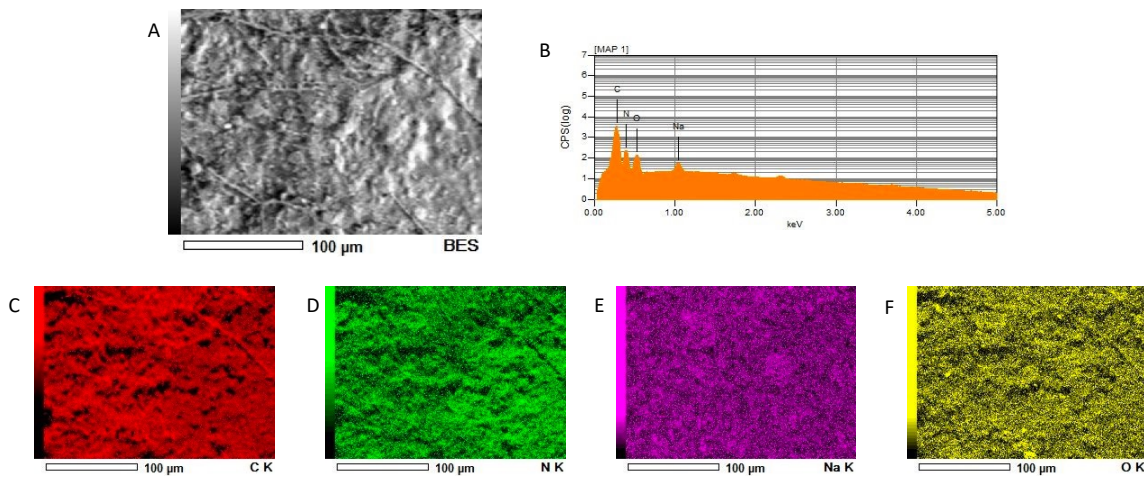


Figure 27. EDX analysis of HPAN. (A) SEM micrograph of area where elemental mapping was done (B) Graph of detected atoms in A and their relative abundance (C) Map showing the areas in A where C was detected (D) Map showing the areas in A where N was detected (E) Map showing the areas in A where Na was detected (F) Map showing the areas in A where O was detected

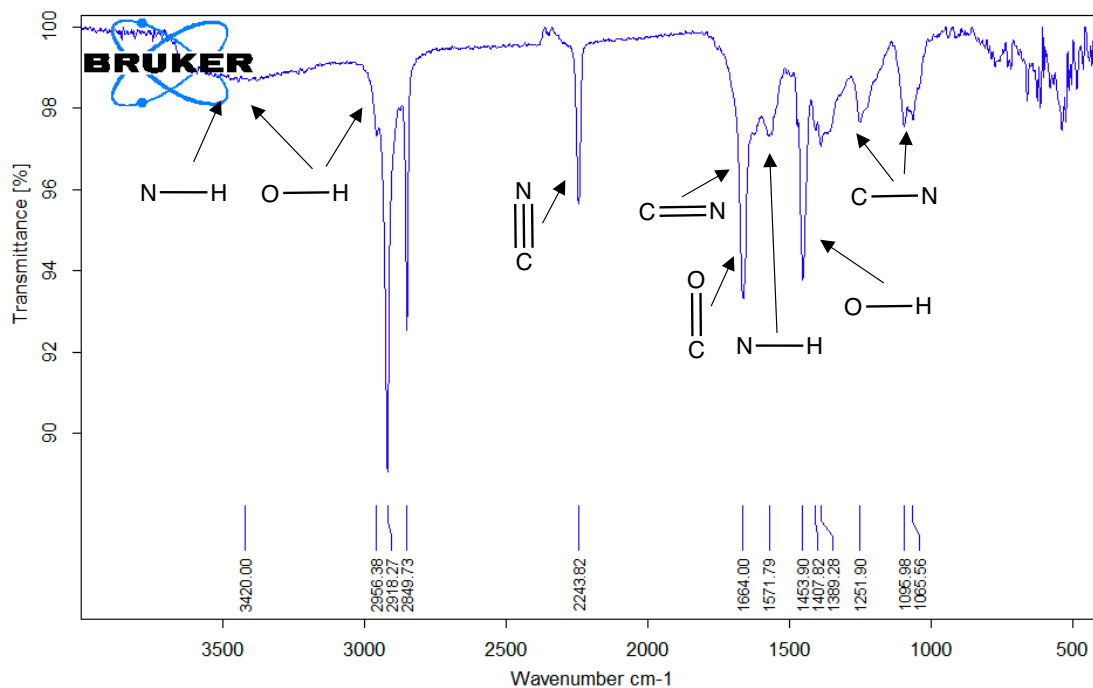
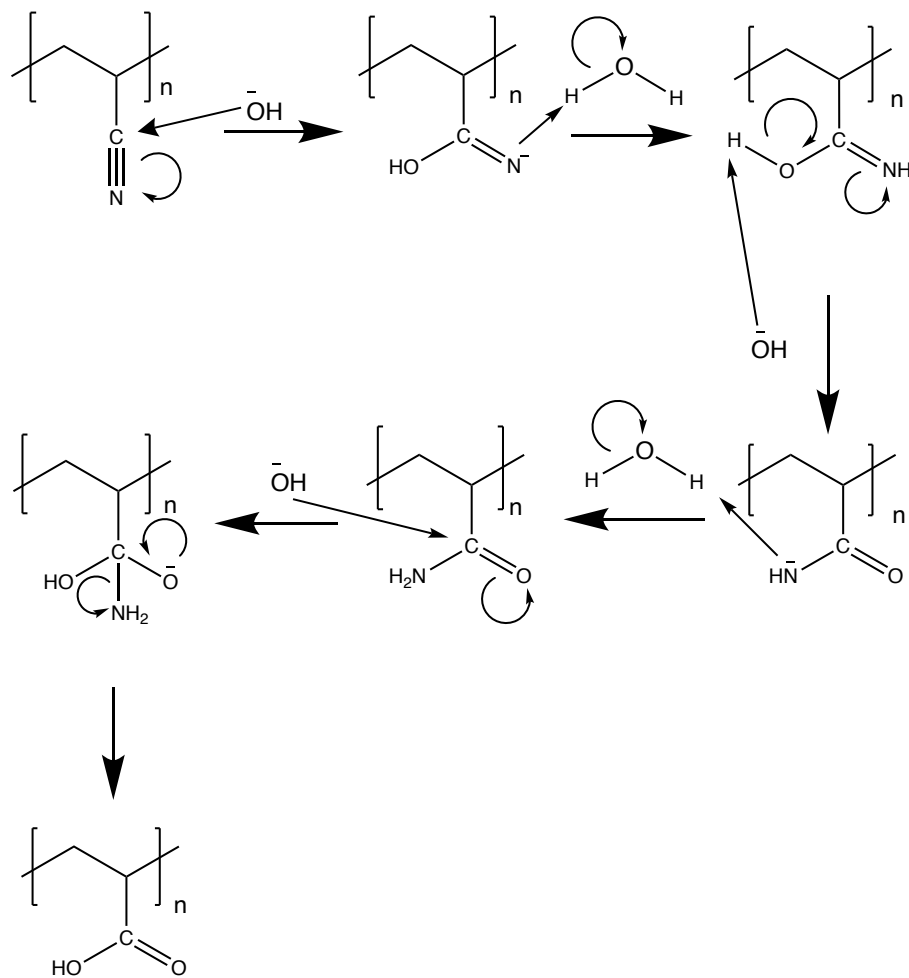


Figure 28. ATR-IR spectrum of electrospun HPAN

As has been noted in the electrospinning of PAN above, these correspond to the carboxylic acid, amide, and imine functional groups formed in hydrolysis, as shown in Scheme 1 below. The formation of the final carboxylic acid product is dependent on

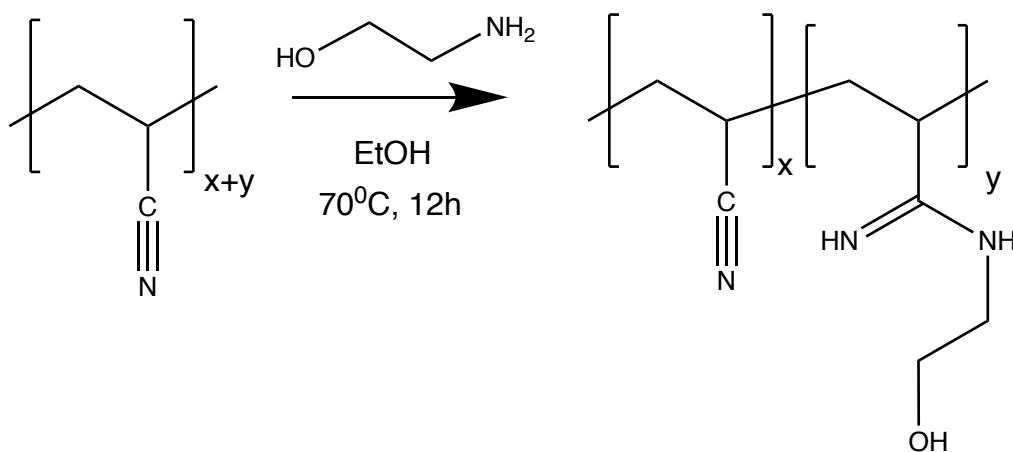
making the base hydrolysis reaction run longer, although it is possible that even after a long hydrolysis time, some imine and amide groups still have not been converted⁶⁰. This reaction and possible route to electrospinning functionalized polymers will be explored further in Chapter 5.



Scheme 1. Proposed mechanism for the alkaline hydrolysis of PAN

Although there was fiber formation in the electrospinning of PAN-co-PAA, it was minimal compared to film formation. This is probably due to solvent DMF evaporating on the surface of the collector instead of in the electric field between the emitter and the collector in the electrospinner. This can be addressed by optimizing any of the process or

solution parameters. It is worth noting, however, that the applied voltage for the electrospinning of this polymer is already at a high value of 25.0 kV, and that electrospinning PAN at the lower applied voltage of 15.0 kV with the same solvent resulted in fiber formation. Thus, the carboxylic acid and amine groups formed during hydrolysis may be responsible for strong hydrogen bonding with the solvent DMF and make evaporation harder. Workman and co-workers previously reported their efforts to electrospin PAN grafted with ethylenediamine⁶⁹, which they then redissolved in DMF and electrospun using the conditions specified in . This was also done as a side experiment, although with the use of ethanolamine (Equation 5). These conditions are milder than the conditions used to attempt to modify PAN-co-PAA and did result in the formation of a fibrous mat, despite having the same functional groups that can hydrogen bond with DMF. Thus, it would prove beneficial to determine the percent conversion of nitrile pendant groups to the ethanolamine-grafted pendant groups in this reaction in the future, and this could provide insight into the extent of hydrogen bonding that can occur between the polymer and the solvent DMF to ensure successful electrospinning.



Equation 5. Grafting of ethanolamine to PAN

Another factor that must be considered is that the hydrolyzed PAN in solution may be a polyelectrolyte and thus conduct charges very efficiently. As has been noted in the previous section, this is undesirable, and leads to lessened electrostatic repulsions in the polymer jet and thus lessened forces which draw the polymer into fibers⁴⁶. Thus, to electrospin hydrolyzed PAN, either or all of the following may be done: dissolution in a suitable, non-hydrogen bonding solvent and increasing the applied voltage and working distance.

2.3.2 Effect of rastering

As can be observed in Figure 29 and Figure 30, the addition of rastering during electrospinning leads to the formation of some fibers that are visually much larger in diameter, and the appearance of areas where solvent may have evaporated on the collector itself. This is a surprising result, as all other parameters in the electrospinning setup were kept constant, and thus solvent should have theoretically evaporated in the space between the emitter and the collector as it has in the electrospinning setup without rastering. As noted in section 2.1.1, electrospinning results in the formation of a loop of polymer solution which eventually deposits on the collector. Solvent may not completely evaporate on the way to the collector, and this looping may allow for solvent in one area of the collector to quickly evaporate while polymer is deposited in another area of the collector. Rastering may thus prevent this dispersal of deposition from happening and overlay still-drying polymer fibers with new polymer to then redissolve in the solvent, resulting in the structure seen in Figure 30. This structure has a much lesser degree of porosity and surface area than that seen in Figure 29, and is thus not advantageous for further use.

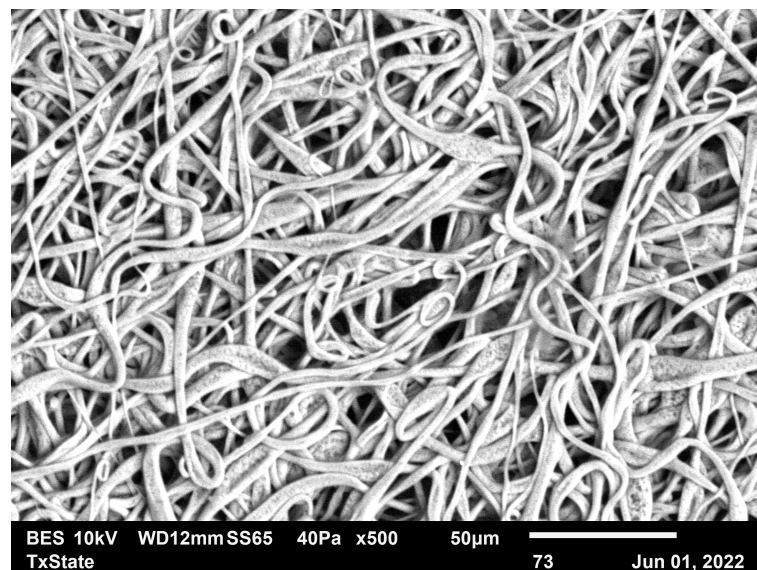


Figure 29. Electrospun PCL without rastering

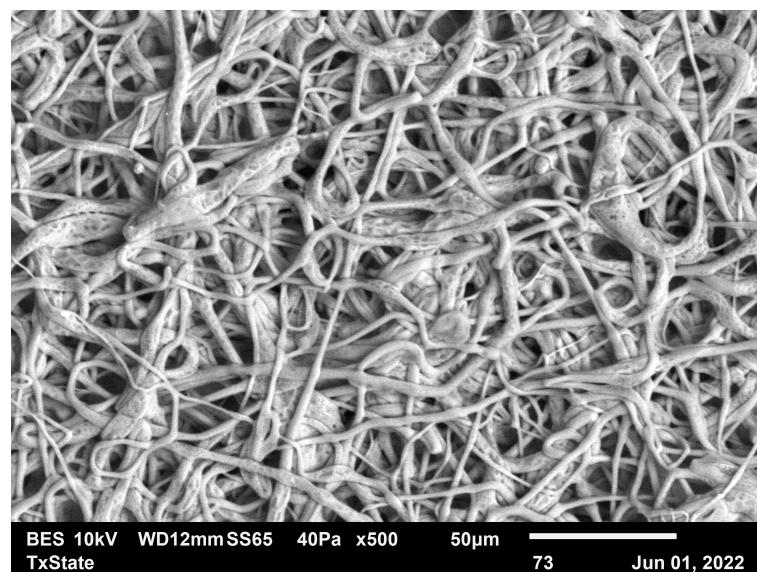


Figure 30. Electrospun PCL with rastering

2.3.3 Effect of collector speed

Figure 31 and Figure 32 show the same polymer, PCL, electrospun using the same solution and process parameters except for the speed of the collector. It can be observed that the speed of the collector is directly related to the degree of alignment of the nanofibers produced. PCL electrospun with collector set to 80 rpm shows randomly

oriented fibers (Figure 31), while PCL electrospun with the collector set to 4000 rpm, shows fibers with a general alignment in the x axis (Figure 32). This alignment, however, is not perfect, as there are some fibers which do align in other directions. This is not necessarily a negative, as this prevents the easy disassembly of the polymer nanofibers by pulling perpendicular to the direction of alignment.

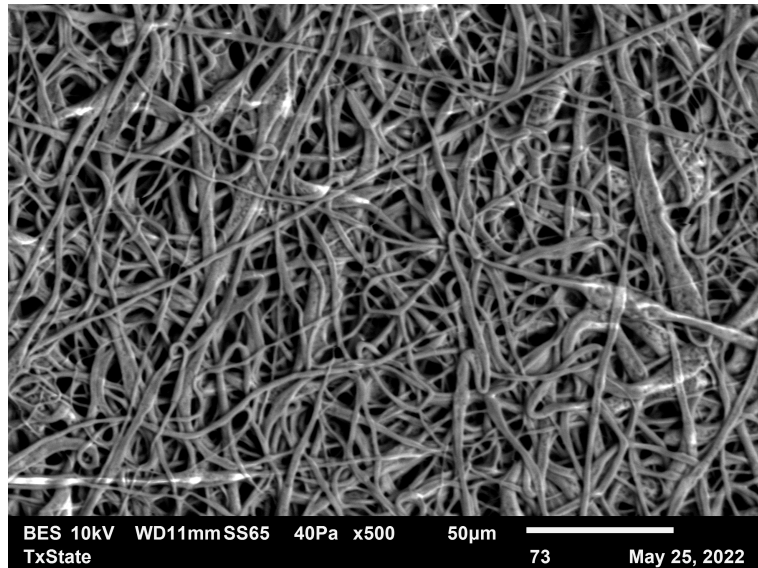


Figure 31. Electrospun PCL with rotating drum collector set to 80 rpm

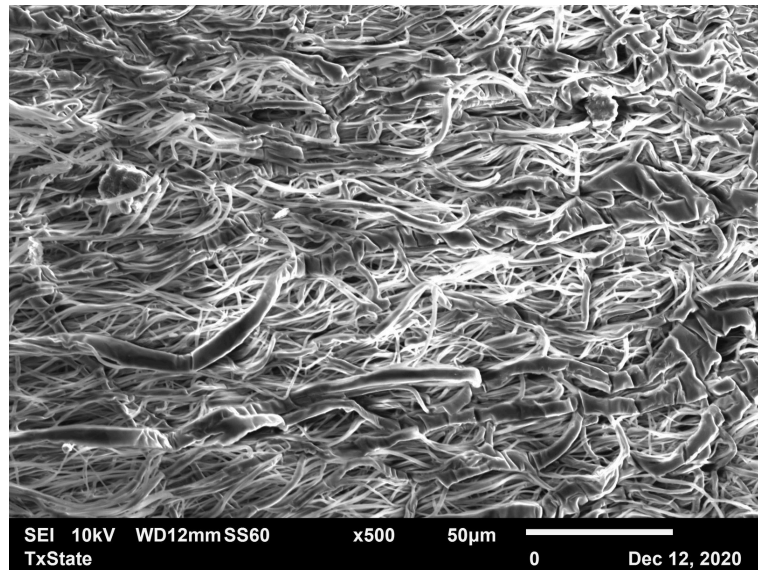


Figure 32. Electrospun PCL with rotating drum collector set to 4000 rpm

Interestingly, Figure 23 shows PMMA that has also been electrospun with the rotating drum collector set to 4000 rpm. The fibers of PMMA can be observed to be much more highly aligned than the aligned fibers of PCL. This may be because PMMA, with a structure shown in Figure 7, only has a flexible hydrocarbon polymer backbone (its carbonyl group is pendant to the backbone), while PCL, with a structure shown in Figure 3, has a backbone containing a stiffening carbonyl group. Flexible polymer chains may be more affected by both the electric field and instabilities in the electrospinning setup and the drawing forces exerted by the rotating drum mandrel to produce more uniform, more highly aligned fibers. However, aligned electrospun PMMA is not a very stable material, and comes apart easily even with careful handling.

2.4 Conclusions and Future Work

This chapter outlines the theory behind electrospinning and demonstrates that it is a viable method to produce nano-to-microfibers of PCL, PAN, PVC, PMMA, and even PAN grafted with ethanolamine. Rastering during electrospinning results in structures which have films of non-fibrous polymer and so must be avoided to prevent reduction in porosity and surface area in the product. Having a rotating drum mandrel as a collector and increasing its speed results in alignment in nanofibers, which may be advantageous for specialized applications such as tissue scaffolds. Future work must be done to optimize the solution and process parameters for the electrospinning of PAN and PVC to result in fibers which are free of beading and films. The effect of hydrogen bonding between the polymer and the solvent on fiber formation must be investigated. Additionally, the effect of polymer backbone structure and molecular weight on their electrospun structure can be explored in the future.

3 COATING ELECTROSPUN POLYMERS WITH INHERENTLY CONDUCTING POLYMERS

3.1 Introduction

3.1.1 Inherently Conducting Polymers

Inherently Conducting Polymers (ICPs), as their name implies, are polymers which are conductive without the addition of conductive fillers such as copper or carbon. The inherent conductivity results from the presence of extended conjugation along the polymer backbone, which allows for the delocalization of electrons. This also results in other properties like low-energy optical transitions, low ionization potentials, and high electron affinity⁷⁰. ICPs are not the only conducting polymers, but these materials are distinguished from filled polymers, which are insulating polymers loaded with conductive material, ionically conducting polymers, which are polyelectrolytes carrying charged or ionizable carriers along their length, and charge transfer materials, which contain polymers with charge transfer groups and oxidants²³. ICPs include polyacetylene, polythiophene (PT), polypyrrole (PPy), polyfuran, polyphenylene (PPP), poly(phenylene vinylene) (PPV), and polyaniline (PANI), and their derivatives (Figure 33). Polythiophenes, polypyrroles, and polyfurans can be further categorized as polyheterocycles due to the presence of a heteroatom in the ring.

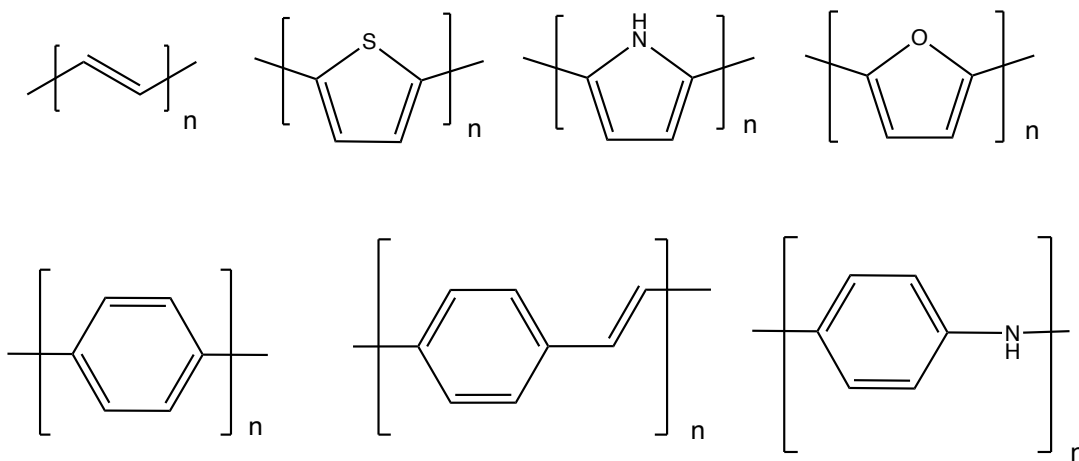


Figure 33. Inherently conducting polymers. (left to right, up to down) polyacetylene, polythiophene (PT), polypyrrole (PPy), polyfuran, polyphenylene (PPP), poly(phenylene vinylene) (PPV), and polyaniline (PANI)

The conductivity of ICPs is due to their unique electronic structure, which can be explained using energy band theory. In the energy band theory, the conduction band is the energy level electrons must be in to travel freely in a material. This is distinct from the valence band, which is the energy level of valence electrons present in a bulk material. In metals, the valence band overlaps the conduction band, and the valence electrons are free to move. In insulators and semiconductors, the valence and conduction bands are separated by an energy gap known as the band gap (E_g). Band gaps of semiconductors are much smaller than those of insulators, so that the energy needed to promote electrons from the valence band to the conduction band is relatively small. The conjugation present in ICPs results in a significantly low E_g in the bulk material. In ICPs, as in semiconductors, the E_g is small and allows for an easy promotion of electrons to the conducting band. This not only allows for current to be conducted in the form of electrons in the conducting band, but also allows for the transport of the positively-charged “holes” left behind in the valence band⁷¹. In ICPs, this is done by raising the energy of the highest occupied molecular orbital (HOMO) of the polymer. This results in

an easier promotion of electrons from the p to the p* orbitals, and thus an easier promotion of electrons from the valence to the conducting bands. Another consequence of this is the lowering of oxidation potentials for polymers with extended conjugation, due to the higher energy of the HOMO and increased resonance stabilization of the resultant radical after oxidation²³.

Increasing the electron density of ICP monomers lowers their oxidation potential. This oxidation potential is important, as it is inversely related to the ease of oxidatively polymerizing a monomer and the probability of side reactions and defects happening. For this reason, the most used PT is PEDOT, which adds a cyclic alkoxy substituent to the thiophene ring. This alkoxy substituent adds electron density to the thiophene ring and lowers its oxidation potential.

In their neutral form, as shown in Figure 33, ICPs are insulating. It is when they are doped that ICPs exhibit their unique electrical properties. In doping, the ICP is either oxidized (called p-doping) and provided with a counter anion, or reduced (called n-doping), providing a counter cation, usually the dopant counter ion⁷². This doping can be achieved using small molecules like chloride salts, or even polymers like poly(styrene sulfonate) (PSS). While small molecule dopants can eventually leach out of the ICP matrix and result in a decrease in the conductivity of ICPs over time, in polymer dopants, the doping species is more stably integrated in the ICP. Doping can occur either by oxidation or reduction: in oxidation, electrons are extracted by the dopant from the HOMO of the valence band of the ICP, and the aforementioned “holes” are created in the polymer backbone; in reduction, electrons are transferred from the dopant to the lowest unoccupied molecular orbital (LUMO) of the conduction band of the ICP⁷¹. Oxidation is

also called p-type doping, and reduction is also called n-type doping. In general, p-type doping results in stable forms of ICPs and are more widely studied.

In the process, the dopants introduce charge carriers into the polymer chain: polarons, which are radical single ions; bipolarons, which are dicitrons or dianions; and/or solitons. Polarons and bipolarons are the charge carriers in ICPs such as PPy and PT, and solitons are the charge carriers in polyacetylene. The formation of polarons is favored by the resonance stabilization of the radical ion over several rings. The formation of bipolarons can be stabilized by the extension of the rings present in a polymer backbone to enforce charge separation for otherwise repelling species. These species can interconvert, as shown in Figure 34²³.

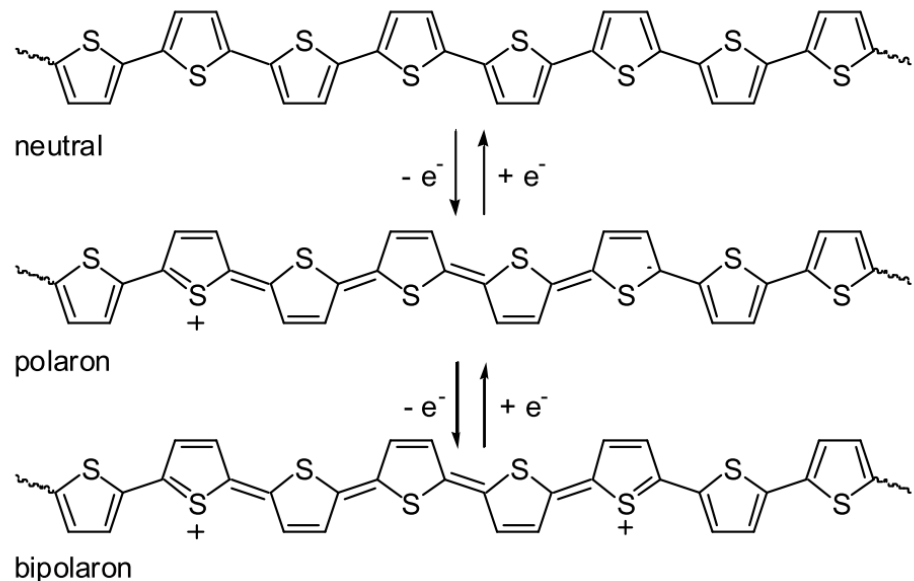
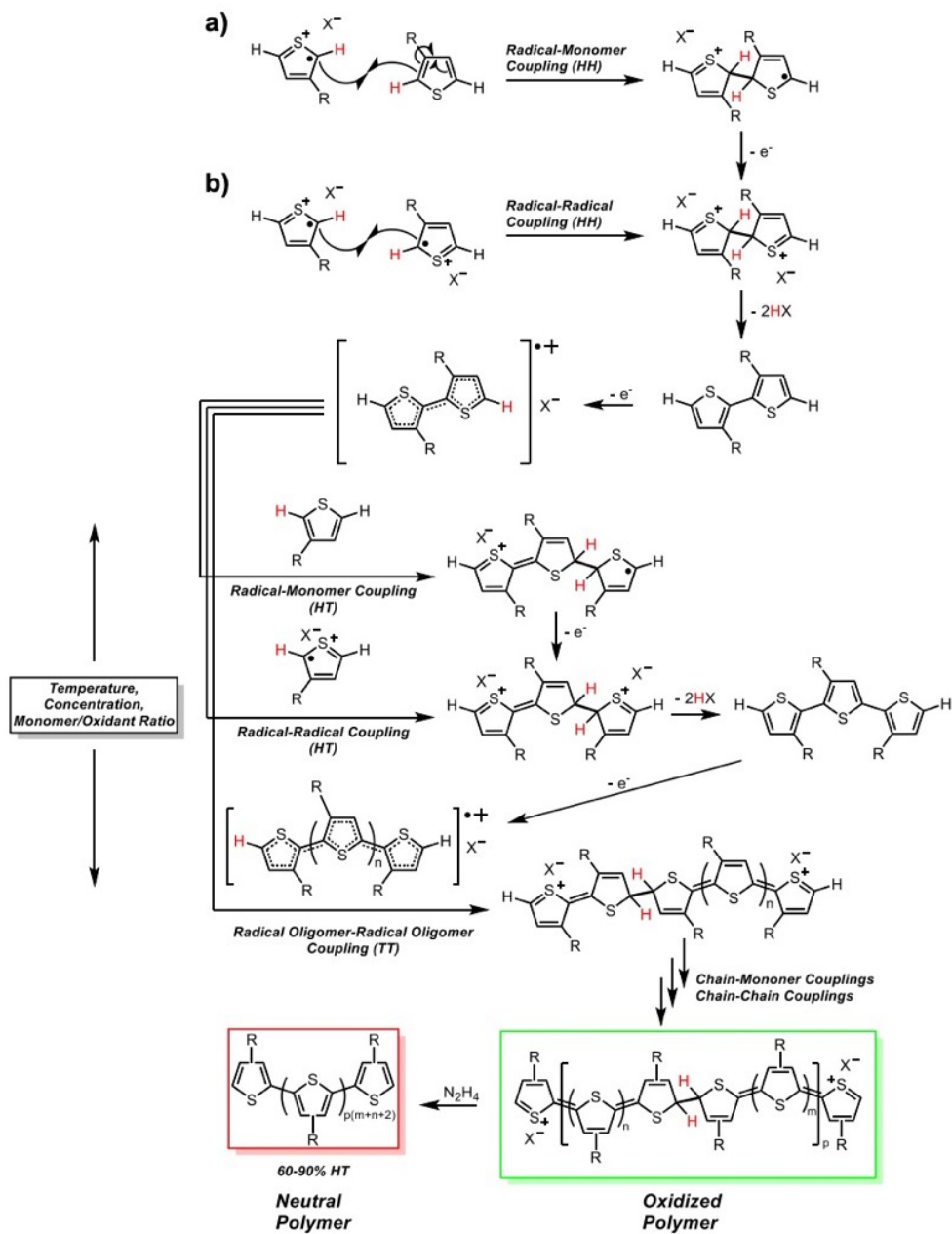


Figure 34. Neutral, polaron, and bipolaron forms of polythiophene. Adapted with permission from ref. 23. Copyright 2003 John Wiley and Sons.

These charge carriers are attracted to the nuclei of atoms in neighboring monomeric units, either in the same or different polymer chain. The movement of charge carriers along the polymer backbone is facilitated by the delocalization offered by conjugation in ICPs. A side consequence of doping is a change in the volume of the polymer, as the polymer adopts conformations to maintain the charge neutrality⁷³.

ICPs of the polyheterocyclic type can be synthesized by oxidative polymerization from their respective monomeric units. Scheme 2 shows the mechanism for the oxidative polymerization of polypyrrole⁷⁴, but this mechanism can be generalized to the polymerization of any polyheterocycle. The initiation step is the oxidation of monomers to form cation radicals. This step is favorable due to the resonance stabilization of the cation radical. The propagation step consists of coupling these cation radicals. This coupling can occur between two radical cations to form dications, or between a radical cation and a monomer, which then loses an electron to form the dication²³. This step occurs with deprotonation. The dications are further reoxidized, and they couple with other radical cations. The termination step consists of nucleophilic attack of the propagating chains by water or impurities. Scheme 2 shows α - α coupling between polyheterocycle units. α - α coupling is favored because the protons in the α position of the heterocycle are more readily eliminated. Polyheterocycle coupling via α - β coupling also occurs, which leads to branching and crosslinking in the polymer. This results in a non-linear and non-planar chain. This is one reason for the insolubility of polyheterocycles in many common solvents.



*Scheme 2. Proposed mechanism for the chemical oxidative polymerization of pyrrole.
From ref. 75.*

This α - β coupling can be circumvented if the β positions are blocked from reacting, as in the case of EDOT, the monomer of PEDOT. The ethylenedioxy bridge in EDOT prevents the 3- and 4- positions of the thiophene ring from coupling. This is another reason why PEDOT is more commonly used than PT. Importantly, oxidatively polymerizing heterocycles results in the synthesis of ICPs in the conductive state, accomplishing both polymerization and doping at the same time⁷³.

There are two main methods of accomplishing oxidative polymerization: electrochemical and chemical oxidative polymerization. In electrochemical oxidative polymerization, thin, free-standing, homogeneous, and self-doped films can be produced at room temperature⁷⁰. Current passing through a monomer dissolved in an electrolyte solution oxidizes it, and insoluble polymer is deposited on the surface of a working electrode⁷². This current can either be constant, have constant potential, or be employed in a potential scanning method⁷⁰, with the oxidation potential of the monomer being a factor in the selection of the potential of the current⁷³. A disadvantage of this method of polymerization is that the insoluble ICP film on the surface of the electrode is difficult to remove⁷²; thus, the electrode to be used in electrochemical polymerization must be the device to which the ICP is used with. Chemical oxidative polymerization overcomes this disadvantage, as it produces powder or very thick films of polymer. In chemical oxidative polymerization, monomers are treated with transition metal oxidants such as ferric salts (e.g. FeCl_3) and copper salts, or other oxidants such as AsF_5 , I_2 , or O_2 ²³.

3.1.2 Properties and applications of ICPs in biomedicine

ICPs couple the strength of polymer design versatility with a unique electronic structure. Because of this, they have the ability of having tunable electrical, optical, magnetic, wettability, and mechanical properties⁷⁶. The primary advantage offered by ICPs is their tunable conductivity coupled with material softness. The optical absorption characteristics can be tuned by designing ICP monomers to tune electron density in the heterocycle and varying the delocalization of charges through altering the doping level. ICPs can also provide a medium for the absorption and conduction of photo-generated carriers. Because structure-property relationships can be established by tuning the ICP molecules and observing effects, information on charge-carrying species and unpaired spins can be obtained in composites of ICPs and magnetic particles, and hydrophilicity can be tuned to selectively adhere particles onto the surfaces of ICPs, or vice versa. The thermal conductivity of ICPs, being polymeric materials, are generally low⁷⁷. However, the mechanical properties of ICPs are poor²³.

Because of these properties, ICPs have seen applications in many fields. Some ICPs are biocompatible and can be processed into flexible devices, and they have consequently been used in biomedical applications. PANI, PPy, and PEDOT have been used in engineering tissue scaffolds whose functions are enhanced by conductivity, such as neural, cardiac, muscular, and skeletal tissue⁷². ICPs have been observed to be suitable matrices for biomolecules and have thus been used as biosensors for the detection and monitoring of drugs, nucleic acids, enzymes, and metabolites⁷⁸, whether *in vitro* or *in vivo*⁷⁹. ICPs processed into nanomaterials have also been used in flexible electronics and supercapacitors⁷⁴.

3.1.3 ICP nanofibers

If ICPs are processed into nanofibers, then this would couple the unique properties outlined above with the high surface area, porosity, and improvement in mechanical properties associated with a nanofibrous structure. For example, this would enhance the applications of ICPs described above. Electrospun ICP tissue scaffolds would have more surface for cells to grow on and align for more efficient conduction of charge. Nanofibrous ICP-based sensors would have more area available for the immobilization of biomolecules and allow for more sensitive detection. Electrospun ICP electronics and supercapacitors would have a greater area available for the storage of charge and would improve the mechanical performance of these devices.

However, unfunctionalized polyheterocyclic ICPs synthesized via chemical oxidative polymerization are difficult to electrospin. This is because they are insoluble in organic solvents, which is required for electrospinning, and they are low-molecular weight, rigid rod polymers with insufficient chain entanglement to form fibers during electrospinning⁸⁰. This insolubility is a consequence of branching and crosslinking because of side reaction α - β couplings in oxidative polymerization. Furthermore, since the ICPs polymerized through this method are synthesized in their oxidized state, with stiffening double bonds between units, free rotation and solvation is very difficult. Oxidatively-polymerized ICPs have low molecular weights due to differences in solubility between the monomer, oxidant, and the growing polymer chains⁸¹. This low molecular weight, coupled with the fact that the polymer backbone of ICPs is a rigid chain made up of stiffening groups that limit chain rotation and flexibility, results in a low chain entanglement⁵⁷, which results in rheological properties unfavorable for

electrospinning. This limitation can be overcome chemically by adding species which increase the chain entanglements in solution, such as in the case of a device made up of PEDOT:PSS which was successfully electrospun with the addition of Mg(NO₃)₂ which acted as a physical crosslinker, to physically entangle the ICP⁸². PANI, a non-polyheterocyclic ICP, has also been successfully electrospun into nanofibers, although this is because the synthesis of PANI proceeds by an acid-base oxidative polymerization mechanism⁸³.

The insolubility and low molecular weights of ICPs do not satisfy the criteria put forth for electrospinning, as stated by Xue et al. in the previous chapter⁴¹, and subjecting conducting polymers to electrospinning by themselves lead to electrospraying. Thus, for example, in an electrospun composite of PCL, collagen, and PPy for neural scaffolds, PPy had to be electrosprayed onto electrospun PCL⁸⁴. Thus, any attempt to process ICPs into nanofibers must address both criteria, or it must proceed to incorporating them into electrospinnable polymers.

Thus, the incorporation of ICPs into electrospun nanofibers has taken the form of either coaxial electrospinning, co-electrospinning with carrier polymers, or coating electrospun nanofibers with ICPs. In coaxial electrospinning, two polymer solutions are electrospun from two concentric nozzles, one inside the other⁸⁵. This forms core-sheath polymer nanofibers, with ICPs being either, and an electrospinnable polymer being the complementary structure. Nanofibers of PANI have been prepared using this method, incorporating PMMA as the sheath⁸⁶. In co-electrospinning with carrier polymers, ICPs are blended into solutions of electrospinnable polymer, and the mixture is spun into nanofibers. This method was used in the fabrication of a composite of poly(3-

hexylthiophene) (P3HT) with PCL⁸⁷. While both methods have resulted in the processing of ICPs into nanofibrous structures, they do result in the lowering of the conductivity of the ICP when compared to ICPs processed into films. This is a surprising result, as nanofibrous structures have more surface area and conduction paths necessary for the transport of charge across a material⁴⁸, which should enhance the conductivity of the material, as has been explained. This is due to the insulating electrospinnable polymer disrupting conduction paths in the material.

Thus, coating electrospun polymers with ICPs would be the ideal way of processing them into nanofibers, while a way to electrospin ICPs by themselves remains to be discovered. This can come in two forms: simply dip-coating polymer nanofibers with ICPs, or *in situ* polymerizing the ICP on the surface of the polymer nanofibers. This former method has been used in coating electrospun polyurethane fibers with PEDOT:PSS dissolved in DMSO and a surfactant⁸⁸. The latter was used in the coating of electrospun cellulose acetate with 3-hexylthiophene and N-vinylpyrrole polymerized on its surface⁸⁹. Dip-coating, although facile, may not be suitable for ICPs which cannot be dissolved in any organic solvent, such as PPy. For this reason, it may be more advantageous to do *in situ* polymerization on the electrospun polymer surfaces.

To satisfy the requirements of percolation theory and retain and enhance the conductivity of the coated ICP, the substrate electrospun polymer must be coated with *in situ* polymerized ICP conformally, without any interruption in the conducting material. *In situ* chemical oxidative polymerization of ICPs on polymer surfaces tends to take the form of adding the electrospun polymer to solutions of either ICP monomer or oxidant, and then adding the opposite to the bulk of the reaction mixture. Thus, the whole of the

solution is polymerized, and some of the ICP adheres to the polymer nanofibers. As a result, the morphology of these composites tends to be clusters of ICP on the surface of the electrospun polymer. While this accomplishes coating, it is uneven, and it results in low conductivities, as mentioned in section 1.4. It may prove useful to have the morphology of the resultant composite to resemble wires instead, to provide clear, delineated conducting paths for charge carriers to follow. To achieve this, pre-treatment of the electrospun polymer in either ICP monomer or oxidant might prove useful. This would enable the adsorption of either the monomer or oxidant onto the surface of the electrospun polymer and take advantage of the high surface area and porosity of the nanofibers. Polymerization would then be on the electrospun polymer alone and would hypothetically more closely follow the morphology of the substrate electrospun polymer, as this prevents the formation of clusters of ICPs, which would lower the surface area of electrospun fibers available.

3.1.4 Applications of nanofibrous ICPs

Because of their unique properties enumerated above, nanofibrous ICPs have seen applications in the fields of biological materials, electronic materials, and sensors.

In the field of biological materials, nanofibrous ICPs have seen use in wound healing and tissue scaffolds, for the biological processes which are enhanced by the application of a current. PT and PPy deposition onto nanofibrous PCL was observed to enhance the growth of human dermal fibroblasts⁹⁰. A tissue scaffold composed of highly-aligned electrospun poly(lactic-co-glycolic acid) coated with PPy has been observed to effectively grow and stimulate nerves⁸⁹ because the aligned morphology of the nanofibers

allows the oriented growth of nerves, and electrical stimulation allows the mimicking of the native electrophysiological environment of neurons²².

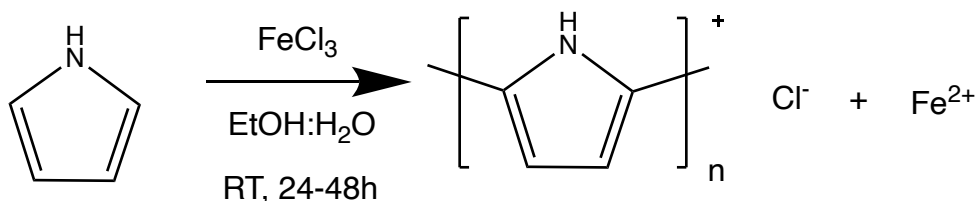
In the field of electronic materials, the softness and enhanced charge transport in nanofibrous ICPs have lent them use in photovoltaics, capacitors, and electronic devices. A device composed of layers of PEDOT:PSS and PPV on electrospun TiO₂ has been successfully fabricated as a hybrid solar cell, and observed to have a high power conversion efficiency and charge conduction capacity⁹¹. PEDOT was coated onto electrospun poly(vinyl alcohol) and graphene oxide and the resultant device was used as a capacitor, which was reported to have a high energy and power density⁹³. An LED has been fabricated from polyfluorene coated onto an electrospun blend of poly(ethylene oxide) and PPV⁹².

The increased surface area of nanofibrous ICPs has made them ideal for use in the highly sensitive detection of analytes in the gas phase and in solution. These analytes can either bind to, interact with, or even oxidize/reduce the ICP layer in these devices. PANI mixed with electrospun Pd:SnO₂ and poly(3-hydroxybutyrate) has been used in the low-temperature sensing of ethanol gas⁹³. PT was incorporated into electrospun PAN and used to detect phosphate anions⁹⁴.

As can be inferred, the successful processing of ICPs into a nanofibrous structure is an enabling technology for the manufacture of composites for many different applications.

3.1.5 Scope and limitations of this Study

This study focuses on the processing of ICPs into a nanofibrous structure. Specifically, it looks at ways to coat electrospun PCL with PPy via *in situ* chemical oxidative polymerization (Equation 6).



Equation 6. Chemical oxidative polymerization of pyrrole

The effect of different methods of coating, specifically, dip coating, and dip coating with different methods of pre-treatment are explored, and the relationship between these methods and the resultant microstructure of the produced composites are looked at. The adhesion of the PPy coating on PCL is also determined via tape test.

3.2 Materials and Methods

3.2.1 Materials

PCL was electrospun as described in Chapter 2. Reagent grade Py, 98% were obtained from Sigma-Aldrich. Anhydrous FeCl_3 , 98% was obtained from Thermo Scientific. For chemical oxidative polymerization, 10 mL BD Luer-LokTM syringes were used.

3.2.2 Instrumentation

For material characterization, analysis was done using a JEOL JSM-6010 PLUS/LA Scanning Electron Microscope in the Shared Research Operations facility at the Texas State University. ATR-IR analysis was done using a Bruker Tensor II FT-IR Spectrometer with a Harrick SplitPea™ Attenuated Total Reflectance accessory in the Department of Chemistry and Biochemistry at the Texas State University.

3.2.3 Polypyrrole coating on electrospun PCL without pre-treatment

In a 20 mL vial, electrospun PCL cut into 1 cm x 1 cm squares was suspended in a 10 mL solution of 2% (w/v) Py monomer in 3:7 (v:v) ethanol:deionized water (EtOH:H₂O). In another container, a 10 mL solution of 1M FeCl₃ oxidant was prepared in the same solvent. This was then transferred to a syringe. The oxidant solution was added dropwise to the monomer solution at room temperature under argon and left to react for an hour, as shown in Figure 35.

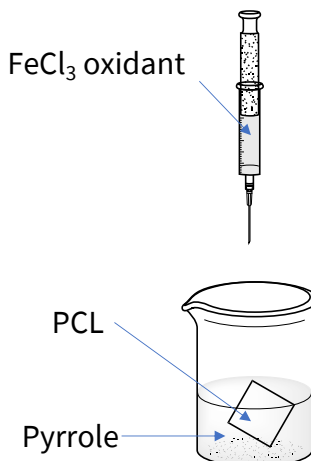


Figure 35. Coating of PPy on PCL without pre-treatment

Afterwards, PPy-coated PCL squares were filtered out of suspension and washed extensively with EtOH until no more PPy was observed being washed away. These were then allowed to air dry for 1 day and stored in vials until further use.

3.2.4 Polypyrrole coating on electrospun PCL with pre-treatment

1 cm x 1 cm squares of PCL were added to 10 mL solutions of either 2% Py or 1M FeCl₃ with stirring for 1h at room temperature. Afterwards, the PCL squares were taken out of suspension, blotted onto paper towels, and then added to 10 mL solutions of 1M FeCl₃ or 2% pyrrole, respectively. These were allowed to stir at room temperature for 24-48 hours, until the squares showed blackening indicating the presence of PPy (Figure 36).

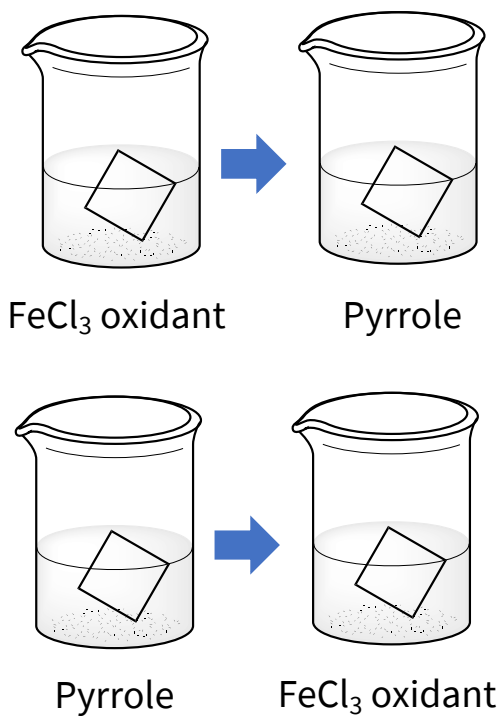


Figure 36. Coating of PCL with PPy with pre-treatment. (Top) Oxidant pre-treatment
(Bottom) Monomer pre-treatment

Afterwards, the PPy-coated PCL squares were removed from suspension and washed extensively with EtOH. These were then allowed to air dry for 1 day and stored in vials until further use.

3.2.5 Tape test

1 in x 1 in PCL squares were coated with PPy with oxidant pre-treatment following the procedure outlined above. Afterwards, these were air dried for 1 day and subjected to the ASTM D3359-17 Standard Test Methods for Rating Adhesion by Tape Test, using Test Method A. The PCL-PPy squares were placed on a flat surface. Two 20 mm incisions were then made to the surface of the squares, forming an X. 2-in Scotch tape was then applied to the X incision, and flattened with an eraser tip of a pencil. After 90 seconds, the Scotch tape was peeled off in a controlled, non-jerked manner, with care taken to keep the angle of peeling as close to 180° as possible. The 1 in x 1 in PCL-PPy squares were then qualitatively examined for peeling.

3.2.6 ATR-IR analysis

1 cm x 1 cm squares of PCL-PPy were analyzed with ATR-IR with no further modification.

3.2.7 SEM-EDX analysis

PPy-coated PCL squares were then analyzed under low vacuum conditions in an SEM without further modification.

3.3 Results and Discussion

It was observed that although Py polymerizes in water, electrospun PCL 1 cm x 1 cm squares do not sink into the bulk of the solution without significant agitation. Not only does this not accomplish a uniform coating of PPy on the surface of electrospun PCL, but agitation would also result in the breakage of PCL fibers. Since PCL sinks in alcohols, an attempt was made to determine the optimal alcohol solvent. Interestingly, Py does not polymerize in absolute EtOH, methanol, or isopropyl alcohol. This may be due

to alcohols being radical scavengers, and thus unsuitable for the chemical oxidative polymerization of Py. Indeed, studies have demonstrated the hydroxyl and hydrogen radical scavenging properties of aliphatic alcohols^{95,96}. Thus, it was decided to have a mix of EtOH and water as the solvent for the *in situ* chemical oxidative polymerization of PPy, with the ratio of 3:7 EtOH:H₂O by volume as the optimal ratio for allowing Py polymerization and electrospun PCL sinking into the solvent. The optimal concentrations of FeCl₃ and PPy in this solvent were also determined. It was furthermore found out that in this solvent, FeCl₃ concentrations above 1M make electrospun PCL squares brittle and Py concentrations above 2% dissolve PCL. These are possibly due to the relative acidity of FeCl₃, which hydrolyzes the ester bonds in PCL, and the possibility of strong hydrogen bonding between the N-H hydrogens in Py and the C=O oxygens in PCL. It was thus decided to use these concentrations as the upper limit for the experiments.

Additionally, it was observed that uniform coating of PPy is facile in 1 cm x 1 cm squares of electrospun PCL and gets more difficult as the size of the PCL squares get larger. This may be because larger nanofiber mats have a greater tendency to fold and stick to each other during the *in situ* polymerization and prevent equal access by the solvent and reagents to the surfaces. This is the reason for conducting all coating experiments with 1 cm x 1 cm electrospun PCL squares except for the tape test, which was difficult to do with 1 cm x 1 cm squares.

3.3.1 No pre-treatment

Figure 37 shows the result of coating PCL with PPy without pre-treatment. As can be observed, there are fibers and white-colored clusters in the microstructure of this material.

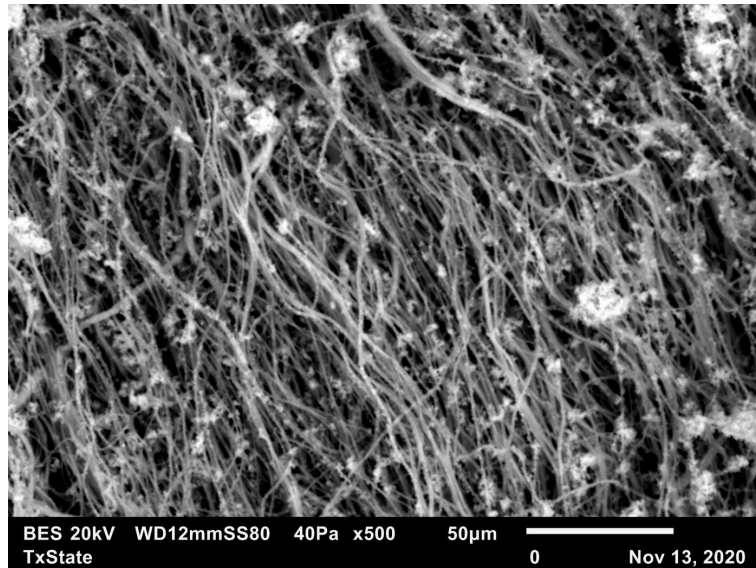


Figure 37. PCL-PPy with no pre-treatment

EDX analysis shows that these are mainly made up of C, N, O, and Cl (Figure 38). The C and O atoms can come from either the PCL (Figure 3) or PPy (Figure 4), but the N atoms can only come from PPy, with the Cl atoms being the counterions of the p-doped PPy formed (Equation 6). It can be observed that the Cl atoms are concentrated on the white-colored clusters, the C and N atoms have been detected on both the fibers and the white-colored clusters, and the O atoms can mostly be detected on the fibers alone. This means that the white-colored clusters are the p-doped PPy, which have also been coated onto the PCL fibers.

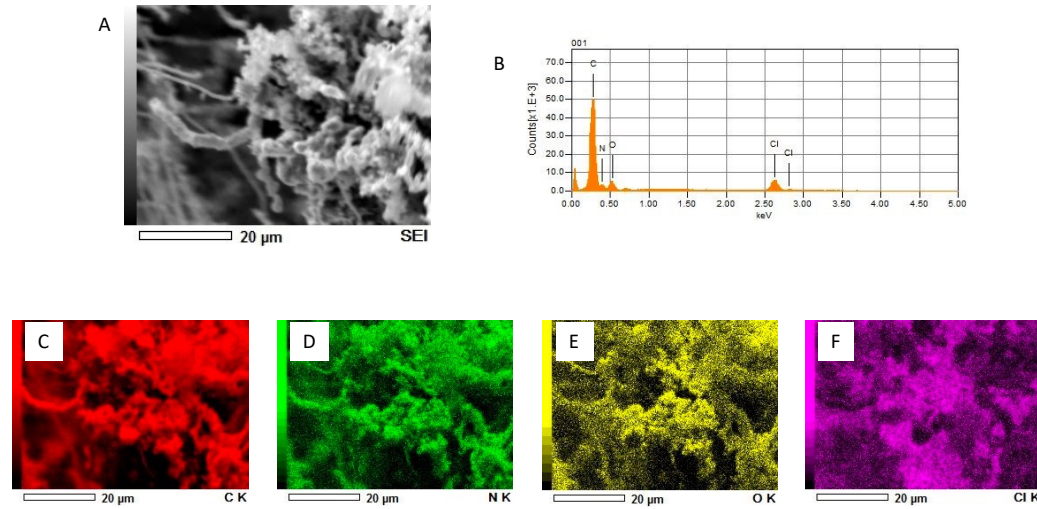


Figure 38. EDX analysis of PCL-PPy with no pre-treatment. (A) SEM micrograph of area where elemental mapping was done (B) Graph of detected atoms in A and their relative abundance (C) Map showing the areas in A where C was detected (D) Map showing the areas in A where N was detected (E) Map showing the areas in A where O was detected (F) Map showing the areas in A where Cl was detected

The ATR-IR spectrum in Figure 39 confirms that PPy has indeed been coated onto PCL. There is a broad absorption centered at around 2710 cm^{-1} , which corresponds to the PPy N-H stretch accounting for a high degree of conjugation. The PCL carbonyl C=O stretch is also retained at 1724 cm^{-1} . PCL-PPy has indeed been fabricated, but the microstructure shows separate domains of PPy-coated PCL and excess clusters of PPy, which, as explained in section 3.1.3, is unfavorable for the conductivity of the ICP.

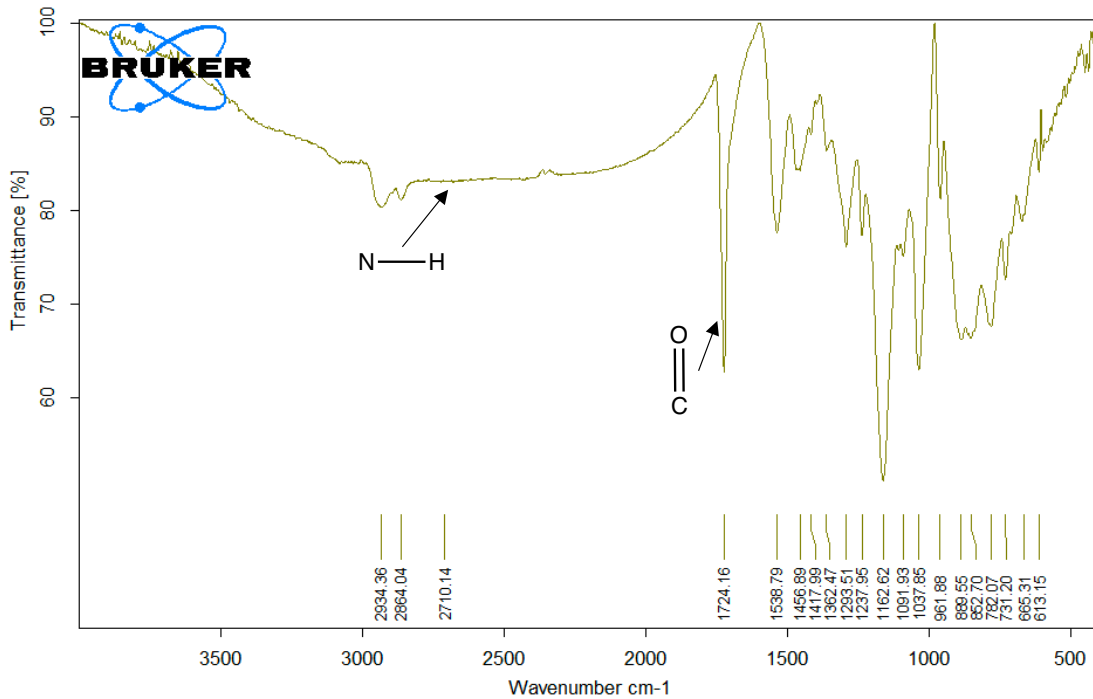


Figure 39. ATR-IR spectrum of PCL-PPy with no pre-treatment

3.3.2 With oxidant pre-treatment

Figure 40 shows the result of *in situ* polymerization of PPy on PCL with oxidant pre-treatment. It can be observed that there are only fibers in the microstructure of this PCL-PPy composite.

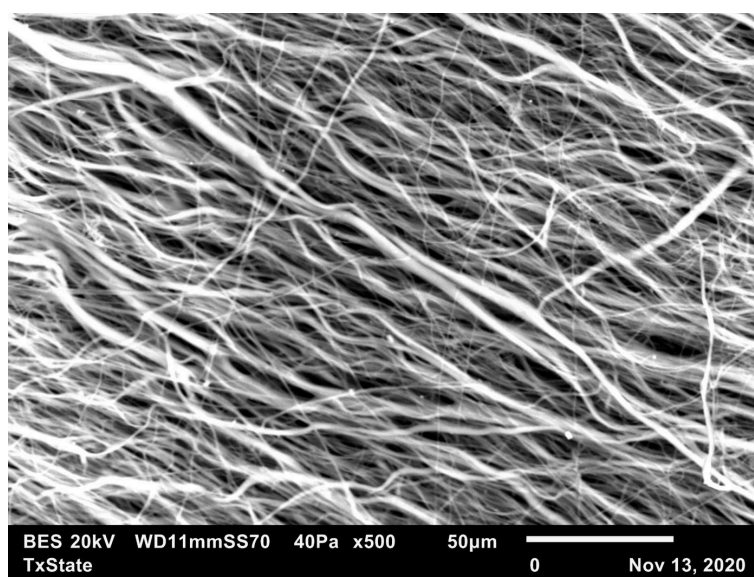


Figure 40. PCL-PPy with oxidant pre-treatment

Figure 41 shows that there are C, N, and O atoms present in these fibers, which, as has been explained earlier, indicates the presence of PPy and PCL, with the PPy completely coating the PCL fibers.

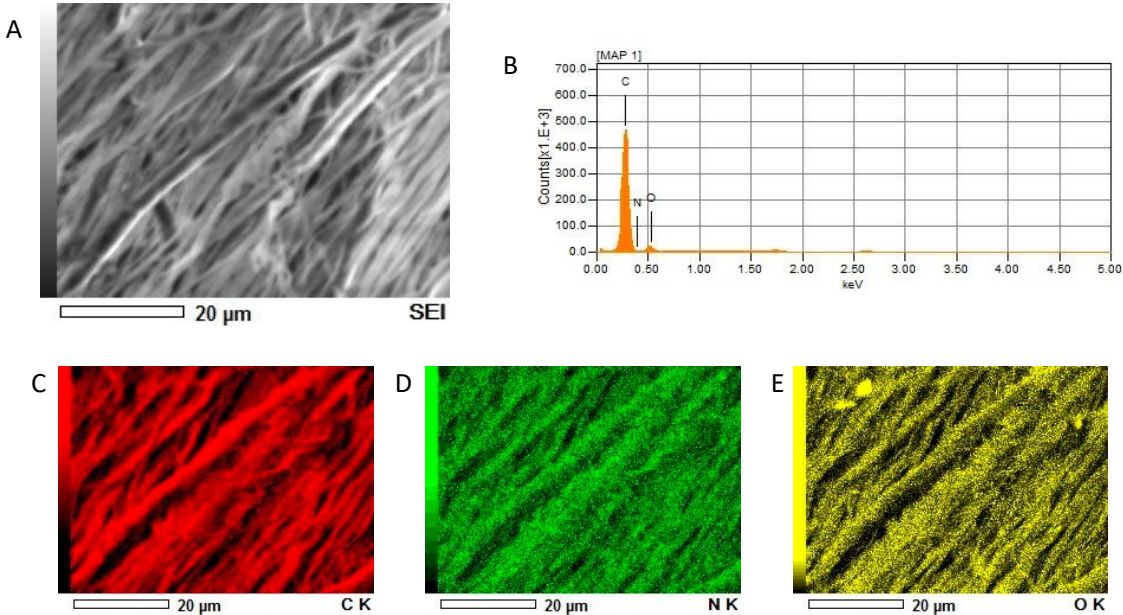


Figure 41. EDX analysis of PPy-coated PCL with oxidant pre-treatment. (A) SEM micrograph of area where elemental mapping was done (B) Graph of detected atoms in A and their relative abundance (C) Map showing the areas in A where C was detected (D) Map showing the areas in A where N was detected (E) Map showing the areas in A where O was detected

Figure 42 verifies this, and again shows the characteristic broad PPy N-H absorption centered at around 3110 cm^{-1} , and the sharp PCL carbonyl C=O stretch at 1723 cm^{-1} . It can be noticed that this sharp absorption is considerably attenuated from the absorption shown in Figure 39. This may be because there is less PPy coated onto the PCL fibers.

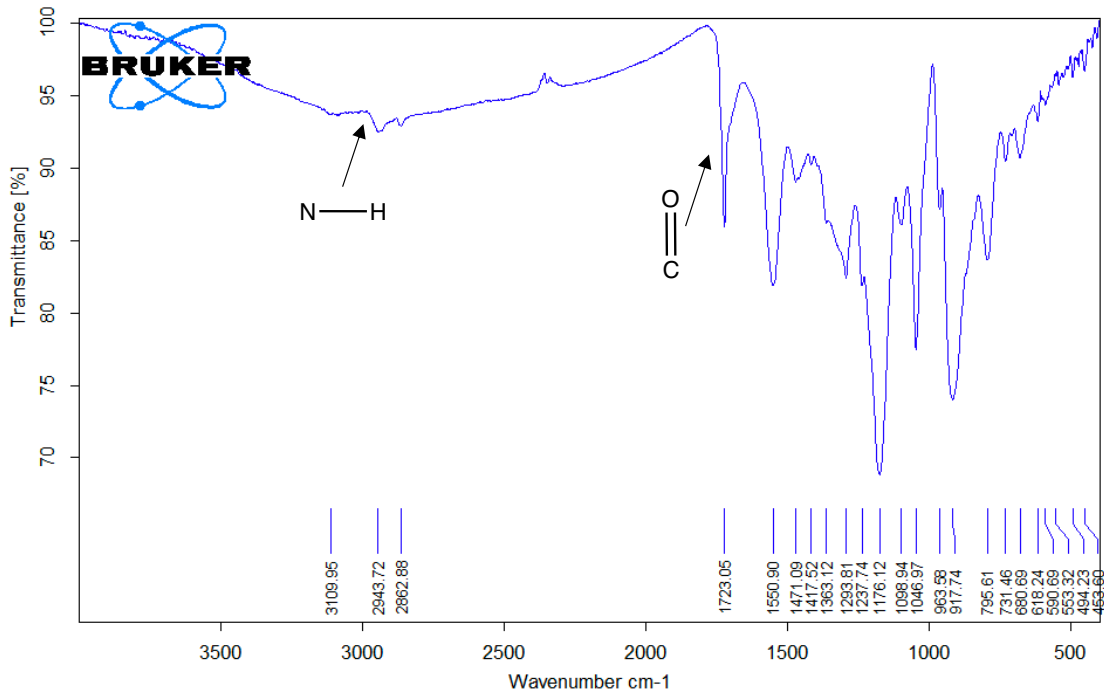


Figure 42. ATR-IR spectrum of PCL-PPy with oxidant pre-treatment

Regardless of this fact, these demonstrate that pre-treatment of electrospun PCL with oxidant before coating with PPy produces a PCL-PPy composite retaining a nanofibrous structure with a conformal coating of PPy, which is advantageous for the retention and possible enhancement of the conductivity of the ICP. This was thus determined to be the best protocol for fabricating PCL-PPy composites, and was used in the tape test, and in the subsequent experiments. The retention of the nanofiber morphology in PPy-coated PCL was interesting, since the same pre-treatment protocol done in our lab by with PEDOT-coated PAN resulted in a microstructure with a beads-on-a-string morphology (Figure 43).

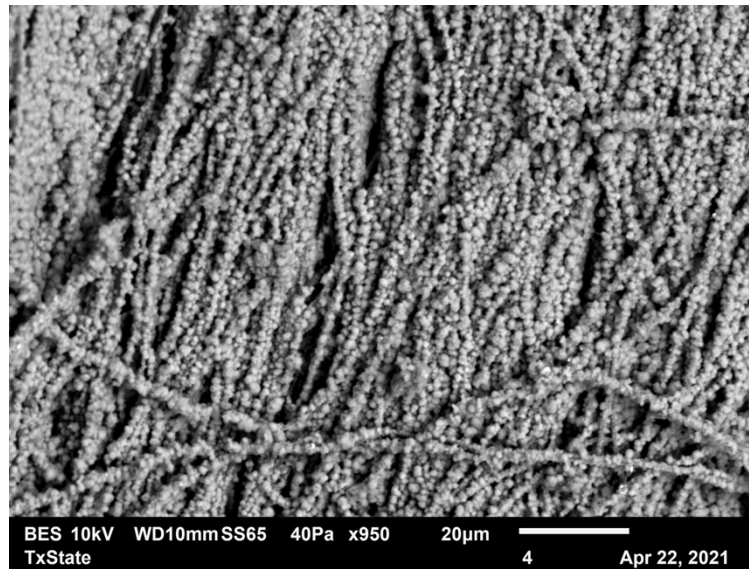


Figure 43. PAN-PEDOT, courtesy of Mariana Ocampo

It is possible that this difference can be explained by the different intermolecular forces of attraction holding the composites together. As mentioned earlier, PPy (Figure 4) contains N-H hydrogens which are capable of strong hydrogen bonding with the C=O and even C-O oxygens of the substrate PCL (Figure 3). On the other hand, PEDOT (Figure 5) does not have any hydrogens capable of hydrogen bonding to the N group in PAN (Figure 7). As a result, this composite is only held together by weaker dipole-dipole interactions, which may result in the microstructure seen in Figure 43.

An attempt was made to measure the conductivity of PCL-PPy using the 4-point probe at the Texas State University Shared Research Operations facility, but the measured conductivities are not reproducible. This may be because this method of making PCL-PPy results in the formation of a thin enough layer of PPy that the 4-point probe is contacting the PCL fibers, not the PPy coating. Further studies must be done in this field.

3.3.3 With monomer pre-treatment

Figure 44 shows that the *in situ* polymerization of PPy on electrospun PCL with monomer pretreatment results in a structure that has both fibers and white-colored clusters.

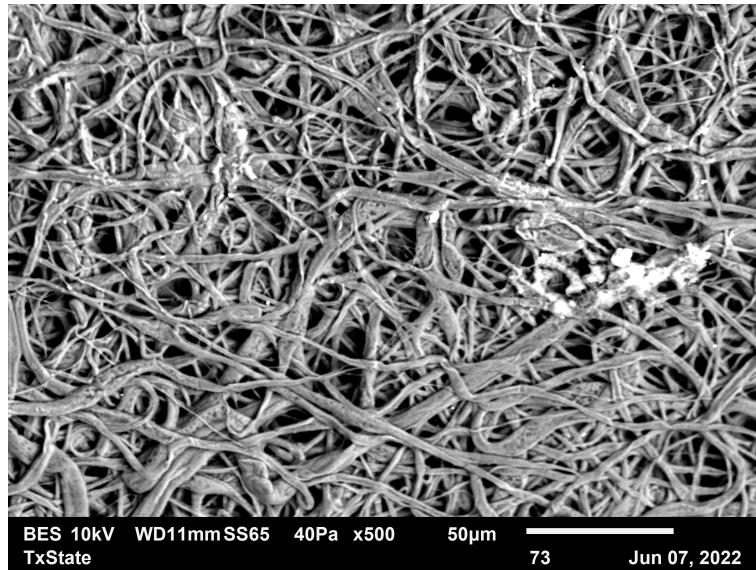


Figure 44. PCL-PPy with monomer pre-treatment

Figure 45 and Figure 46 prove the presence of PPy coating on electrospun PCL, with the presence of N together with C and O, and the faint broad PPy N-H stretch centered at 3524 cm^{-1} , a strong PCL carbonyl C=O stretch at 1732 cm^{-1} , and PPy N-H bends at 1577 and 1542 cm^{-1} . Interestingly, the N-H stretch is not as strong for monomer pre-treated PCL-PPy as it is for un-pre-treated and oxidant pre-treated PCL-PPy, even showing the CO₂ peak at 2350 cm^{-1} that was obscured in their ATR-IR spectra due to the broadness of the N-H stretches. This may be because Figure 44 shows unevenness in the PPy coating, and thus, the area subjected to ATR-IR could have been coated with a thinner layer of PPy.

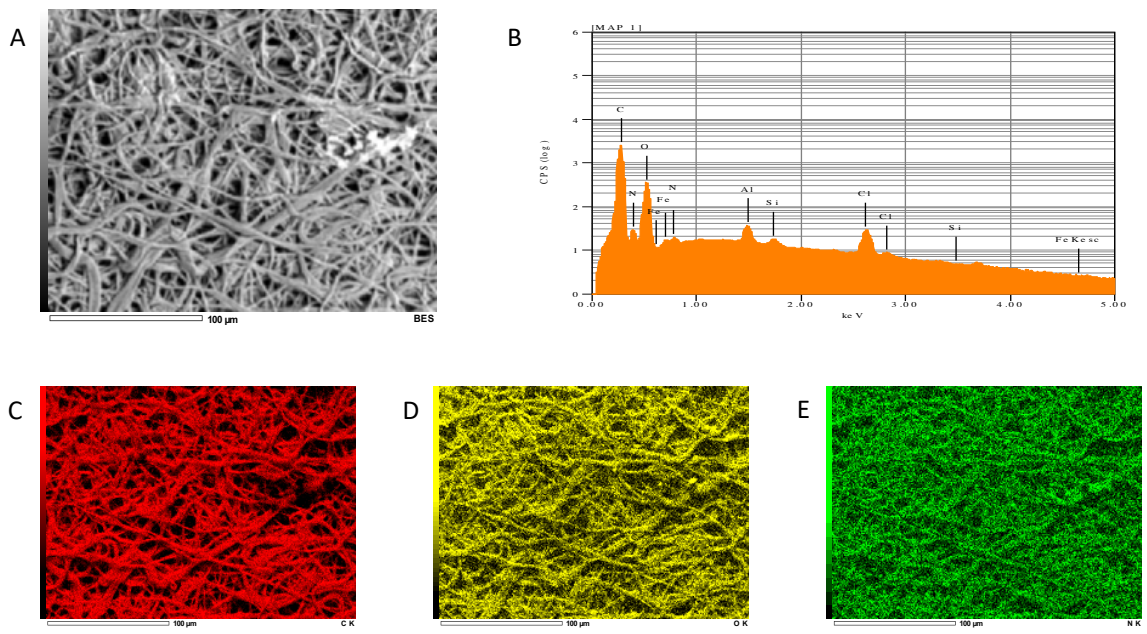


Figure 45. EDX analysis of PCL-PPy with monomer pre-treatment. (A) SEM micrograph of area where elemental mapping was done (B) Graph of detected atoms in A and their relative abundance (C) Map showing the areas in A where C was detected (D) Map showing the areas in A where O was detected (E) Map showing the areas in A where N was detected

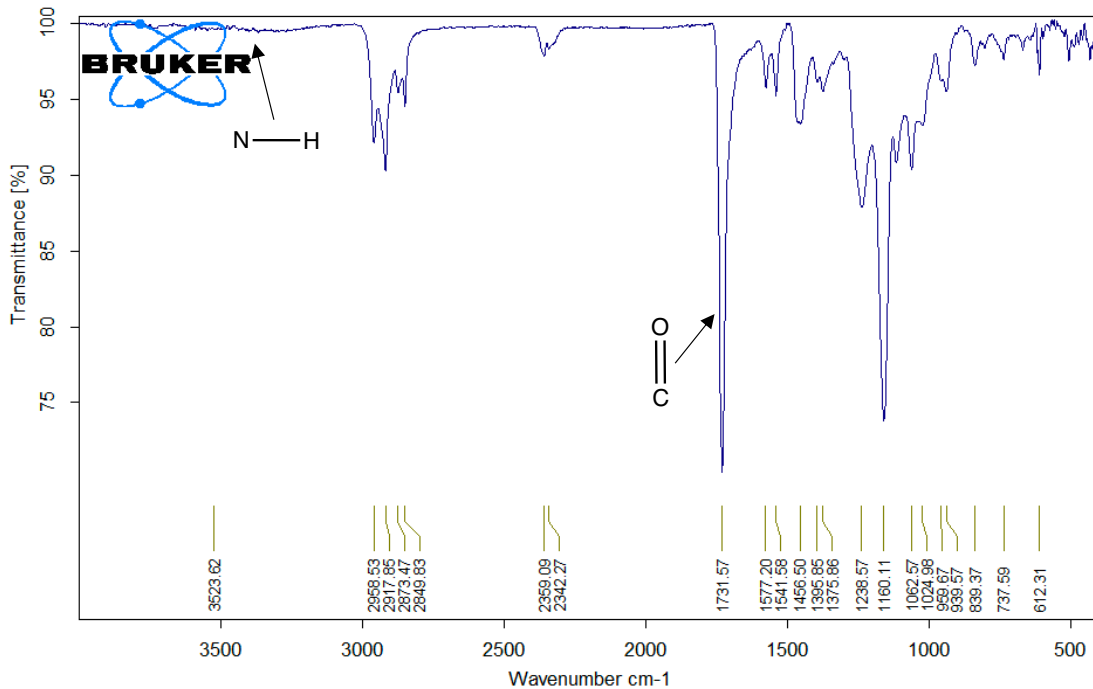


Figure 46. ATR-IR spectrum of PCL-PPy with monomer pre-treatment

3.3.4 Tape test

Figure 47 shows the result of the tape test being done to 1 in x 1 in squares of electrospun PCL coated with PPy via the oxidant pre-treatment route. As noted earlier, coating 1 in x 1 in squares evenly has proved to be challenging, and it was decided that doing the tape test on areas with the thinnest coating of PPy would give a better measure of the adhesion of PPy on PCL and not the adhesion of successive layers of PPy with each other. The determination of the area of the thinnest coating was done qualitatively and was determined to be the area with the lightest shade of black or gray. As can be observed, there was little to no delamination of PPy from PCL after the tape test, as evidenced by the unnoticeable change in color of the PCL-PPy square, and the trace amounts of black powder on the tape used for the test. This would merit the PPy adhesion a 4A on the ASTM D3359-17 standard. This indicates that the coating of PPy on these

substrates are strong. This, however, is preliminary data, and other ways of testing adhesion strength should be explored, such as subjecting the composite to ultrasonication.

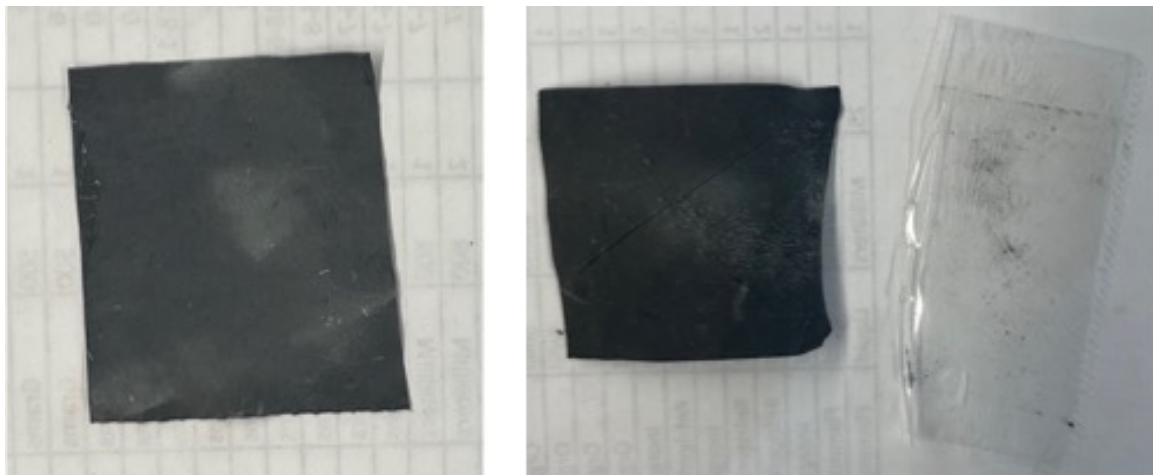


Figure 47. (Left) 1 in x 1 in electrospun PCL coated with PPy. (Right) The same electrospun PCL square after being subjected to the Tape Test, and the tape used

3.4 Conclusions and Future Work

This chapter has shown that PPy can be processed into a nanofibrous structure by *in situ* chemical oxidative polymerization onto an electrospun PCL substrate. Pretreatment of the electrospun PCL substrate with FeCl₃ oxidant achieves the best conformal coating of PPy. The ASTM Tape Test shows that this adhesion of the PPy coating onto the electrospun PCL substrate is strong. This method of fabricating the composite is hypothesized to retain the advantageous high surface area and porosity of nanofibrous structures and enhance the conductivity of PPy. This also is hypothesized to apply to other combinations of ICPs and electrospinnable polymers and is thus an enabling technology for soft materials which have applications in biomedical engineering, energy storage, sensing, and electronics. This protocol for fabricating PCL-PPy is then used in the next chapter. Future work in this area will concentrate on testing the conductivity of the fabricated PCL-PPy composites, testing different combinations of

ICPs and electrospun polymers, determining the mechanical properties of the composites, quantitatively determining the adhesion of PPy if possible and exploring other ways of trying to delaminate PPy if not (such as through ultrasonication), and determining their degradation behavior.

4 PCL-MNP-PPy FOR NERVE REGENERATION

4.1 Introduction

4.1.1 *Nerve regeneration and strategies for enhancement*

In general, nerve regeneration after damage is difficult to achieve unaided in the CNS. This is because scars that form during CNS nerve injury which serve to protect the CNS also block the transport of growth factors and extension of axons⁹⁷. While PNS nerves are able to regenerate by themselves, anything which helps accomplish this regeneration quicker results in better outcomes for the regeneration of function in the damaged nerve⁴.

The process of nerve regeneration involves Wallerian degeneration and reinnervation, as shown in Figure 48⁹⁸. Immediately after injury to the nerve, axons send signals via transport of proteins to the soma or the nerve cell body containing the nucleus, alerting it of injury. Wallerian degeneration then happens, which is the breaking down and clearing of the axon at the site of injury. In Wallerian degeneration, there is an increase in the uptake of calcium by the cell to maintain the motility of the mitochondria in the cell which accomplishes this breaking down and clearing of the axon. White blood cells then accomplish the digestion of myelin and axon debris, while also producing growth factors which regulate the contents of the ECM¹¹. The next step is the actual regeneration of the nerve. The signal sent from the site of injury or the lack of signals traversing the axon causes changes in Schwann cells to make them more suited to promoting cell growth. In this process, the Schwann cells at the site of injury switch from producing myelin to producing cell adhesion molecules and growth factors and their receptors, which go to the ECM. Reconnection in the axons happens due to the formation

of longitudinal cell columns in the basal lamina, called the Bands of Bungner. New axons are grown and elongated from the ends of these bands with the mediation of growth cones. This happens at a rate of about 2-5 mm a day.

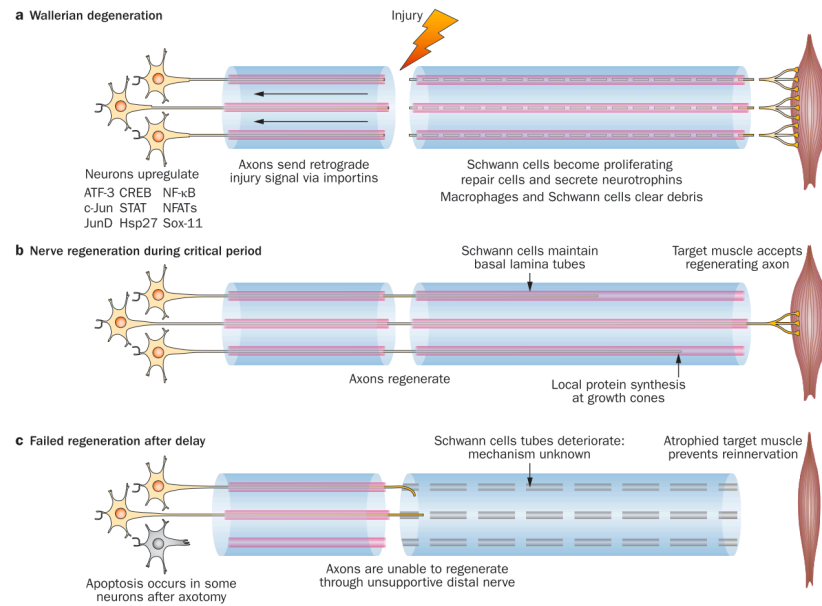


Figure 48. The process of nerve regeneration and consequence of failed regeneration.
Adapted with permission from ref. 98. Copyright 2013 Springer Nature.

If this happens slowly, whether due to the length of the nerve that needs regrowing or defects in the nervous system, then the Schwann cell tubes eventually deteriorate. This causes cell death in the parent neuron and structural changes in other cells the nerve is attached to. Furthermore, axons regrown in this manner are oriented randomly⁹⁷. These two effects may be the reason why the regaining of full functionality in nerves after injury is difficult to achieve. Hence, current strategies to address nerve injury focus on this part of nerve regeneration. These strategies focus on improving the intrinsic growth capacity of axons, ameliorating the effects of growth-inhibiting molecules, prevention of cell death in neurons, modulating the response of the immune system to growth, or a combination of any of these⁹⁸. Genetic engineering can be used to

induce Schwann cells to shift more quickly to producing more growth factors and produce more enzymes to degrade growth-inhibiting proteoglycans. The same can be done to promote the growth of white blood cells with a phenotype that specifically suppresses inflammation in the site of injury and promote repair. Surgical and pharmacological methods can also be used to prevent neuronal apoptosis by forcibly reinnervating them through nerve grafting or protecting neurons from cell death directly through coating with acetyl-L-carnitine or N-acetylcysteine. Because of their utility, these last two methods have seen the most clinical use in the treatment of nerve damage.

Nerve grafting involves the replacement of damaged nerve tissue with healthy nerves⁹⁷. The most used form of nerve grafting is autografting, which is the replacement of damaged nerves by healthy nerves sourced from another part of the body. This goes around the need for suppressing the negative immune response induced when nerve tissue from outside the body is used. However, in autografting, the available donor sites are limited, with potentially inherent deformities and differing functions, and these sites lose nerve function permanently. Additionally, a second surgery is needed to retrieve the healthy nerve from the donor site¹¹. Thus, the use of tissue engineering to fabricate synthetic nerve grafts has seen increased interest. This strategy has the advantage of potentially minimizing harmful side effects to induced nerve regeneration by designing the composition and topography of these implanted synthetic nerve grafts.

4.1.2 Nerve scaffolds and use of polycaprolactone as material

These synthetic nerve grafts, which are also called nerve guidance channels/conduits or nerve scaffolds, have five main functions: directing axonal growth from the site of injury back to the soma, mechanically supporting these growing axons, providing for the efficient transport of growth factors, nutrients, and cellular waste produced from Wallerian degeneration, preventing the growth of scar tissue which inhibits growth, and creating an environment conducive for the accumulation of growth factors and proteins necessary for axon regrowth¹¹. In clinical use, nerve scaffolds are tubular devices which are wrapped around a site of injury. These scaffolds can be modified with to have structures such as filaments, porosity, and many channels, and can further be functionalized with Schwann cells and growth factors, as shown in Figure 49⁹⁷.

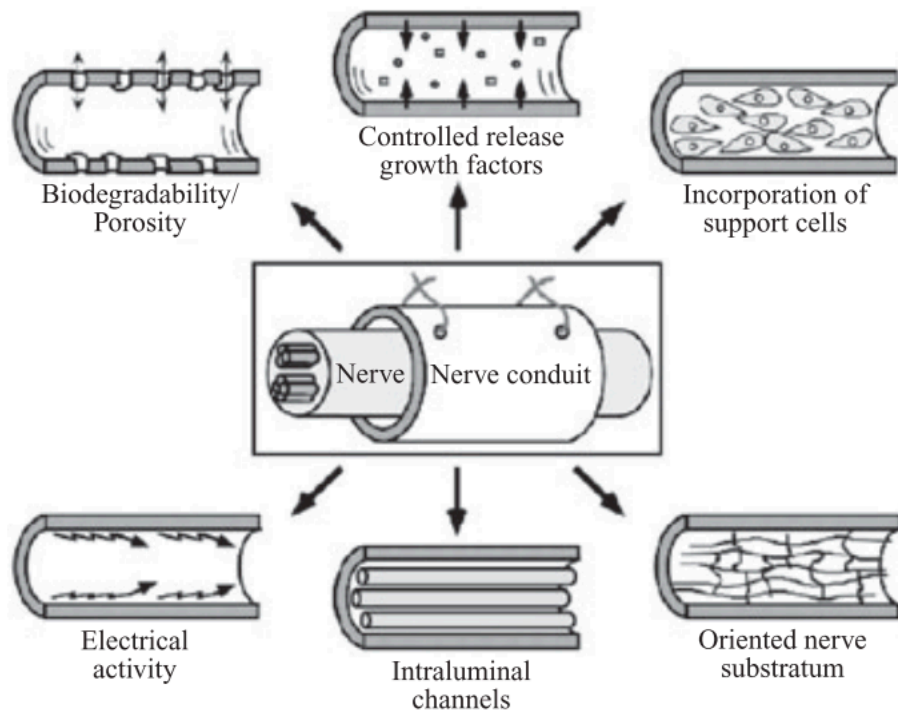


Figure 49. Structure of a nerve conduit for *in vivo* use. Adapted with permission from ref. 97. Copyright 2006 John Wiley and Sons.

There are several properties which are advantageous in the fabrication of these synthetic scaffolds: biocompatibility, mechanical stability, biodegradability, high surface area, surface modifiability, permeability, alignment, and electrical conductivity^{11,97}. Scaffolds should be biocompatible: not only should they support the growth of cells on them, but also not induce an inflammatory response or cell death. Scaffolds should have good mechanical properties and not fail during nerve regeneration or normal patient activities. Scaffolds should be biodegradable in the body and not require a second surgery to be removed. The rate of this degradation should match the rate of new tissue formation. Scaffolds should have a very high surface area and porosity to allow for the attachment of Schwann cells and take advantage of their inherent ability to promote nerve growth. Scaffolds should be able to accomplish a controlled release of growth factors necessary for nerve growth. Importantly, nerve scaffolds should have anisotropically-distributed properties: they should be oriented in a specific direction and guide oriented axonal growth physically across a site of injury. This takes advantage of the formation of growth cones in nerve regeneration⁹⁹. This helps retain the native organization of cells. Scaffolds should mimic the ECM of nerve tissue to allow them to better induce cell attachment. Interestingly, electrical stimulation can also be used to help in the growth of axons across the injury site⁹⁸. Thus, finally, nerve scaffolds should be able to support the conduction of direct current electrical fields, as this promotes the rearrangement of the cytoskeleton in nerves along the direction of growth.

Polymer microfibers and nanofibers fabricated through electrospinning satisfy these criteria and have been used in nerve tissue regeneration. As has been discussed in Chapter 2, synthetic biocompatible and biodegradable polymers can be electrospun to yield a micro- to nanofibrous structure, which has a high surface area and a high degree of porosity. To allow for anisotropically-distributed properties, a rotating drum mandrel collector can be used in electrospinning and align the nanofibers in a certain direction. The biological performance and mechanical properties of the scaffold can be tuned by altering the electrospinning parameters and polymer choice. Polymers that can be used in scaffolds must have functionality that can be hydrolytically or enzymatically-cleaved, such as esters, amides, and even ethers¹⁷. Polyesters offer a wide range of possible favorable mechanical properties and are readily hydrolytically cleaved, and thus are widely used as scaffolds.

PCL, a semicrystalline polyester, has a high ductility and intermediate modulus of elasticity. It has a melting temperature between 59-64 °C, and a glass transition temperature of -60 °C which means it stays solid and flexible at body temperature. These properties allow PCL to be processed into structures which have comparable mechanical properties to native tissue. Because of this, it has seen extensive use in nerve regeneration applications, together with molecules which promote the adhesion and even growth of cells such as chitosan and collagen¹², or ICPs which enhance nerve growth. As has been explained above, the application of electrical current enhances nerve growth. The use of soft ICPs coated on soft substrates such as electrospun PCL more closely mimics the mechanical properties of native tissue, and lessens the strain mismatch associated with the growth of new cells in the tissue¹⁰⁰, as opposed to implanting other conductive

substrates, such as metal electrodes. The ICP of choice for this application is PPy, because of its biocompatibility and observed enhanced surface affinity for cell adhesion¹⁰¹.

PCL coated with PPy has been proven to be effective in nerve regeneration. PCL nanofibers coated with PPy has been observed to exhibit anti-clotting and anti-inflammatory properties with the application of a current¹⁰², grow and allow the differentiation of neural stem cells⁶², and be effective for the proliferation of Schwann cells¹⁸. It is thus a viable composite for nerve regeneration, and it is hypothesized that applying the knowledge obtained from conformally coating electrospun nanofibers with ICPs as described in the previous chapter will enhance neural cell attachment, growth, and differentiation in these scaffolds because of the preserved high surface area and enhanced conductivity of the ICP coating.

4.1.3 Magnetic nanoparticles for nerve regeneration

Another area that has been explored in nerve regeneration is the use of magnetic nanoparticles (MNPs). MNPs for use in biomedical applications are composed of a core of magnetite (Fe_3O_4) or maghemite ($\gamma\text{-Fe}_2\text{O}_3$), and an organic or inorganic shell¹⁰³, which is incorporated for stability or compatibility. This coating can also be composed of small molecules or drugs, depending on the end application and desired mechanism of action of the MNP.

The use of MNPs in biomedical applications is due to their ability to be functionalized, remote controlled, and undergo hyperthermia or localized heat generation⁶. MNPs can be functionalized with nerve growth factors to protect them from degradation, and with drugs to assist nerve growth. These can then be directed to a

particular region of injury in the body by an external magnetic field, which allows for targeted treatment. This also offers the advantage of allowing the monitoring of the progress of these treatments, as MNPs are excellent contrast agents for magnetic resonance imaging¹⁰³. Additionally, MNPs can be controlled by external magnetic fields to generate a small mechanical tensile force in the local environment of growing nerves, which serve to induce the sprouting, elongation, and outgrowth of axons.

When MNPs are subjected to an alternating magnetic field, they generate heat. This is because of two competing mechanisms: Brownian motion, and Néel relaxation⁶. In Brownian motion, the alternating magnetic field causes a physical rotation of the particles in the MNP. In Néel relaxation, the atomic magnetic moments are altered and rotated by the application of the same alternating magnetic field. The dissipation of energy because of these two mechanisms results in the local production of heat. It has been observed that the addition of Zn and Co in magnetic nanoparticles optimizes both their magnetic properties and heat dissipation efficiencies⁸.

These two properties have been taken advantage of in the field of nerve regeneration. Dr. Gabriela Romero-Uribe, currently at the University of Texas at San Antonio, and colleagues have observed the potential of MNPs to be used in stimulation of areas deep in the brain⁷. This was done by directing Fe₃O₄ MNPs with an external magnetic field to areas in mice brain with heat sensitive TRPV1⁺ neurons, and then hysteretically heating them by changing the frequency of the applied magnetic field, resulting in widespread and reversible neural function. Moreover, MNPs have been successfully functionalized with a thermally-labile agonist, which was successfully selectively delivered to its specific receptor via remote control and hysteresis⁹.

Importantly, this localized heating was observed to have had only minimal thermal damage to surrounding tissues.

It is thus hypothesized that incorporating MNPs into neural scaffolds would add these advantages to the composite. MNPs would allow remote control of neural scaffolds to areas of the body which need treatment, and the application of an alternating magnetic field would induce local heating which would enhance the proper functioning of nerves growing on the scaffolds. The thermal damage to surrounding unaffected tissue would be further minimized by the low thermal conductivity of the composite, being composed of polymers. Interestingly, the application of an alternating, changing magnetic field to a conductor induces an electromotive force and current in it, as per Faraday's law of induction¹⁰⁴. Since the neural scaffold is coated in PPy, a conductive material, it is plausible that the application of an alternating magnetic field would also cause the induction of current. This would remove the need for continuous external stimulation of these neural scaffolds to take advantage of their conductivity.

Incorporating MNPs into electrospun polymer nanofibers can take the form of simply dispersing MNPs in polymer solutions²⁹. These mixtures can then be electrospun as is, or the grounded collector in the electrospinner can be embedded with magnets to enforce alignment in the MNP distribution in the composite, which is different from the nanofiber alignment. Care must be taken in the incorporation of MNPs, as too much MNPs were observed to damage polymer nanofibers. Neat electrospinning has been used to successfully produce composites of electrospun poly(vinyl alcohol), Fe₃O₄ MNPs, and magnetic graphene¹⁰⁵, and even a multilayered neural scaffold of PCL, melatonin, and

Fe_3O_4 MNPs, which was demonstrated to induce remyelination, regrowth of the axon, and restoration of peripheral nerve function in rats¹⁰⁶.

4.1.4 Scope and limitations of the study

This study aims to fabricate a composite of PCL, MNPs, and PPy for nerve regeneration by mixing MNPs in a solution of PCL, which is then electrospun, and then PPy is then polymerized on its surface. This study is done in collaboration with Dr. Gabriela Romero-Uribe's group from the University of Texas at San Antonio, who are responsible for providing MNPs and conducting cell adhesion and function tests on the composites.

4.2 Materials and Methods

4.2.1 Materials

PCL was electrospun following the procedure developed in Chapter 2. Core 40 MNPs composed of Fe and Zn were sourced from Dr. Romero-Uribe's group, with a cubic structure shown in Figure 50, and elemental analysis shown in Figure 51.

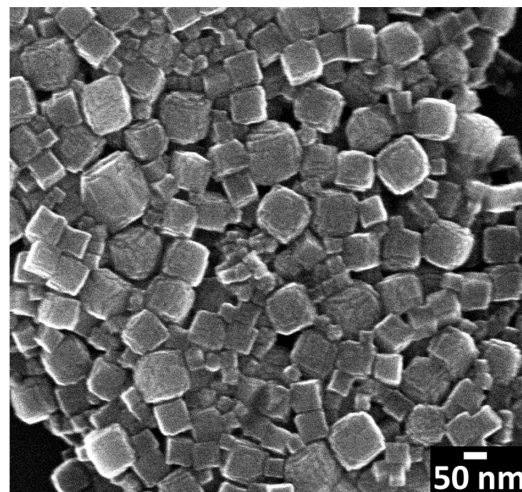


Figure 50. TEM of Core 40 MNPs, courtesy of Dr. Romero-Uribe's group

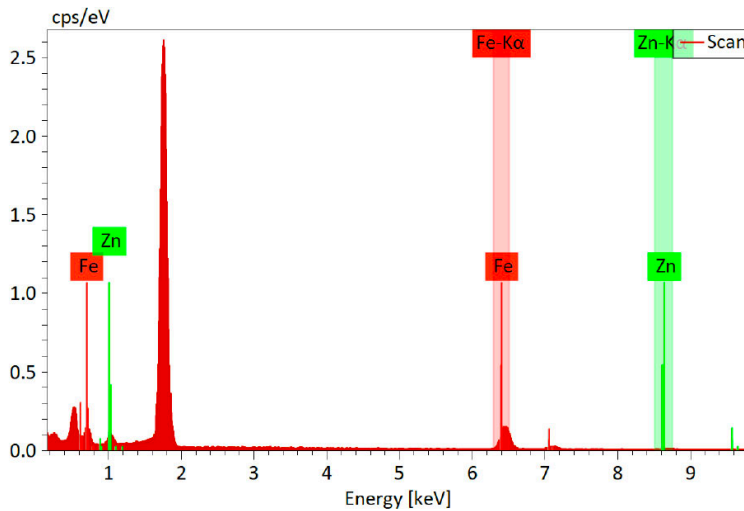


Figure 51. EDX of Core 40 MNPs, courtesy of Dr. Romero-Uribe's group

4.2.2 Instrumentation

An electrospinning setup composed of a New Era Pump Systems syringe pump, Gamma High Voltage Research high voltage power supply, and Spraybase electrospinning rotating drum collector were used. For homogenization, a Fisher Scientific FS30H sonicator and S56 miniRoto vortexer were used. For material characterization, analysis was done using a JEOL JSM-6010 PLUS/LA Scanning Electron Microscope in the Shared Research Operations facility at the Texas State University. ATR-IR analysis was done using a Bruker Tensor II FT-IR Spectrometer with a Harrick SplitPea™ Attenuated Total Reflectance accessory in the Department of Chemistry and Biochemistry at the Texas State University.

4.2.3 Electrospinning of PCL-MNPs

In a 10 mL vial, 1.5g of PCL was dissolved in 9 mL of 1:1 THF/DMF with stirring at room temperature for 24-48 hours, until fully dissolved. In a separate vial, 25 mg of organic-soluble MNPs were dissolved in 10 mL of 1:1 THF/DMF to make a stock suspension of 2.5 mg/mL MNPs. This solution was then sonicated for 30 minutes and vortexed for 5 minutes, until a clear brownish solution was formed. 1 mL of this stock solution was then added to the 15% PCL solution. This was then sonicated for 30 minutes and vortexed for 5 minutes to ensure homogeneity. The mixture was then electrospun with the following process parameters: 14.0 kV applied voltage, 130 mm working distance, and 0.05 mL/min flow rate. The speed of the rotating drum mandrel were modified to 4000 rpm as needed for the production of highly aligned nanofibers. After electrospinning, the nanofiber mat produced was cut out of the rotating drum mandrel and stored in a drawer until further use.

4.2.4 Effect of MNP concentration

To probe the effects of MNP concentration on both the structure of the composite and its biological activity, two concentrations of MNPs were used: 25 and 2.5 $\mu\text{g}/\text{mL}$.

4.2.5 Polypyrrole coating

Combinations of PCL and MNP were coated with PPy following the oxidant pre-treatment procedure developed in Chapter 3.

4.2.6 ATR-IR analysis

The developed composites were analyzed using ATR-IR with no further modification.

4.2.7 SEM-EDX analysis

SEM and SEM-EDX analysis was done on the fabricated composites under low vacuum conditons with no further modification done to the samples.

4.2.8 Cell adhesion tests

Cell adhesion tests of the produced PCL-MNP-PPy composites were done by the research group of Dr. Gabriela Romero-Uribe at the University of Texas at San Antonio. C2C12 and ND7/23 cells were seeded in a solution of 10% Fetal Bovine Serum and antibiotics in Dulbecco's Modified Eagle Medium. The PCL-MNP-PPy composites were cut into 10 mm x 3 mm rectangles and glued to a polystyrene 24-well plate with a 0.3 g/mL solution of polystyrene in CHCl₃. The samples were then sterilized by exposure to UV light for 60 minutes. Afterwards, the PCL-MNP-PPy composites were coated with fibronectin to aid the adhesion of cells with the help of Sulfo-SANPAH crosslinker. Next, 1 mL of the seeded C2C12 cells were added to each PCL-MNP-PPy-containing well and fixed using 4% formaldehyde 24 h post-seeding. The same was done with the ND7/23 cells, which were fixed using 4% formaldehyde 48 h after seeding. The cells were then permeabilized with Triton X100. They were then stained with DAPI and Alexa Fluor 488 phalloidin and visualized using a Leica TCS SP8 Confocal Microscope. These visualize the nuclei and the actin cytoskeletons of the cells, respectively. As of writing, the following samples have been tested by Dr. Romero-Uribe's group:

Table 2. Samples tested for cell adhesion at UTSA

Sample	Collector speed	MNP concentration
1	4000 rpm (aligned)	2.5 µg/mL
2	4000 rpm (aligned)	25 µg/mL
5	4000 rpm (aligned)	0 µg/mL
6	80 rpm (unaligned)	0 µg/mL

4.3 Results and Discussion

4.3.1 PCL-MNP

Figure 52 shows that the microstructure of the PCL-MNP composite is composed of fibers with clusters of white material.

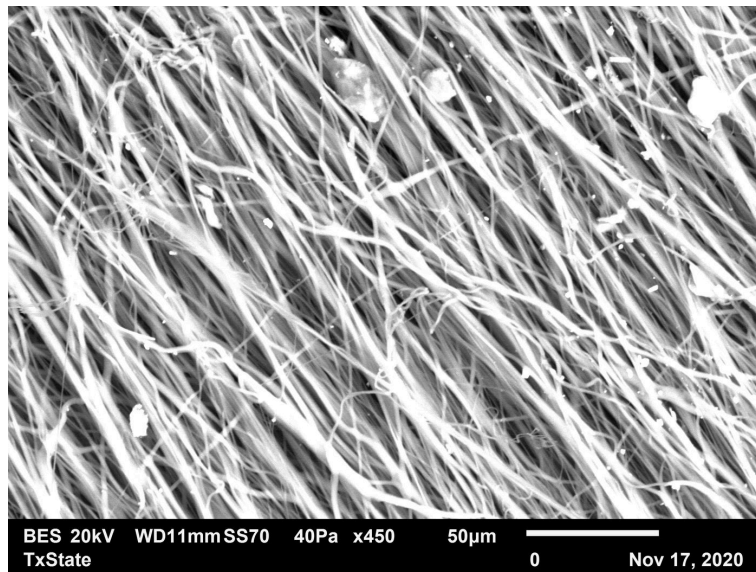


Figure 52. PCL-MNP

Figure 53 shows that there are amounts of C, O, Fe, and Zn, as well as Si, Al, and Cl, with the fibers being composed of C and O, and the white-colored clusters being composed of O, Fe, and Zn. As has been mentioned in previous sections, Si is a pervasive contaminant and could have come from any source such as glassware contacted or sand in the laboratory. The presence of Al can probably be attributed to the sample stub used in SEM analysis. Cl can be attributed to sweat that can have contacted the PCL-MNP at any time during the fabrication and analysis of the material. Fe and Zn can only come from the MNPs, which means that the Core 40 MNPs are in electrospun PCL, especially since the areas where Fe and Zn, as well as O have been detected roughly correspond to the same areas. Furthermore, it can be observed that although the MNPs appear to be

dispersed across the viewing area, clumping of the MNPs can be observed, especially in the upper right region in Figure 53A.

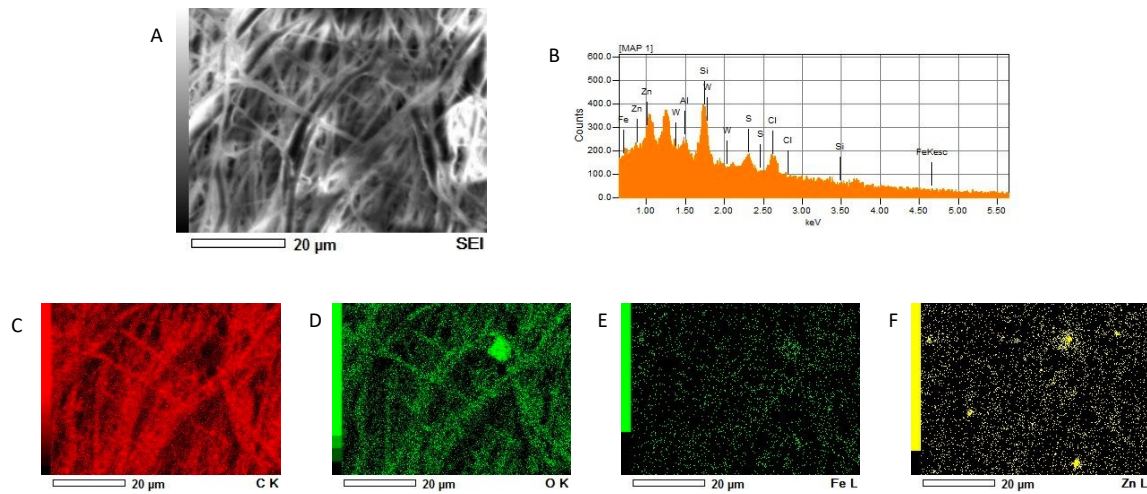


Figure 53. EDX analysis of PCL-MNP. (A) SEM micrograph of area where elemental mapping was done (B) Graph of detected atoms in A and their relative abundance (C) Map showing the areas in A where C was detected (D) Map showing the areas in A where O was detected (E) Map showing the areas in A where Fe was detected (F) Map showing the areas where Zn was detected

Comparing Figure 54 and Figure 16, it can be observed that there are no significant changes in the ATR-IR spectrum between the two, which means that the incorporation of MNPs has not caused degradation in the chemical structure of PCL.

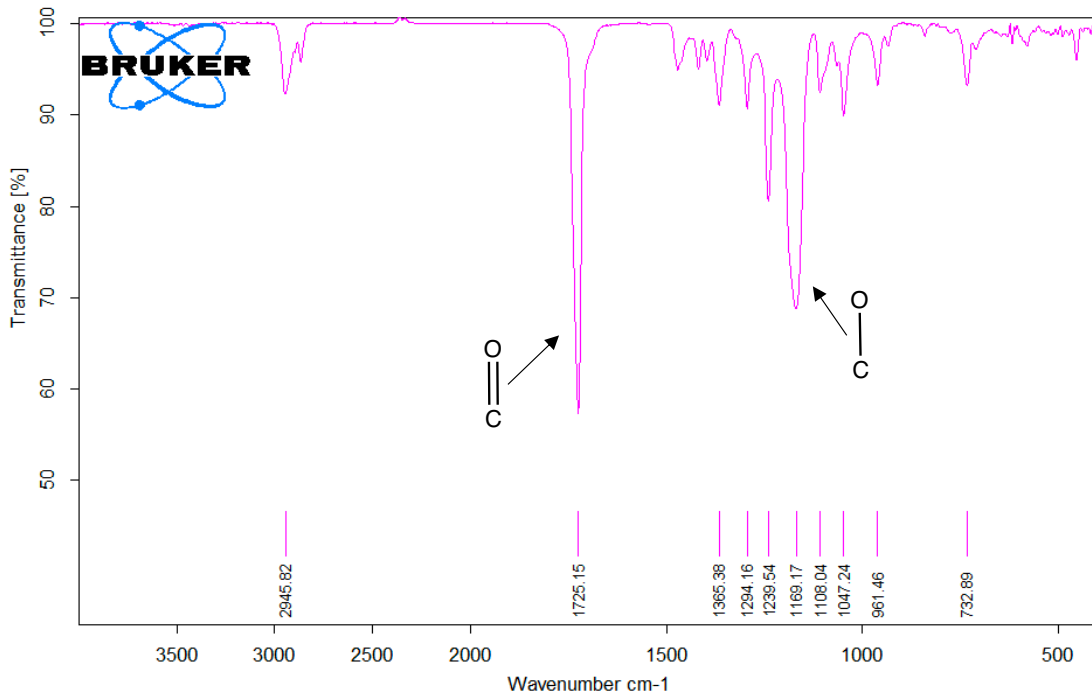


Figure 54. ATR-IR spectrum of PCL-MNP

Thus, MNPs have been successfully embedded into the matrix of electrospun PCL and dispersed, although more work needs to be done to disperse the MNPs uniformly. This however assumes that the level of concentration of MNPs in a single area as shown in the preceding figures is significant (given the scale) and produces an adverse biological effect in the resultant composite for nerve regeneration, and further dispersal might not be needed if this is not the case. The presence of MNPs was not determined apart from SEM-EDX analysis. Future work may also be done to use more methods to validate the presence and quantitatively measure the properties of MNPs in electrospun PCL, such as using a Quantum Design Physical Property Measurement System (PPMS). Another area that can be explored is attempting to align the MNPs in a single direction, such as through the embedding of a magnet or the application of a magnetic field to the electrospinning collector.

4.3.2 Effect of MNP concentration

It can be observed in Figure 55 that the nanofibers of PCL electrospun at 4000 rpm gradually lose alignment as more and more MNPs are blended into the polymer solution. At 2.5 µg/mL MNP loading, the degree of alignment is retained. However, increasing that concentration 10x to 25 µg/mL results in a decrease in the degree of alignment of the nanofibers. This phenomenon of decrease in alignment because of increasing magnetic nanoparticle content has also been observed in the magnetic electrospinning of PLGA blended with MNPs¹⁰⁷. As has been discussed in Section 4.1.4, the motion of magnetic materials induces the formation of an electric field. This induced electric field may be acting against the electric field produced by the electrospinning setup between the emitter and the grounded collector and introduce instability forces which act against the drawing, aligning force exerted by the rotating collector. This effect may be negligible up to a certain threshold, after which this induced electric field acts to reduce the nanofiber alignment.

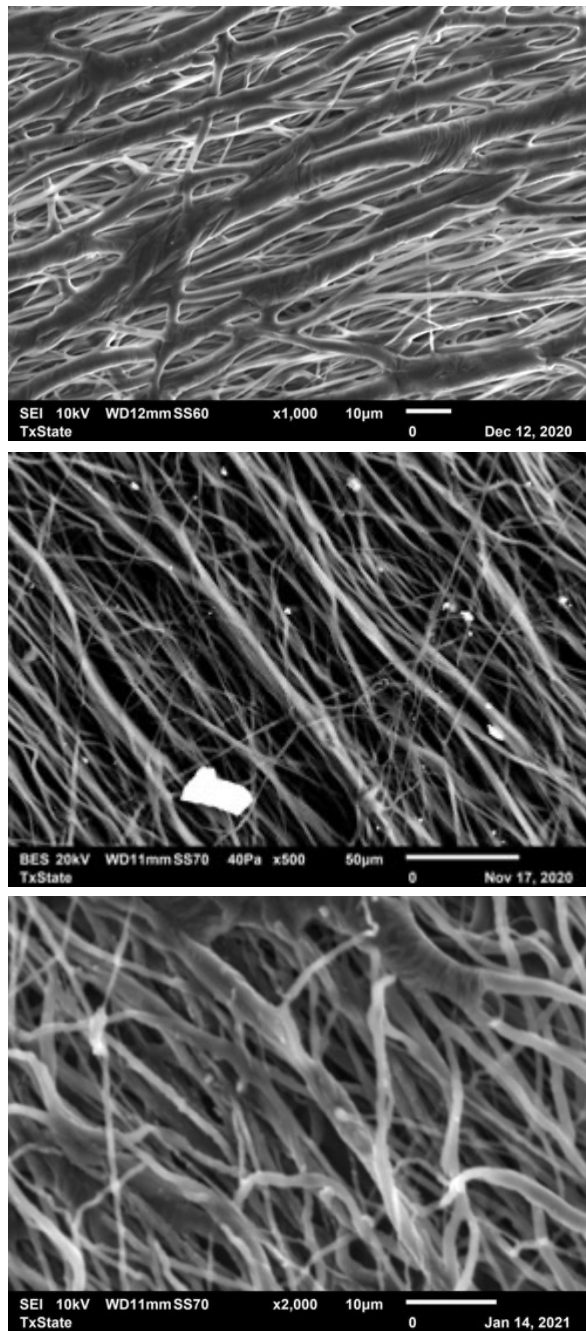


Figure 55. (Top to bottom) PCL electrospun at 4000 rpm with 0, 2.5, and 25 μ g/mL MNPs

However, it was deemed necessary to probe the effect of MNP concentration in the nerve regeneration capacity of PCL-MNP-PPy scaffolds. Thus, both 25 and 2.5 $\mu\text{g/mL}$ MNP concentrations were used in biocompatibility studies.

4.3.3 PCL-MNP-PPy

Figure 56 shows the microstructure of PPy coated on PCL-MNP following the protocol developed in the last chapter.

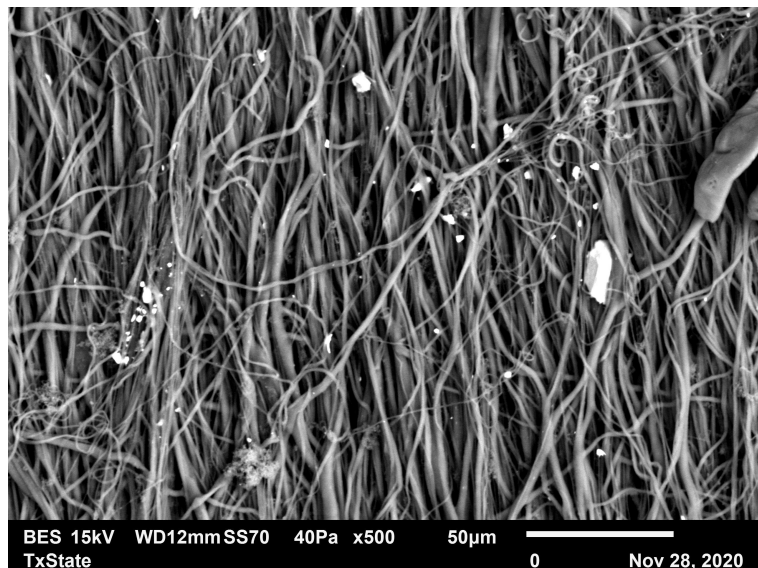


Figure 56. PCL-MNP-PPy

As expected, Figure 57 shows that the fibrous structure is composed of C, O, and N atoms, which are from PCL and PPy evidenced by the PPy N-H broad stretch centered at around 3000 cm^{-1} and the strong PCL C=O stretch at 1725 cm^{-1} in Figure 58, and the white colored clump is made up of Fe.

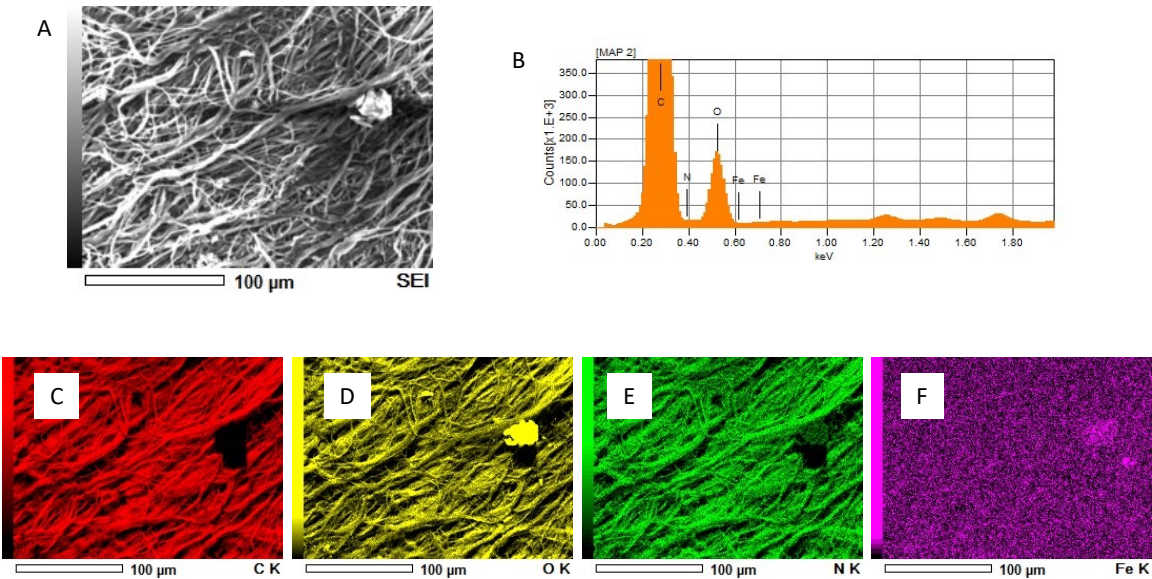


Figure 57. EDX analysis of PCL-MNP-PPy. (A) SEM micrograph of area where elemental mapping was done (B) Graph of detected atoms in A and their relative abundance (C) Map showing the areas in A where C was detected (D) Map showing the areas in A where O was detected (E) Map showing the areas in A where M was detected (F) Map showing the areas where Fe was detected

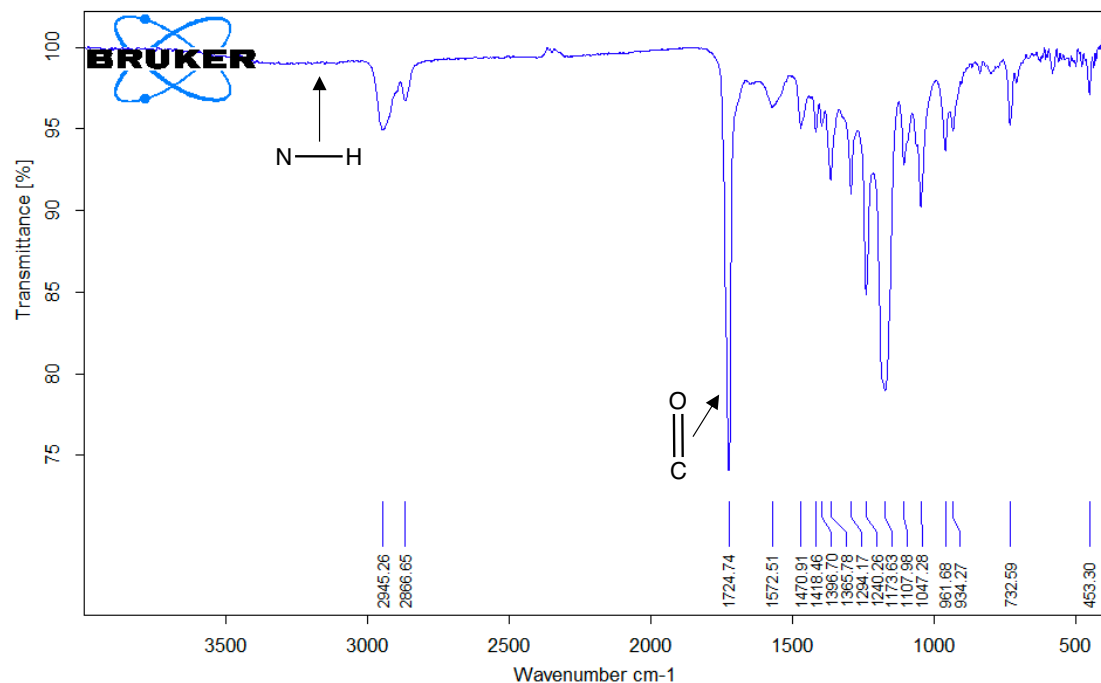


Figure 58. ATR-IR spectrum of PCL-MNP-PPy

Thus, PCL-MNP-PPy has been successfully made, combining three strategies for nerve regeneration into one composite. Because of this, it is hypothesized that this would be a good candidate material for neural tissue scaffold. Thus, samples of this composite were sent to our collaborators at the University of Texas at San Antonio for further testing.

4.3.4 Cell adhesion test results (Courtesy of Dr. Nicolas Muzzio, UTSA)

Cell adhesion studies were done by the group of Dr. Gabriela Romero-Uribe at the University of Texas at San Antonio, who developed the technique of using MNPs for hysteretic deep brain stimulation. Composites with different combinations of PCL, MNP, and PPy were made and sent, and the group was able to successfully test the adhesion of cells of 4 samples as outlined in Table 2. The results are shown in Figure 59, with the blue stain corresponding to the cell nuclei, and the green stain corresponding to the cell cytoskeleton. It was reported that there was a difficulty in obtaining images of the setups of the cell adhesion experiments, as it was observed that PPy exhibits blue fluorescence. Hence, faint bluish lines can be seen in the background of all micrographs.

C2C12 cells are mouse myoblasts, which eventually differentiate into muscle tissue. Figure 59 shows their adhesion on Sample 2 and Sample 5, which, from Table 2, are both aligned PCL nanofibers with 25 and 0 µg/mL MNPs, respectively. It can be observed that the presence of fibronectin as a cell adhesion aid does not affect the seeding and adhesion of cells, and that C2C12 cells adhere to PCL-PPy and PCL-MNP-PPy. What does affect these are the alignment and the presence of PPy on the substrates. On cells seeded on bare PCL or PCL-MNP, alignment of the cytoskeleton can be observed in the direction of the alignment of the substrate. This alignment can also be observed in the

cells seeded on the PCL-MNP-PPy sample, although it appears that the degree of alignment is lesser. This lessened alignment can also be observed when comparing the cells seeded on PCL alone with the cells seeded on PCL-PPy. Notably, however, it appears that coating PCL with PPy almost makes the substrate completely unviable for cell adhesion. This is a surprising result, given that C2C12 cells seeded on PCL-MNP-PPy just fine; thus, a hypothesis involving the cytotoxicity of the Fe^{3+} salts used to prepare PPy can be eliminated.

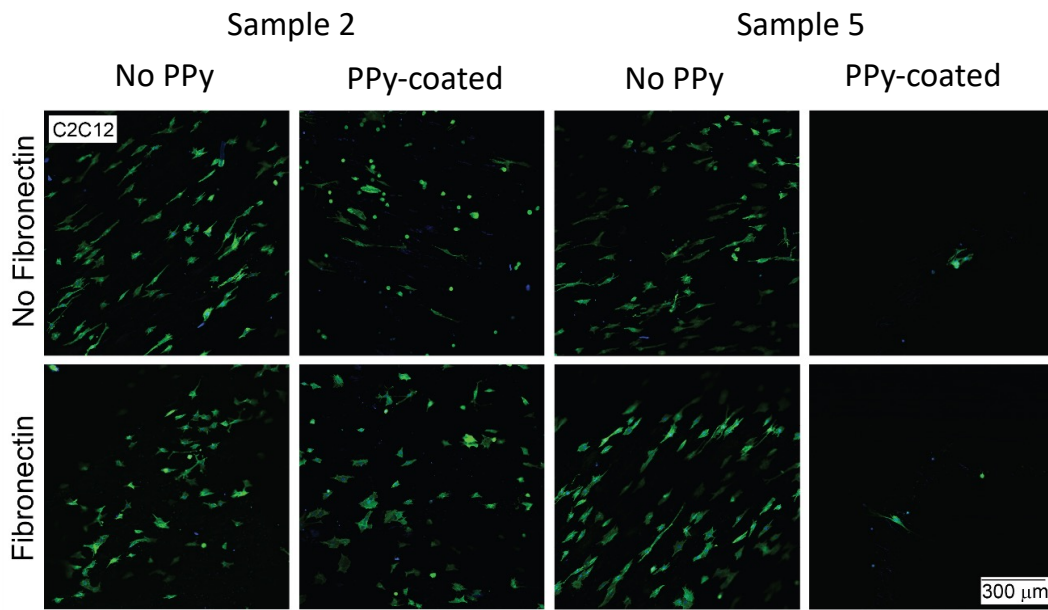


Figure 59. Confocal images of C2C12 cells seeded on composites (blue: DAPI stain; green: phalloidin stain)

Two explanations can therefore be offered, both of which hinge on the process of *in situ* chemical oxidative polymerization on pre-treated PCL substrates.

Firstly, the presence of MNPs may provide extra anchoring for cells to adhere to. As has been established in the previous chapter, the coating of PPy via the optimized protocol results in a thick, strong coating, with the exact amount deposited being subject to further studies. Although this coating results in a conformal coating that preserves the

nanofibrous structure of the substrate, as shown in Figure 40, it may also obscure its surface roughness and porosity. This nanoroughness, and, ultimately, surface energy may be important in the adhesion and viability of cells^{108–110}. This may be overcome by the presence of MNPs, which, as shown in Figure 56, may be big enough to provide this roughness. These, however, are qualitative observations, and future work may be done to quantitate roughness, such as through Atomic Force Microscopy, and its effect on cell adhesion and, ultimately, growth.

Second, the decrease in cell adhesion may be explained by a simple mishandling of the production of the PCL-PPy composites. FeCl₃•6H₂O has been demonstrated to be cytotoxic to BALB/3T3 and HepG2 cells, which are mouse embryo fibroblasts and liver cancer cells, respectively¹¹¹. This was attributed to the ability of Fe to either oxidize or reduce cellular molecules and generate reactive oxygen species which cause damage to cellular components. Since the protocol established in the earlier chapter involved oxidant pre-treatment, subsequent soaking in a solution of Py, and then washing with excessive amounts of EtOH before drying and use in cell adhesion studies, the decrease in adhesion and viability of PCL-PPy may simply be due to excess FeCl₃ remaining in the composite that has not been successfully washed away at the last step. Work is currently underway in our laboratory to test this hypothesis.

ND7/23 cells are mouse neuroblastomas, which eventually differentiate into neurons. Figure 60 shows their growth on Sample 1 and Sample 6, which, from Table 2, are aligned PCL samples with 2.5 µg/mL MNPs and unaligned PCL samples without any MNPs, respectively. Just as in the case of the C2C12 seeding experiment, it appears that ND7/23 cells seeded on the composites of PCL, MNP, and PPy follow the alignment of

the substrate. It can be observed that the presence of MNPs in the composite does not affect the adhesion of cells seeded. Interestingly, contrary to the results obtained from C2C12 cell seeding experiment, it can be observed that the coating of these samples with PPy increased cell adhesion and have led to differentiation, as can be observed by the observable increase in the size of the cytoskeleton. These findings can be interpreted to rule out the first explanation for non-adhesion of C2C12 cells on PCL-PPy explained previously, although it would still be worth probing the effect of PPy coating on the roughness and adhesion of cells on electrospun PCL, especially as more results come in from our collaborators at UTSA.

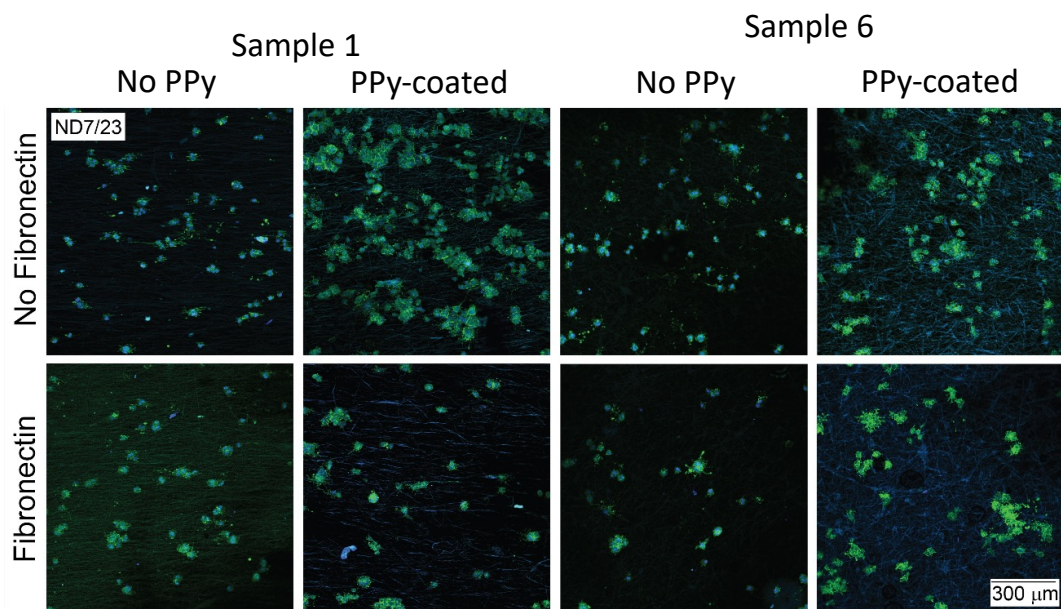


Figure 60. Confocal images of ND7/23 cells seeded on PCL (blue: DAPI stain; green: phalloidin stain)

Figure 61 shows one of these cells grown on PCL-MNP. It can be observed that there is a structure composed of cytoskeleton components radiating from the cell nuclei, oriented along the direction of alignment of the substrate. It was determined that this is evidence for the formation of dendrites, which are important cellular organelles in

neurons, as shown in Figure 1. Although this was observed in uncoated Sample 1, which corresponds to aligned PCL-MNP (at 2.5 $\mu\text{g/mL}$), this can also be easily observed in the PPy-coated samples. This is important, as this means that our PCL-MNP and PCL-MNP-PPy aligned composites are not only viable for the adhesion of cells, but also allow for cellular differentiation.

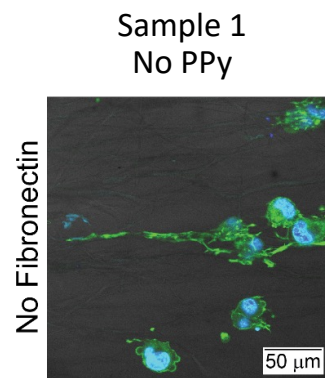


Figure 61. Confocal image of ND7/23 cells seeded on electrospinning samples (blue: DAPI stain; green: phalloidin stain)

It should be noted that these are simply cell adhesion tests, and the property of these composites to enhance nerve growth with and without electrical stimulation remains to be seen. This is important, as this is the reason for including PPy in the first place. The response of these composites to an external magnetic field, whether remote-controllability, hysteretic heating, or induction of electric fields, is also yet to be tested. Work is underway in the laboratory to produce more of these composites for further testing at UTSA.

4.4 Conclusions and Future Work

This chapter has shown the successful fabrication of a scaffold composed of PCL, MNP, and PPy which is hypothesized to be a good material for nerve tissue regeneration. The combination of the nanofibrous structure of aligned electrospun PCL mimicking the ECM of native nerve tissue; the remote-control, hysteretic, and drug-delivering capacity of MNPs plus their potential use as anchors for cellular attachment; and the softness, biocompatibility, and conductivity of PPy are hypothesized to synergistically enhance the attachment, growth, and differentiation of neurons. The adhesion of cells on composites of PCL-MNP and PCL-MNP-PPy has been demonstrated using seeded mouse myoblast C2C12 cells and mouse neuroblastoma ND7/23 cells, with cells attaching and orienting along the alignment of the substrate. Evidence of neuroblastoma cell differentiation leading to dendrite formation has even been found.

Future work in this regard will focus on evenly dispersing MNPs on the composite; comparing the surface roughness of PCL, PCL-MNP, PCL-PPy, and PCL-MNP-PPy; determining ways to completely remove potentially cytotoxic FeCl_3 ; and the effects of all these variables on the adhesion of cells and biocompatibility of the composite. Studies will be conducted to test the effects of electrical stimulation and the application of an external magnetic field onto the integrity, biocompatibility, and, ultimately, the ability of these composites to enhance nerve regeneration.

5 CHEMICAL MODIFICATION OF POLYMER NANOFIBERS

5.1 Introduction

5.1.1 *Stability of electrospun composites and graft copolymerization*

In the literature studies discussed above involving the fabrication of composites of electrospun polymer substrates and coated ICPs for various applications, there are no extensive attempts at studying either the delamination of the ICP coating or the degradation of the whole composite. There is mention of non-delamination of the PPy coating on poly(lactic-co-glycolic acid) after 2 weeks of storage⁶², and non-delamination of reduced graphene oxide coated onto hot-pressed electrospun PAN during processing¹¹². Delamination has been explored more extensively in studies which do not involve coating electrospun substrates: electrochemically-polymerized PPy delaminated from ITO glass electrodes after mild washing⁴⁹, “modest” to good adhesion was observed on solvent-cast and electrodeposited PPy onto an aluminum alloy¹¹³, bioactuators with coatings of PPy and PANI films have the disadvantage of being susceptible to delamination⁷², and unmodified PEDOT coated on ITO can delaminate after just 5 seconds of ultrasonication³⁹. As an aside, however, it should be noted that the protocol developed for conformally coating PPy on electrospun PCL described in Chapter 3 was determined to result in good adhesion, as per ASTM standards.

The literature studies illustrate not just the need to study the stability of ICP coatings on electrospun substrates but also the need to find a way to make these composites more stable. One factor that can be looked at is the fact that the aforementioned composites are just held together by secondary interactions. It is hypothesized that making covalent bonds between the substrate electrospun polymer and

the ICP coating would introduce primary interactions between them and thus make for a more robust coating. Indeed, a fabric of poly(ethylene terephthalate) was modified with a phosphonyl group which was reacted with an alcohol-modified Py which was then polymerized. The resultant graft copolymer was much less susceptible to delamination while retaining the conductivity of PPy¹¹⁴. Interestingly, in the study involving the coating of PPy onto an Al alloy, the authors posited that the increase in strength of adhesion observed in electrodeposited PPy vs. solvent-cast PPy may be due to higher PPy molecular weights attained during electropolymerization, resulting in increased chain entanglement and cohesion¹¹³.

Essentially, this method of modifying polymer nanofibers involves the formation of a graft copolymer. This method imparts long term chemical stability to these composites¹¹⁵. Graft copolymerization is advantageous as it allows for the retention of conjugation in the modifier ICP. This copolymerization occurs with either the coupling of previously-synthesized polymers to the surface of these substrate polymers, which can be termed “grafting to”, or chain growth from reactive sites on the surface, which can be termed “grafting from”¹¹⁶. There is a third method, “grafting through”, which involves the *in-situ* polymerization of a macromonomer tethered to a side chain. All these methods produce what is called a polymer brush, as shown in Figure 62¹¹⁷.

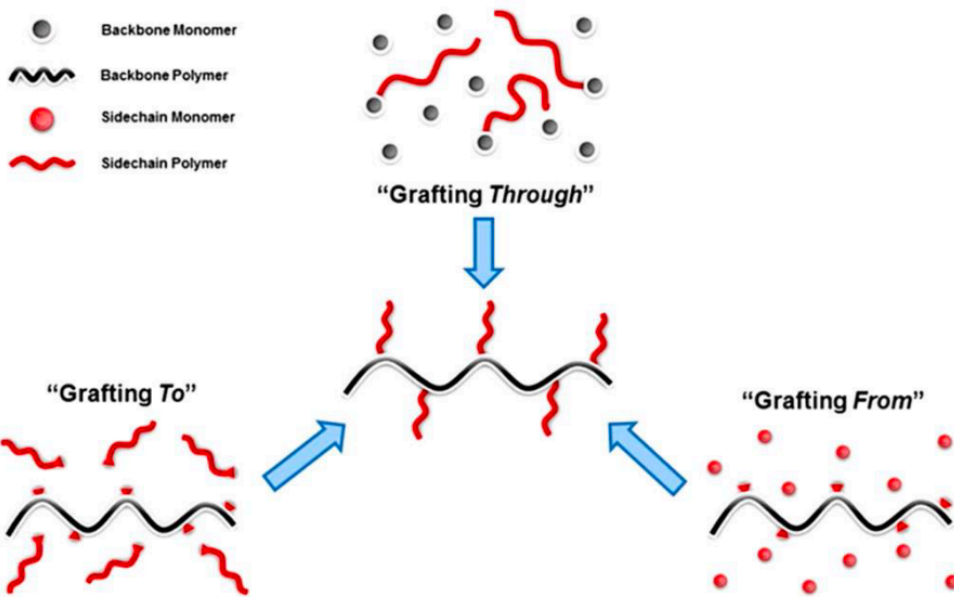


Figure 62. The three methods of graft copolymerization. From ref. 117. CC BY 4.0.

The “grafting to” method relies on the presence of reactive functionality on both the substrate and the modifier polymers. This method relies on the accumulation of modifier polymer chains on the surface to be modified, and the proximity of the reacting functionalities. These can be hard to achieve in solution due to strong osmotic repulsion¹¹⁸. In the case of ICPs such as PPy, poor solubility of the ICPs makes the “grafting to” approach largely infeasible. “Grafting through” is not relevant in the modification of electrospun substrates simply because the substrates are already polymerized. The “grafting from” method only relies on the presence of reactive functionality on the substrate polymer, which makes it more attractive. “Grafting from” produces a thick homogeneous polymer layer, and this process is unaffected by the bulkiness of the substrate polymer¹¹⁹. This process furthermore results in a retention of the morphology of the substrate polymer surface and tunability in the mixture of the properties of the substrate and modifier polymer, dependent on the extent of the

modification. This work focuses on the “grafting from” method because of these advantages.

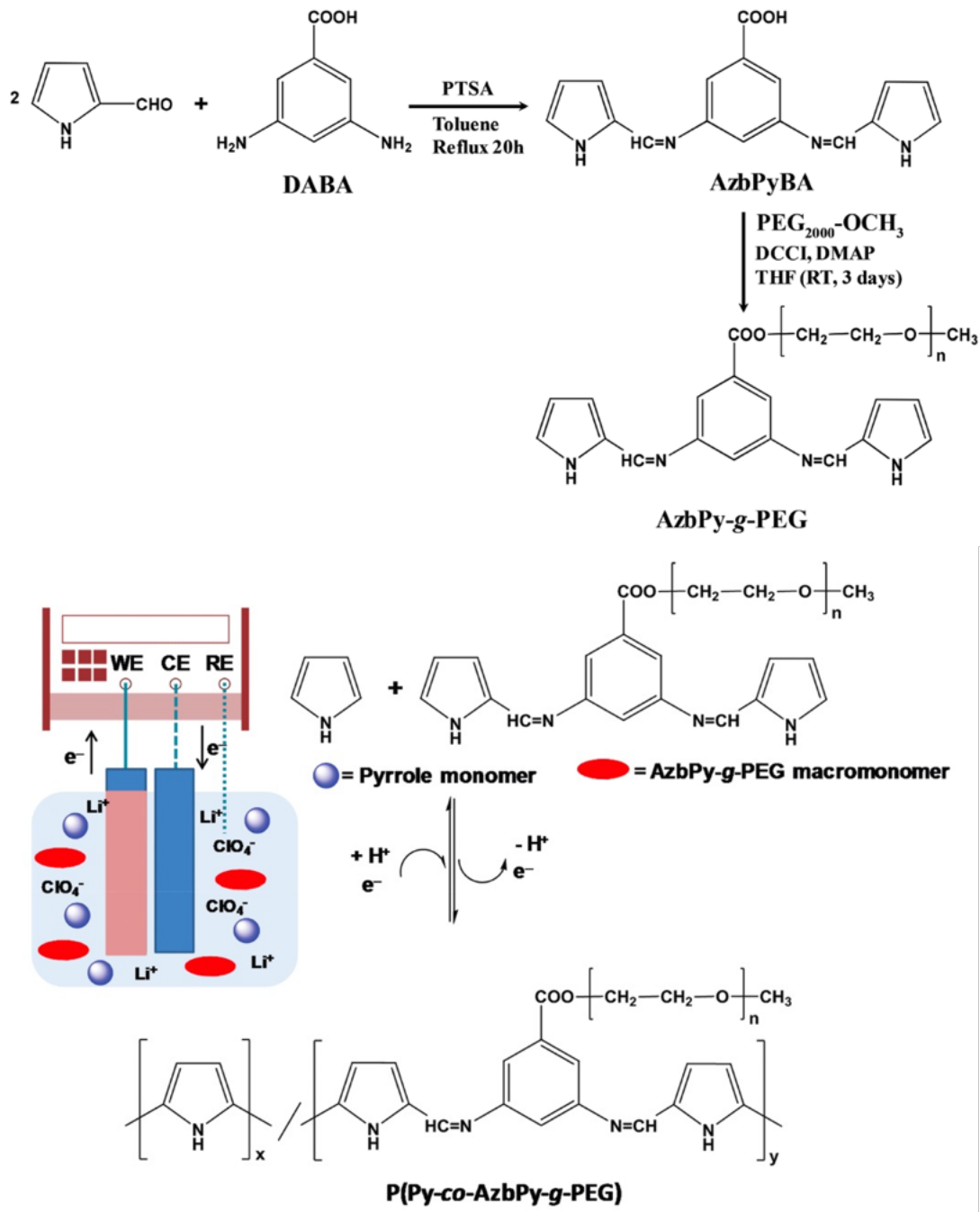
“Grafting from” requires reactive functionality on the substrate, and this can be accomplished by irradiation or plasma treatment to generate reactive species such as radicals, or by direct chemical modification. The former process has the potential to degrade the polymer substrate and can result in side reactions, such as coupling of radicals generated on the surface to accomplish crosslinking. As these have the effect of degrading the desirable properties of electrospun polymers, this work instead relies on the latter process for grafting. Direct chemical modification relies on the presence of reactive pendant functional groups on the surface of the electrospun substrate polymer. Because of these criteria, the polymers chosen for this work are PAN and PMMA, which have a nitrile group and an ester group, respectively, both of which can undergo further reaction to enable “grafting from” via direct chemical modification.

5.1.2 Graft copolymerization considerations and electrospun polymer-ICP graft copolymers

The main factors to be considered when performing a graft copolymerization include the nature of the polymer substrate, the nature of the modifier monomer, and the solvent¹²⁰. The effect of the initiator on the polymer substrate is also a factor, especially if the polymer grafted onto it is grown via atom-transfer radical polymerization. However, for the specific type of graft copolymerization that this work attempts to accomplish, which is the growth of ICPs on the surface of electrospun polymers, the effect of the initiator can be ruled out, since the ICP polymerization occurs via chemical oxidative polymerization. The size, solubility, crystallinity, and intermolecular forces present in the

polymer substrate influence its accessibility and thus its reactivity to modifiers in solution, which in turn influences the rate and extent of grafting. Because chemical reactions are involved, the structure and steric bulk as well as the concentration of the modifier monomers affect grafting. Increasing the concentration of monomers increases grafting efficiency up to a certain limit, over which homopolymerization of the modifier monomer occurs. The solvent has the role of making sure that monomers reach reactive sites in the substrate polymer: solvents which cause swelling in the substrate polymer allow monomers to diffuse more readily into the polymer structure, resulting in more grafting. The solvent should also not have an affinity for scavenging radicals from the subsequent polymer growth step.

There have been examples of grafting ICPs onto polymer substrates. Poly(ethylene glycol) has been modified in solution with Py and then electrochemically polymerized with the addition of more pyrrole units to fabricate an antibacterial device for serotonin detection (Scheme 3)¹²¹.



Scheme 3. Synthesis of Py-modified PEG and subsequent oxidative polymerization. Adapted with permission from ref. 121. Copyright 2018 Royal Society of Chemistry.

Xanthan gum was modified in solution in a two-step process involving reaction with aniline and dopant, and then subsequent polymerization was accomplished with the addition of initiator. The resultant device was then used as an ammonia sensor with a rapid, sensitive response¹²². As of writing, there seems to be no examples of “grafting from” copolymers utilizing both ICPs and electrospun polymers.

Performing graft copolymerization on electrospun substrates presents a whole new list of factors which need to be considered: the sequence of the modification, electrospinning, and polymerization, solubility factors, and extent of grafting. The modification of the substrate polymer with monomer can happen either before or after electrospinning, and can be accomplished either directly (i.e., reaction of monomer with polymer), or in a two-step process (i.e., reaction of monomer with modified polymer), so long as the sequence yields an electrospun substrate which includes the ICP monomer covalently attached to it. The degree of functionalization with monomer is important in modulating the properties of the product, the most important of which is the insolubility of this product in solvents suitable for polymerization and must be tuned as a result. Lowering this concentration would also lead to avoiding homopolymerization, as explained in the beginning of this section. To overcome the limitations presented by blend electrospinning ICPs as discussed in Chapter 3, the actual “grafting from” polymerization of ICPs needs to occur after electrospinning. This polymerization, which for the sake of simplicity can be accomplished via chemical oxidative polymerization, must take place in a two-phase system to preserve the integrity of the electrospun substrate. The electrospun substrate must be suspended in a solution of monomer and oxidant, and not itself dissolve. As discussed at the beginning of this section, this solvent

must allow monomers to diffuse into the polymer structure during polymerization by swelling the polymer. However, too much swelling could also cause a decrease in the electrospun substrate's surface area and porosity.

5.1.3 Scope and limitations of the study

This study aims to synthesize graft copolymers of electrospun PAN and PMMA, and PEDOT, using the “grafting from” method. PAN and PMMA have been chosen because these are commodity polymers that have the necessary chain entanglement to be electrospun directly from solution. Importantly, these polymers also have pendant functional groups that can be reacted further. PEDOT has been chosen because of the ease in modification of the ethylene bridge of the monomer EDOT with functional groups that can react with the pendant functional groups in PAN and PMMA, or groups that these functional groups can easily be transformed into. Two methods are explored in the modification of PAN: direct reaction with amine-modified EDOT, and hydrolysis and subsequent reaction with amine- and alcohol-modified EDOT. PMMA modification through amidolysis with amine-modified EDOT is also explored.

5.2 Materials and Methods

5.2.1 Materials

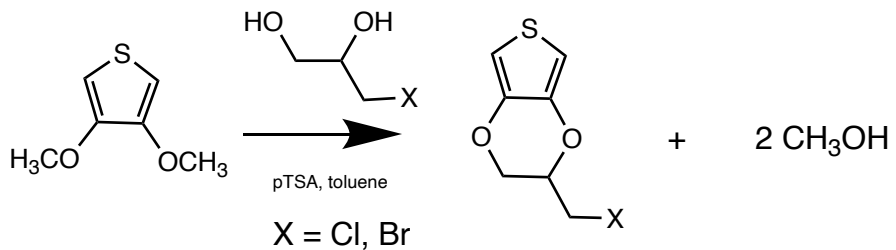
3,4-Dimethoxythiophene was obtained from Ambeed. (+/-) 3-Chloro-1,2-propanediol, 98% was obtained from Alfa Aesar. Sulfuric acid (Certified ACS plus) was obtained from Fisher Scientific. Hydrochloric acid (ACS grade, 36.5-38%) was obtained from VWR chemicals. p-Toluenesulfonic acid monohydrate was obtained from TCI Chemicals. Triphenylphosphine (PPh_3) (99%), toluene (99.85%, extra dry over molecular sieves), and diethyl ether (99% pure) were obtained from Acros Organics. Sand (washed

and dried) was obtained from Mallinckrodt. Silica gel (60-200 mesh) was obtained from Sigma Aldrich. Molecular sieves (4Å, grade 514) and hexanes were obtained from Macron Fine Chemicals. Magnesium sulfate ($MgSO_4$) (anhydrous) was obtained from Fisher Chemical. Sodium azide (NaN_3) (99%) was obtained from Beantown Chemicals. Borate buffer (pH=9.0) was obtained from Electron Microscopy Sciences. DMF (Drisolv, anhydrous) and THF (Drisolv, anhydrous) were obtained from EMD Millipore. Dichloromethane (ACS reagent, stabilized with amylene, 99.6%) was obtained from Thermo Scientific. All reagents were used without purification.

5.2.2 *Instrumentation*

ATR-IR analysis was done using a Bruker Tensor II FT-IR Spectrometer with a Harrick SplitPea™ Attenuated Total Reflectance accessory. NMR analysis was done using a Bruker Avance III 400 MHz NMR. Both instruments are in the Department of Chemistry and Biochemistry at the Texas State University.

5.2.3 *Synthesis of modified EDOTs*



Equation 7. Synthesis of halomethyl EDOTs

5.2.3.1 Synthesis of 2-(Bromomethyl)-2,3-dihydrothieno[3,4-b][1,4]dioxine (EDOT-MeBr)

EDOT-MeBr was synthesized via acid-catalyzed transesterification following literature (Equation 7)³⁸. A Soxhlet extraction setup was used with 4Å molecular sieves. In a three-necked round bottom flask, 3,4-Dimethoxythiophene (4.10 g, 28.4 mmol), 3-Bromo-1,2-propanediol (11.10 g, 71.62 mmol), and p-Toluenesulfonic acid (0.80 g, 4.7 mmol) were dissolved in 300 mL of dry toluene and stirred at 100 °C for 48 h under flowing argon. Afterwards, the mixture was allowed to cool to room temperature, and then extracted three times with saturated Na₂CO₃ and three times with deionized water. The organic phase was then dried with MgSO₄. Afterwards, the drying agent was filtered out, and toluene was removed under reduced pressure. The crude mixture was then filtered through a short plug with silica gel as the stationary phase and heptane as the mobile phase. The final product was yellowish oil (1.18 g, 5.01 mmol) in 27% yield. ¹H NMR (250 MHz, CDCl₃, ppm): δ obtained from literature³⁸ = 3.4-3.6 (m, 2H, CH₂-Br); 4.44 (m, 3H, O-CH₂-CH-O); 6.36/6.37 (dd, 2H, S-CH). Found (400 MHz, CDCl₃, ppm): 3.51 (m, 2H); 4.22 (m, 3H); 6.35 (dd, 2H).

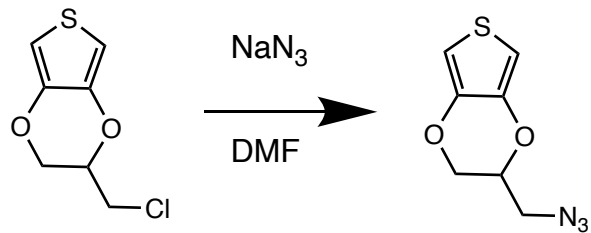
5.2.3.2 Synthesis of 2-(Chloromethyl)-2,3-dihydrothieno[3,4-b][1,4]dioxine (EDOT-MeCl)

EDOT-MeCl was synthesized via acid-catalyzed transesterification following a literature procedure (Equation 7)¹²³. A Soxhlet extraction setup was used with 4Å molecular sieves. In a three-necked round bottom flask, 3,4-Dimethoxythiophene (5.77 g, 40.0 mmol), 3-Chloro-1,2-propanediol (9.81 g, 88.7 mmol), and p-Toluenesulfonic acid (0.68 g, 4.0 mmol) were dissolved in 100 mL of dry toluene and stirred at 90 °C for 24 h

under flowing argon. Afterwards, 3-Chloro-1,2-propanediol (9.92 g, 89.7 mmol) was added again, and the reaction was left to stir for 3 h. The mixture was then allowed to cool to room temperature, and then toluene was allowed to evaporate at reduced pressure. A small amount of dichloromethane was then added to dissolve solid and high-viscosity liquid residues. The crude product was then subjected to flash chromatography with silica gel as the stationary phase and 4:1 (v:v) hexane:dichloromethane as the mobile phase. The final product was white solid (3.07 g, 16.1 mmol) in 40% yield. ^1H NMR (400 MHz, CDCl_3 , ppm): δ obtained from literature¹²³ = 6.37 (s, 2H, S-CH), 4.35–4.40 (m, 1H, O-CH₂), 4.27–4.35 (m, 1H, O-CH₂), 4.14–4.18 (m, 1H, CH-O), 3.65–3.75 (m, 2H, CH₂-Cl). Found (400 MHz, CDCl_3 , ppm): 6.36 (s, 2H), 4.37 (m, 1H), 4.28 (m, 1H), 4.18 (m, 1H), 3.70 (m, 2H). Because of significantly higher yields and less expensive starting materials, EDOT-MeCl was used in the succeeding experiments.

5.2.3.3 Synthesis of 2-(Azidomethyl)-2,3-dihydrothieno[3,4-*b*][1,4]dioxine (EDOT-*MeN*₃)

EDOT-*MeN*₃ was synthesized via SN_2 reaction following literature (Equation 8)¹²⁴. The reaction was performed in a reflux setup using EDOT-Cl.

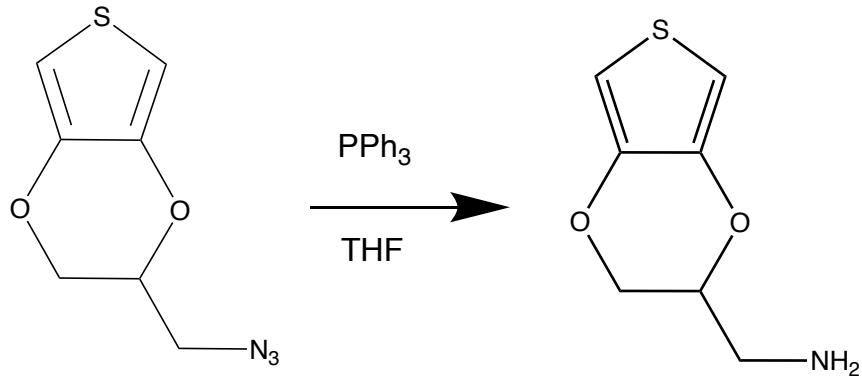


Equation 8. Synthesis of EDOT-*MeN*₃ from EDOT-Cl

In a three-necked round bottom flask, EDOT-MeCl (1.52 g, 7.97 mmol) and NaN₃ (0.55 g, 8.4 mmol) were dissolved in 65 mL dry DMF. The reaction mixture was then stirred at 120 °C for 3 h under flowing argon. The organic fractions were collected, and then washed three times with water. The mixture was then dried with MgSO₄. Lastly, the diethyl ether was removed under reduced pressure. The final product was yellow oil (1.50 g, 7.63 mmol) in 96% yield. ¹H-NMR (300 MHz, CDCl₃, ppm): δ obtained from literature¹²⁴ = 6.36 (d, 2H, CH-S), 4.30 (m, 1H, CH-O), 4.18 (dd, 1H, CH₂-O), 4.04 (dd, 1H, CH₂-O), 3.56 (dd, 1H, CH₂-N₃), 3.47 (dd, 1H, CH₂-N₃). Found (400 MHz, CDCl₃, ppm): 6.36 (d, 2H), 4.31 (m, 1H), 4.18 (m, 1H), 4.03 (m, 1H), 3.53 (m, 2H).

5.2.3.4 Synthesis of 2-(Aminomethyl)-2,3-dihydrothieno[3,4-b][1,4]dioxine (EDOT-MeNH₂)

EDOT-MeNH₂ was synthesized via Staudinger reduction following literature (Equation 9)³⁹.



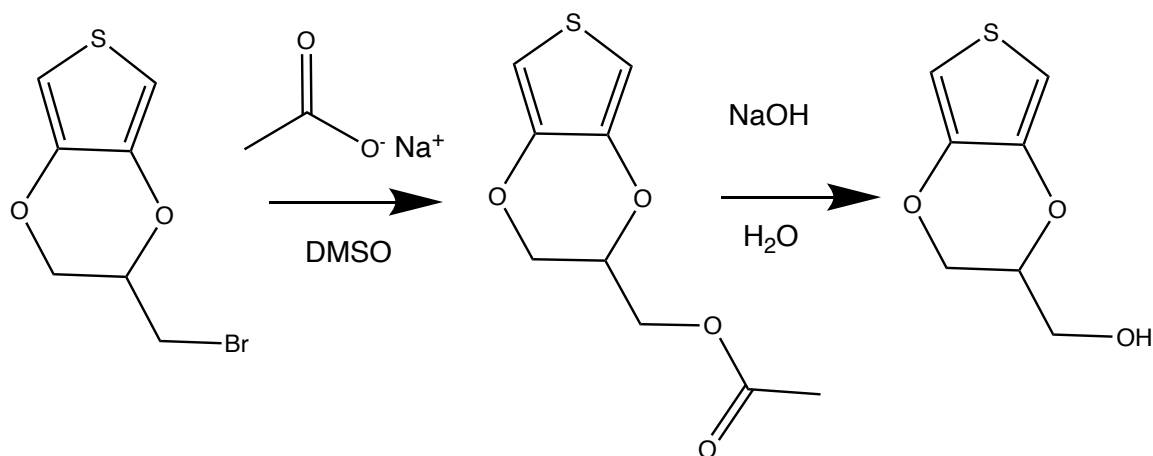
Equation 9. Synthesis of EDOT-MeNH₂ from EDOT-MeN₃

The reaction was done in a reflux setup. In a three-necked round bottom flask, EDOT-MeN₃ (0.51 g, 2.6 mmol) and PPh₃ (0.81 g, 3.1 mmol) were dissolved in 15 mL dry THF and stirred at 50 °C for 1 h under flowing argon. 25 mL 2M NaOH was then added, and then the mixture was left to react for 2 h more. Afterwards, the mixture was

allowed to cool to room temperature. Concentrated HCl was then added dropwise to the mixture to lower its pH to <3. Then, THF was removed under reduced pressure. Triphenylphosphine oxide was removed by washing the mixture three times with dichloromethane. The mixture was then basified with 2M NaOH to pH >10. Afterwards, the mixture was extracted three times with dichloromethane. The organic fractions were then dried with MgSO₄. Dichloromethane was then removed under reduced pressure. The product was yellow oil (0.38 g, 2.2 mmol) in 85% yield. ¹H NMR (400 MHz, CDCl₃, ppm): δ obtained from literature³⁹= 6.36/6.34 (dd, 2H, S-CH); 4.25-4.0 (m, 3H, O-CH₂-CH-O); 3.0-2.9 (m, 2H, CH₂-N), 1.5 (broad s, 2H, NH₂). Found (400 MHz, CDCl₃, ppm): 6.32 (d, 2H); 4.21-4.01 (m, 3H); 2.97 (m, 2H); 1.32 (broad s).

5.2.3.5 Synthesis of 2-(Hydroxymethyl)-2,3-dihydrothieno[3,4-b][1,4]dioxine (EDOT-MeOH)

EDOT-MeOH was synthesized via S_N2 reaction followed by ester hydrolysis (Equation 10)¹²³.



Equation 10. Synthesis of EDOT-MeOH from EDOT-MeBr

A reflux setup was used for the reaction. In a three-necked round bottom flask, EDOT-MeBr (0.93 g, 4.3 mmol) and sodium acetate (0.65 g, 8.0 mmol) were dissolved in 30 mL of DMSO. The mixture was then stirred at 120 °C for 1 h under flowing argon. Afterwards, the mixture was allowed to cool to room temperature. Then, the mixture was added to 50 mL deionized water. The mixture was then extracted three times with dichloromethane. Dichloromethane was then removed under reduced pressure, yielding yellow oil (0.93 g, 4.3 mmol), which is the acetate-functionalized EDOT or EDOT-MeOAc. This was then used in the next step without purification. In another three-necked round bottom flask, all the yellow oil synthesized from the previous step was dissolved in 20 mL water together with NaOH pellets (0.68 g, 17 mmol). The mixture was then stirred at 100 °C for 1 h under flowing argon. Afterwards, the mixture was cooled to room temperature. 10 mL of water was then added, and then concentrated HCl was added dropwise until the pH of the solution was <7. The mixture was then extracted three times with dichloromethane. The organic fractions were then dried with MgSO₄, filtered, and then dichloromethane was removed under reduced pressure. The crude product was then filtered through flash chromatography with silica gel as the stationary phase and hexane:dichloromethane (4:1, v:v) as the mobile phase. The solvent was then removed under reduced pressure to yield a yellowish oil product (0.33 g, 2.0 mmol) at 45% yield. ¹H-NMR (400 MHz, CDCl₃, ppm): δ obtained from literature¹²³= 6.34 (s, 2H, S-CH), 4.24 (d, 2H, O-CH₂), 4.07–4.12 (m, 1H, CH-O), 3.84–3.87 (m, 2H, CH₂-OH). Found (400 MHz, CDCl₃, ppm): 6.34 (d, 2H), 4.23 (d, 2H), 4.11 (m, 1H), 3.86 (m, 2H).

5.2.4 Polymer modification

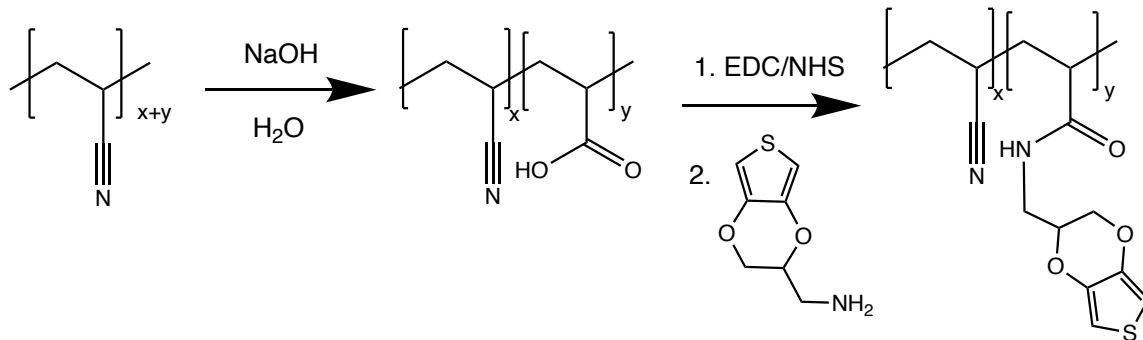
5.2.4.1 PAN modification

PAN modification was attempted using two methods: reaction of modified EDOTs with hydrolyzed PAN, and direct reaction with EDOT-MeNH₂.

5.2.4.1.1 PAN modification via hydrolysis and EDC/NHS coupling

The first group of attempts to modify PAN are two-step processes: first, PAN was base hydrolyzed following the scheme in Equation 4. Afterwards, modified EDOTs were reacted to HPAN/PAN-co-PAA.

A literature procedure for esterifying brushes of poly(acrylic acid) (PAA) with L-leucine methyl ester¹²⁵ was adapted for the amidation of HPAN/PAN-co-PAA (Equation 11).



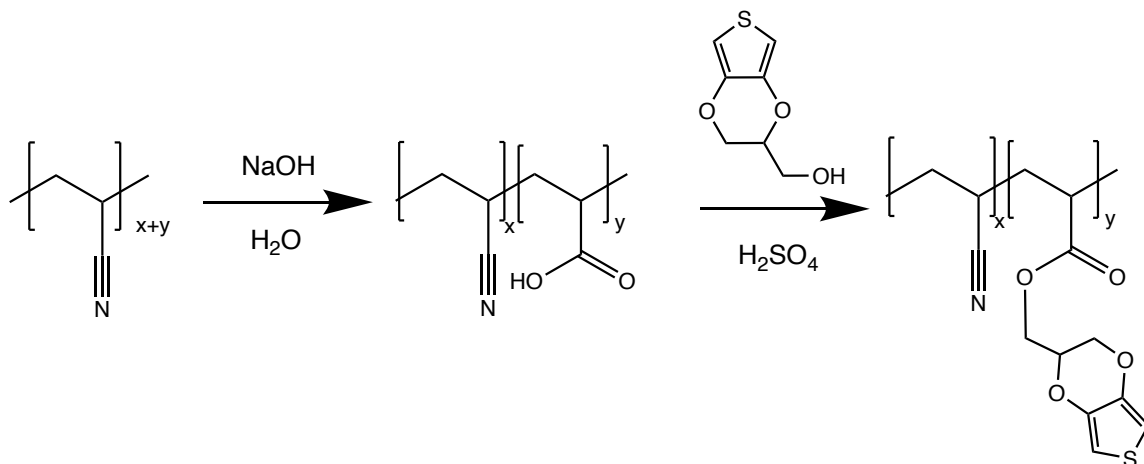
Equation 11. Reaction of EDOT-MeNH₂ with HPAN via EDC/NHS coupling

This reaction was performed in a 20 mL scintillation vial. HPAN powder/PAN-co-PAA (0.1 g) was suspended in 10 mL of a mixture of 0.1M EDC and 0.2M NHS in deionized water and left to stir for 1h at room temperature. Afterwards, the powder was filtered out, washed extensively with deionized water, and air dried. Next, this powder was suspended in 10 mL of a solution of 0.1mM EDOT-MeNH₂ in borate buffer, with the pH adjusted to 10. This mixture was left to stir for 1 h at room temperature. Lastly, the

powder was filtered out, washed extensively with deionized water, and air dried for 1 day. The reaction yielded orange-colored solid (0.1 g). This product was dissolved in DMF-d₇ for ¹H NMR analysis. ¹H-NMR (400 MHz, DMF-d₇, ppm): δ= 6.55 (d, EDOT S-CH), 4.35 (m, EDOT O-CH₂), 4.11 (m, EDOT CH-O), 3.99 (m, EDOT CH₂-N), 3.63 (broad, EDOT N-H), 3.32 (d, PAN CH-CN), 2.68 (m, PAN-co-PAA/PAN-co-PAA-graft-EDOT-MeNH₂ CH-C=O), 2.27 (s, PAN CH₂), 1.79 (m, PAN-co-PAA/PAN-co-PAA-graft-EDOT-MeNH₂ backbone CH₂).

5.2.4.1.2 PAN modification via hydrolysis and Fischer esterification

Fischer esterification was used to react hydrolyzed electrospun PAN (HePAN) /PAN-co-PAA with EDOT-MeOH (Equation 12).



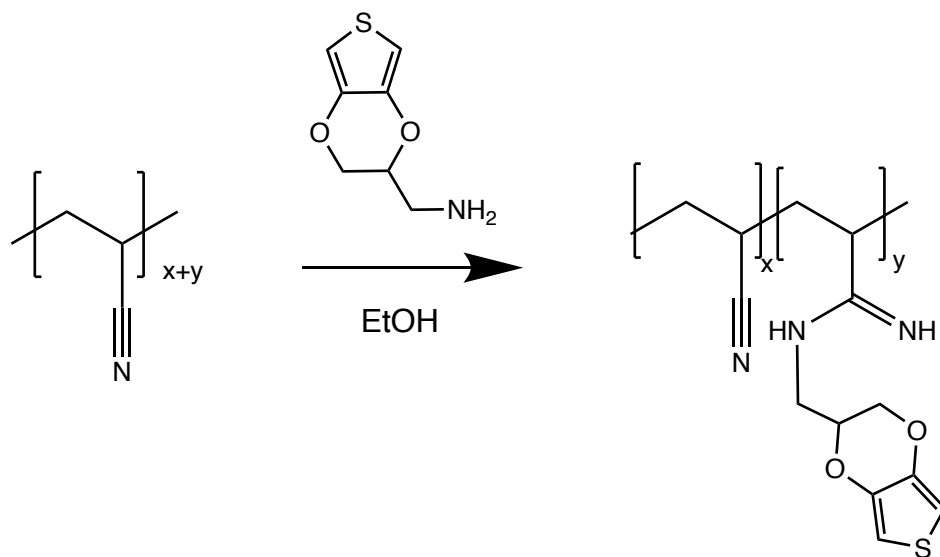
Equation 12. Reaction of EDOT-MeOH with HePAN via Fischer esterification

This reaction was performed in a reflux setup comprised of a three-necked round bottom flask outfitted with a Dean-Stark trap and a high efficiency condenser. For this reaction, 1 cm x 1 cm squares of HePAN were used instead of hydrolyzed PAN powder. HePAN (0.01 g), EDOT-MeOH (0.1 g, 0.6 mmol), and H₂SO₄ (0.001 g, 0.01 mmol) were mixed in 10 mL of dry toluene. The mixture was allowed to react without stirring at 100 °C for 24 h under flowing argon. Afterwards, the fibers were filtered out and washed

extensively with toluene to remove unreacted EDOT-MeOH, and air dried for 1 day. The reaction yielded black squares (0.001 g). This was subjected to ATR-IR analysis without further modification.

5.2.4.1.3 PAN modification via direct reaction

The second group of attempts to modify PAN involved direct reaction with EDOT-MeNH₂ (Equation 13), adapting a previously-reported modification of PAN with ethylenediamine⁶⁹.



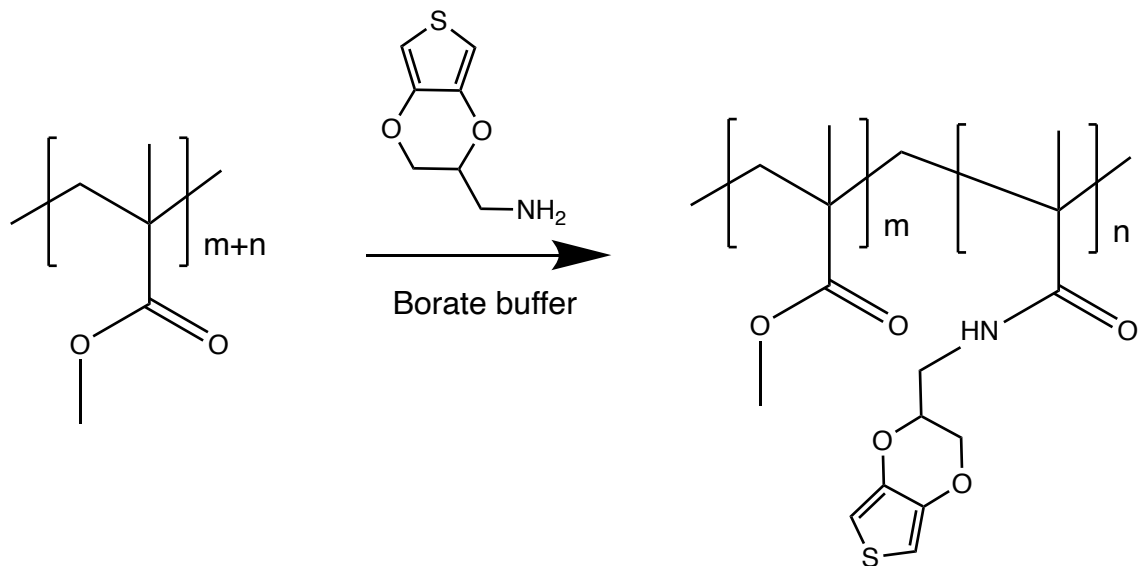
Equation 13. Direct reaction of PAN with EDOT-MeNH₂

This reaction was performed in a 20mL scintillation vial. PAN (0.01 g) in powder form was mixed with (0.1 g, 0.6 mmol) of EDOT-MeNH₂ in 10 mL of 95% EtOH in water. The reaction was stirred at 70 °C for 12 h under flowing argon. Afterwards, the reaction was allowed to cool to room temperature. PAN-graft-EDOT-MeNH₂ was then filtered out and washed with an excess of EtOH to remove unreacted EDOT-MeNH₂. The product was brownish solid (0.01 g), which was dissolved in DMF-d₇ for ¹H NMR analysis. ¹H-NMR (400 MHz, DMF-d₇, ppm): δ= 8.37 (s, EDOT =N-H), 6.56 (dd, EDOT

S-CH), 4.00-4.20 (broad, EDOT O-CH₂-CH-O, CH₂-N), 3.32 (d, PAN CH-CN), 2.27 (s, PAN CH₂), 2.12 (s, PAN-graft-EDOT CH-C=N), 1.28 (s, PAN-graft-EDOT-MeNH₂ NH).

5.2.4.2 PMMA modification

PMMA was amidolyzed with EDOT-MeNH₂ (Equation 14) adapting a reported procedure on the modification of PMMA surfaces with hexamethylenediamine¹²⁶.



Equation 14. Amidolysis of PMMA with EDOT-MeNH₂

This reaction was performed in a 20 mL scintillation vial. PMMA powder (0.01 g) and (0.07 g, 0.4 mmol) of EDOT-MeNH₂ were suspended in 10 mL borate buffer with pH adjusted to 11.5. This mixture was stirred at room temperature for 2 h. Afterwards, the powder was filtered out and washed extensively with EtOH to remove residual unreacted EDOT-MeNH₂, and air dried for 1 day. The resultant product was orange-colored solid (0.01 g), which was dissolved in CDCl₃ for ¹H NMR analysis, and then cast into a film for ATR-IR analysis. ¹H-NMR (400 MHz, CDCl₃, ppm): δ= 6.37 (d, EDOT S-CH), 3.93-4.38 (m, EDOT O-CH₂-CH-O), 3.60 (s, PMMA O-CH₃), 2.97 (s, EDOT CH₂-

N), 1.82-1.95 (m, PMMA/PMMA-graft-EDOT-MeNH₂ CH₃), 1.75 (b, EDOT NH), 0.85-1.02 (d, PMMA backbone CH₂).

5.3 Results and Discussion

5.3.1 *Modified EDOTs*

As can be observed from Figure 63 and Figure 64, EDOT-MeBr and EDOT-MeCl were successfully synthesized via acid-catalyzed transesterification following literature procedures, with the relevant peaks labeled. There are either separate peaks for each hydrogen in the ethylene bridge of the modified EDOTs or they are coupled in complex patterns. This is consistent with the 3D models of modified EDOTs, which are not completely planar. There also are peaks corresponding to toluene and hexane, which are to be expected since these correspond to the solvent for the reaction and the mobile phase for the chromatography step, respectively. Water is also seen, which is a pervasive contaminant in organic reactions. It can also be noticed that the percent yields of these reactions are quite low: 27% for EDOT-MeBr and 40% yield for EDOT-MeCl. These yields are somewhat lower than literature yields: 37% for EDOT-MeBr³⁸ and 62% yield for EDOT-MeCl¹²³.

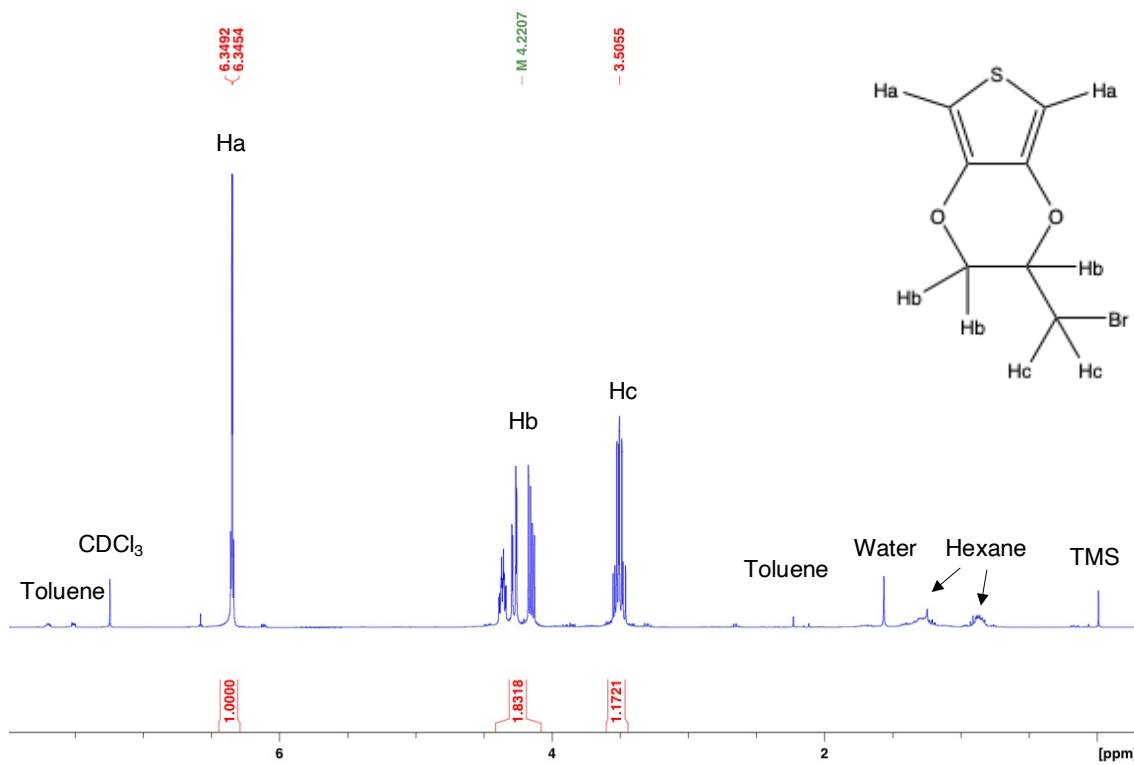


Figure 63. ^1H NMR of synthesized EDOT-MeBr

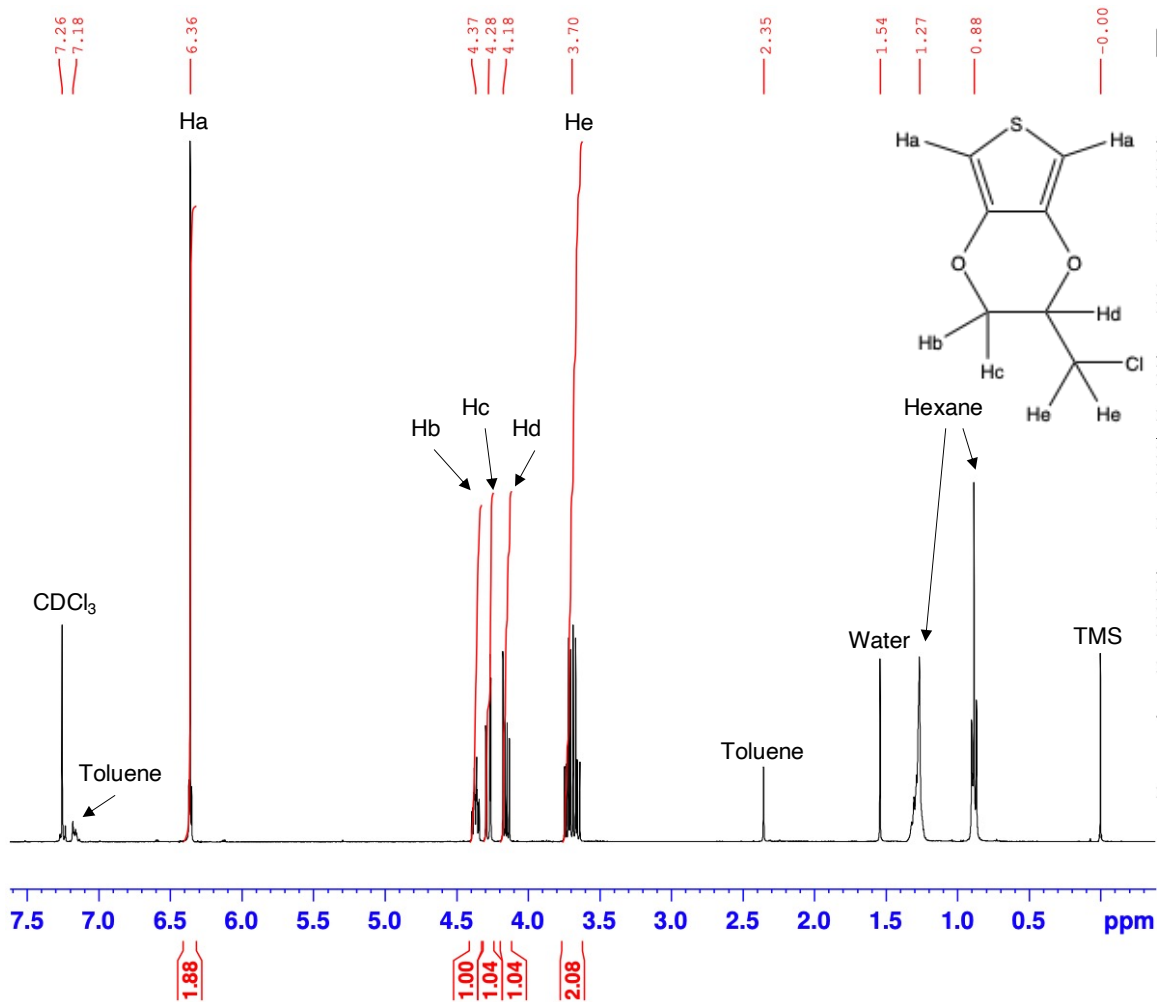
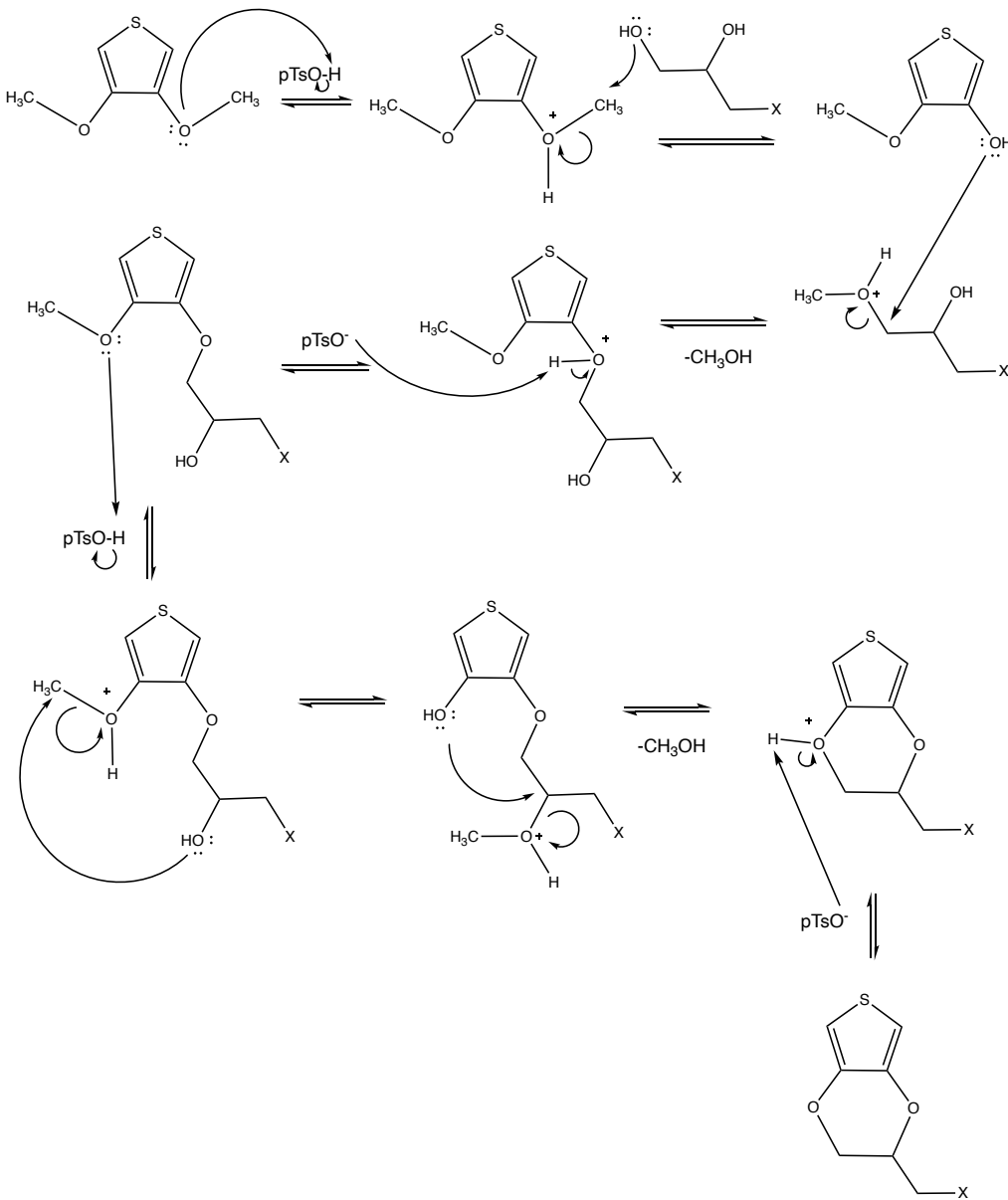


Figure 64. ^1H NMR of synthesized EDOT-MeCl

Scheme 4 below gives a proposed mechanism for this reaction, which has not yet been elucidated in literature but has been proposed by a previous thesis from our laboratory⁷⁵.



Scheme 4. Proposed mechanism of acid-catalyzed transesterification of 3,4-dimethoxythiophene with 3-halo-1,2-propanediols

The proposed mechanism gives insights into what may be responsible for the low yields. Firstly, the presence of the electron-withdrawing halogen functionality in the diol may be exhibiting the inductive effect and reduce the nucleophilicity of the hydroxyl group which attacks the oxygen of the ether group in the thiophene molecule in the second step of the mechanism. Second, looking at the sixth step of the mechanism, it is

possible that the other oxygen In the ether group of the thiophene molecule attacks a carbon in another molecule of the diol instead of doing an intramolecular attack as shown here. Although the reaction was performed in an inert atmosphere, polymerization may still have happened between any of the combinations of the starting material, the desired end-product EDOT-MeCl/Br, and any of the side products mentioned above. This is evidenced by the presence of insoluble material in the reaction mixture as well as the presence of substances which stick and do not come out of the column during the final step of purification of the product. The Irvin research group and others have attempted to increase the percent yield of this reaction using Soxhlet extraction to continuously remove the byproduct MeOH from the reaction mixture and favor the formation of more product as per Le Chatelier's principle. It is possible that a higher percent yield may still be reached at higher temperatures to extract more MeOH from the mixture, although this runs the risk of polymerizing the reaction mixture contents even further. Interestingly, a relatively-high yield of 72% has been reported in the synthesis of EDOT-MeCl in the literature with the addition of the inhibitor 2,6-di-tert-butyl-4-methylphenol¹²⁴, although this creates the new problem of having to remove this from the reaction mixture. As has been noted in section 5.2.2, because of the significantly higher yields and less expensive starting materials, it was decided to use EDOT-MeCl for further reactions.

Figure 65 shows the ¹H NMR spectrum of the EDOT-MeN₃ synthesized in this study. As has been noted in Figure 65, all the peaks reported in literature are present, suggesting that the azide-functionalized EDOT has been successfully synthesized. The product also contains traces of the solvents mentioned in the previous paragraph as well as DMF, which is to be expected as the reaction was conducted in this solvent.

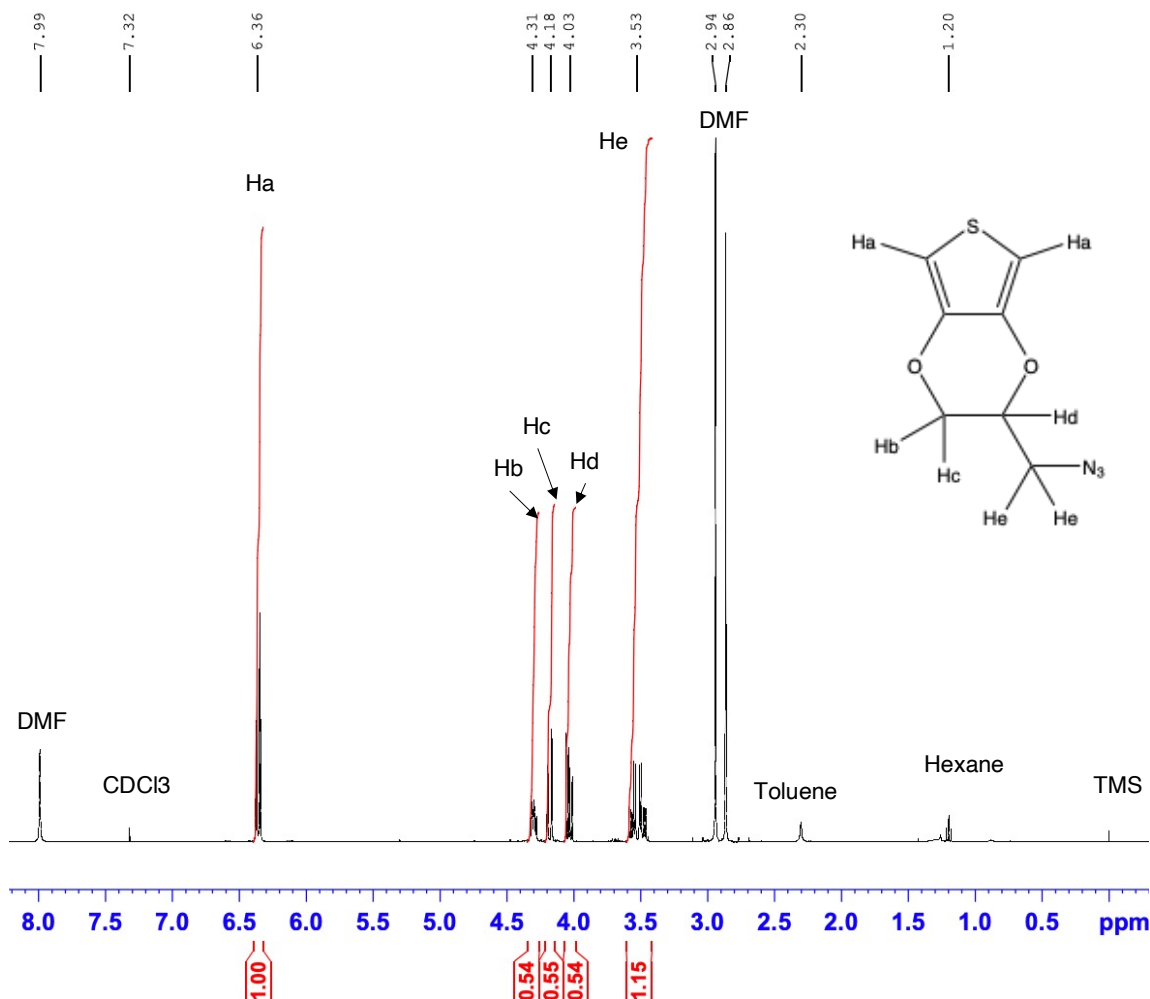
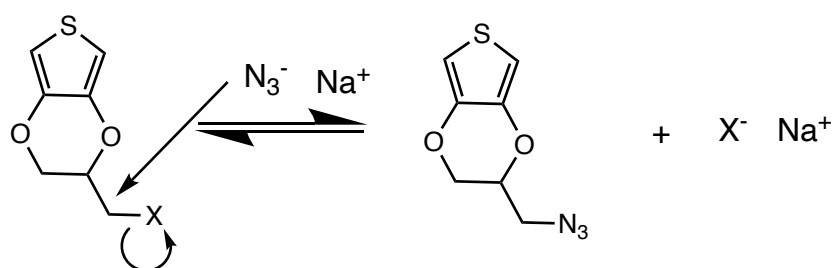


Figure 65. ^1H NMR of synthesized EDOT- MeN_3

The percent yield for this reaction has been high at 96%, comparable to a literature-reported yield of 97%³⁸. This can be explained by looking at the proposed mechanism for this reaction shown in Scheme 5 below.



Scheme 5. Proposed EDOT- MeN_3 synthesis mechanism

As can be observed, this is a simple S_N2 reaction. The good yield can be explained by the formation of NaCl/NaBr salt, which is insoluble in the DMF solvent used in this reaction. As in the previous paragraph, the precipitation of this byproduct from the reaction mixture results in the formation of more product, as per Le Chatelier's principle.

EDOT-MeOH has been successfully synthesized, as evidenced by the ¹H NMR shown in Figure 66. Interestingly, although the NMR analysis was performed in CDCl₃, the literature-reported synthesis of EDOT-MeOH does not report ¹H NMR shifts attributed to the hydroxyl hydrogen, which is understandable given the exchange of these hydrogens with the solvent. There is a faint broad peak at around 1.75 ppm which is possibly this very hydrogen. Further experiments could ascertain the identity of this peak; for example, the spectrum of EDOT-MeOH could be taken at different temperatures, or D₂O could be added to the NMR solution prior to spectral acquisition.

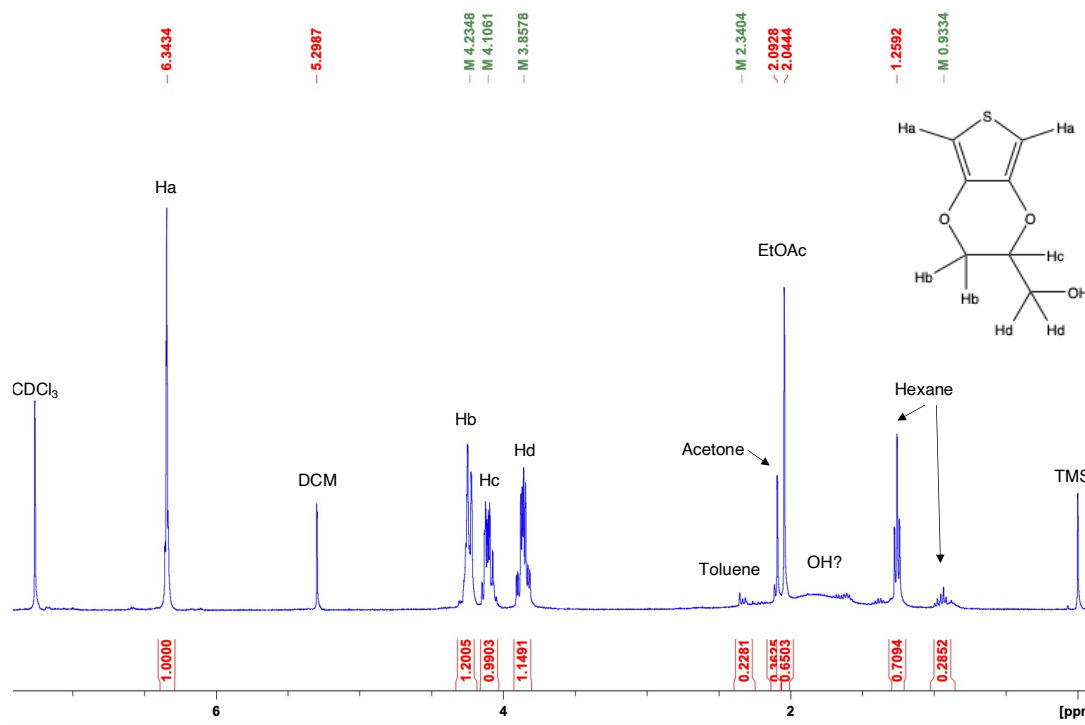
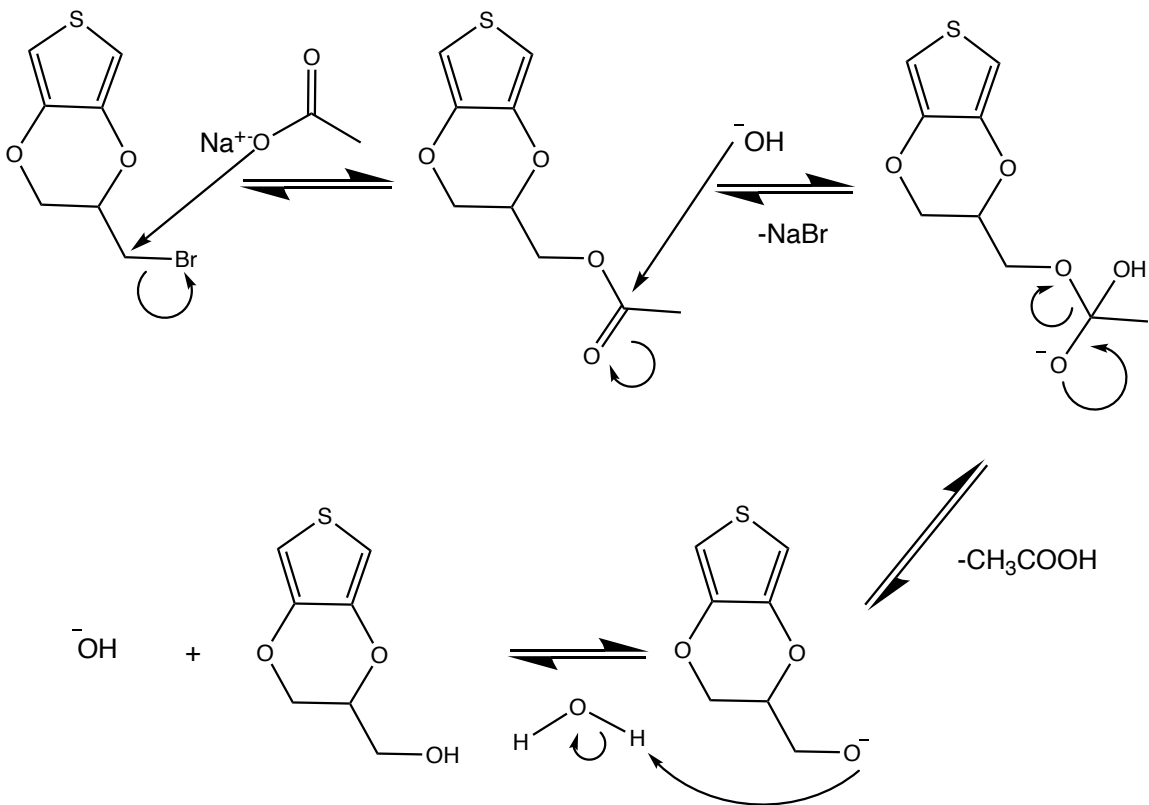


Figure 66. ¹H NMR of synthesized EDOT-MeOH

The overall yield for the two-step conversion of halomethyl EDOT to EDOT-MeOH is at a low 45% compared to the literature reported value of 85%¹²³. This may be because the synthesized EDOT-MeOAc in the first step may not have been measured correctly and may still have contained solvent DMSO. Scheme 6 below shows a proposed mechanism for the synthesis of EDOT-MeOH, involving an S_N2 reaction where acetate displaces the halogen in the modified EDOT, followed by base hydrolysis of the ester.



Scheme 6. Proposed EDOT-MeOH synthesis mechanism

If, for example, not enough base was added in the second step because of an error in measuring the synthesized intermediate, then a significant amount of unreacted EDOT-MeOAc may be present in the reaction mixture. This would drive down the yield significantly. It should be noted that the reaction was conducted in DMSO, a high-boiling solvent. It might be possible to completely remove DMSO via vacuum distillation for future syntheses, but it is possible that the high temperatures required for DMSO removal might result in product decomposition. Instead, DMSO could replace other, lower-boiling polar aprotic solvents, such as DMF.

EDOT-MeNH₂ has been successfully synthesized, as evidenced by the ¹H NMR spectrum shown in Figure 67. Interestingly, there seems to be a signal for the amine hydrogens which appears as a broad peak at 1.32 ppm. This may be further proof that hydrogen-bonding hydrogens in modified EDOTs do appear in their ¹H NMR spectra in CDCl₃. There also is an unknown trace contaminant at 2.61 ppm.

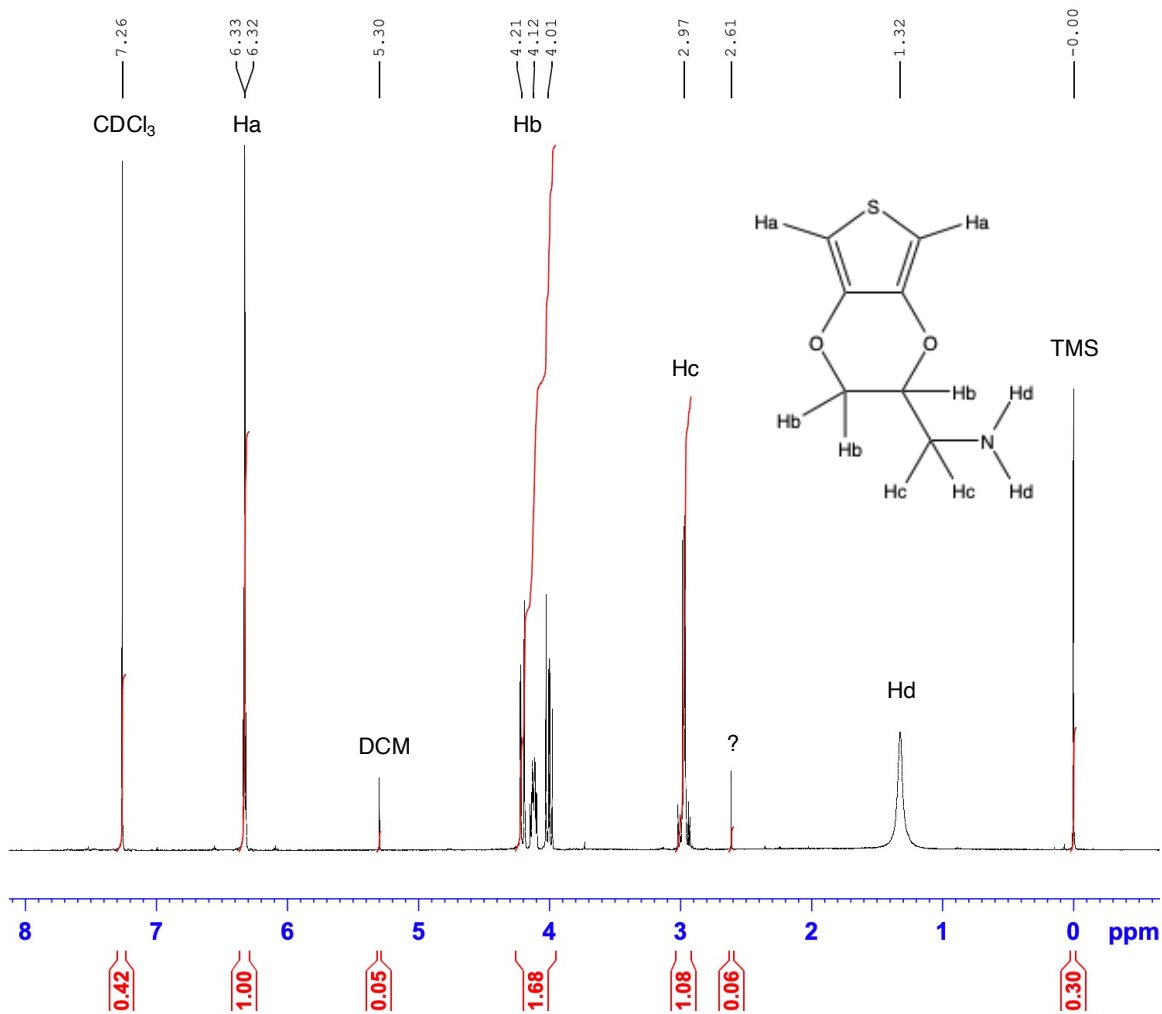
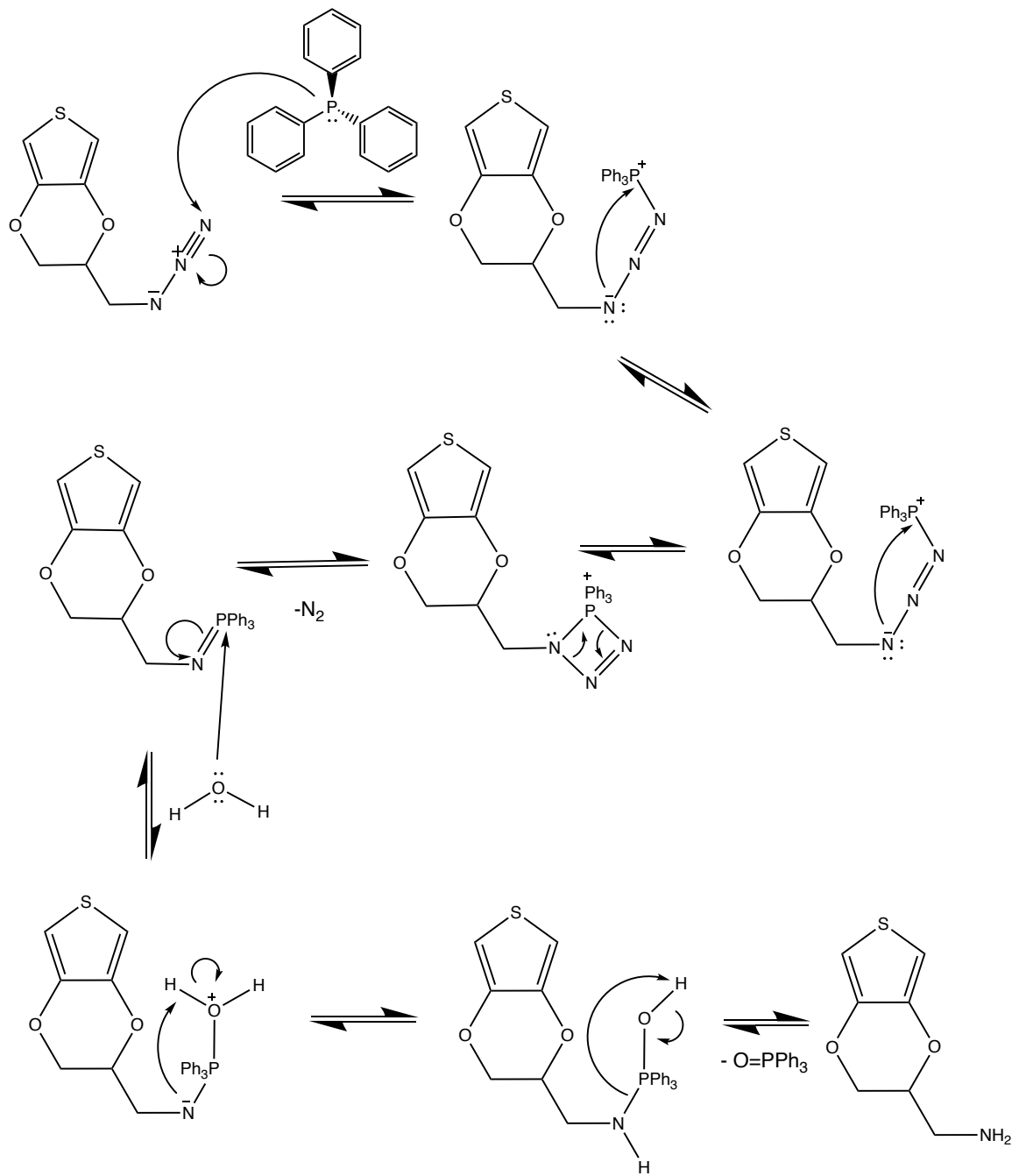


Figure 67. ¹H NMR of synthesized EDOT-MeNH₂

This reaction had a high yield of 85%, although there is no literature-reported yield to compare this with. Scheme 7 below shows the proposed mechanism for this Staudinger reduction.



Scheme 7. Proposed mechanism for the reduction of EDOT-MeN₃ into EDOT-MeNH₂

5.3.2 *Polymer modification*

In the modification of electrospun polymers, combinations of electrospinning then reacting and reacting then electrospinning were explored. In the first case, the electrospun polymer is suspended in a solvent that does not dissolve it, but dissolves modified EDOTs completely. After modification, the polymer grafted with monomer should remain in solid, nanofibrous form for the actual “grafting from” polymerization. Because of solubility problems encountered in experiments using this method, as will be explained below, it was decided to also attempt the reverse process, reacting then electrospinning. In this method, polymer powder is suspended in a solvent that dissolves the modified EDOTs completely.

5.3.2.1 *Surface PAN modification via hydrolysis and esterification*

The first method used in grafting PAN was using alkaline hydrolysis in aqueous solution. The first attempt to accomplish this reaction involved hydrolysis of electrospun PAN samples following a literature-reported procedure⁶⁰. The attempt to hydrolyze electrospun PAN with retention of solidity and nanofibrous form was successful, and this solid had an ATR-IR spectrum as shown in Figure 68. It can be observed that there are indicators of the presence of carboxylic acid groups: the appearance of a broad strong O-H or N-H stretch centered at 3368 cm⁻¹, the strengthening of the C=O stretch at 1667 cm⁻¹, and the appearance of an absorption at 1561 cm⁻¹, which can be attributed to the amine N-H bending. In addition, the attenuation of the nitrile stretch at 2244 cm⁻¹ can also be observed. It should also be noted that, as per the discussion of electrospun HPAN as described section 2.3.1, there are amine, amide, and imine groups present; however, the literature-reported procedures cited have stated that the reaction conditions reported have

been optimized to accomplish the conversion of nitrile groups into carboxylic acid groups. All in all, these indicate that PAN-co-PAA has been formed.

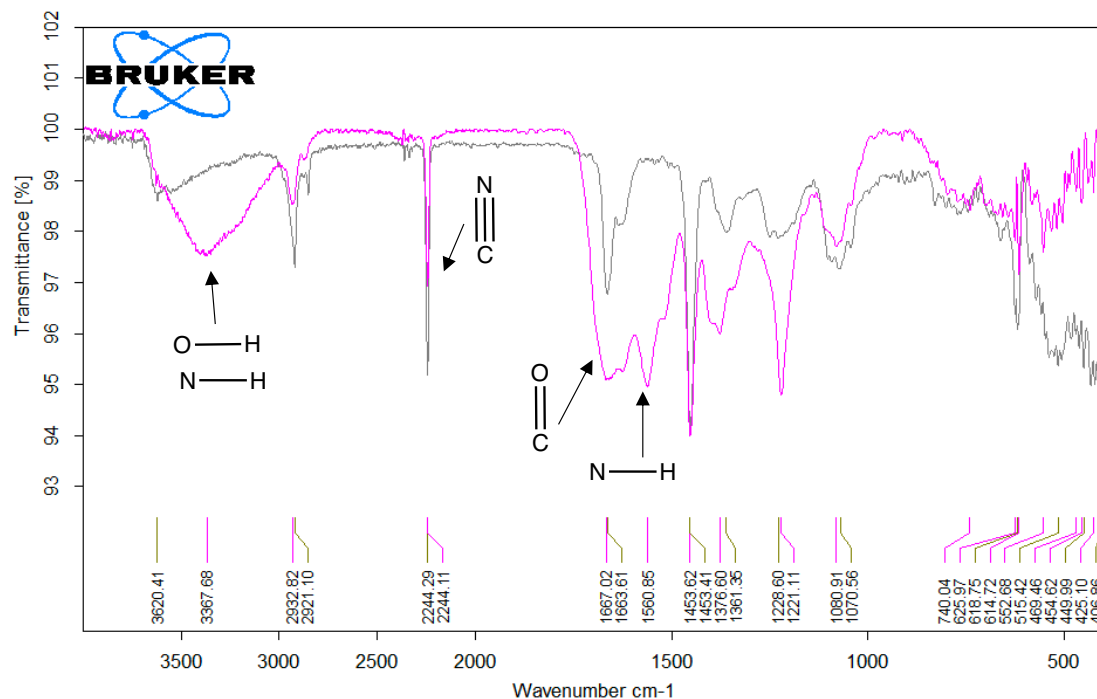


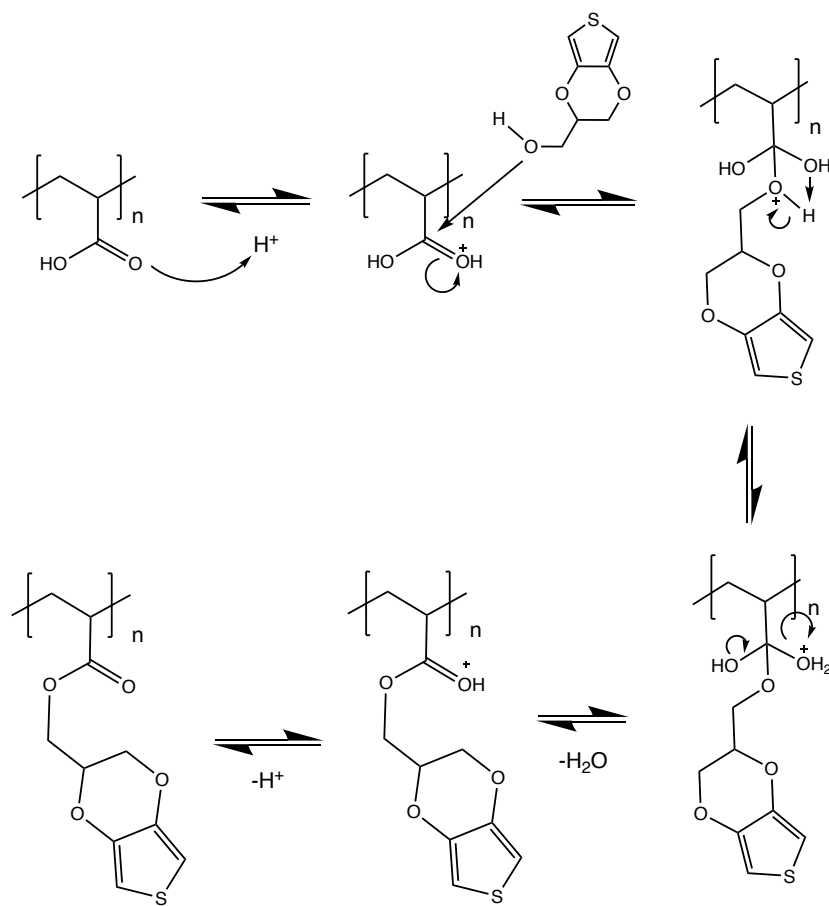
Figure 68. ATR-IR spectrum of PAN (grey) and base-hydrolyzed PAN (pink)

Because of this, it was decided that this hydrolyzed electrospun PAN (HePAN) was to be used in the next step of modification, which is the actual grafting of the modified EDOT monomers. An attempt was made to elucidate the structure of HePAN further via redissolution in DMF-d₇ and ¹H and ¹³C NMR analysis; however, it was determined that HePAN does not dissolve in it, or in DMSO-d₆. This may be due to the extent of conversion of the nitrile pendant groups in PAN into carboxylic acids, amides, and imines which modify the solubility of the native PAN, which is soluble in both the solvents mentioned. The further elucidation of the structure, as well as the extent of conversion, is left to future work.

There were several problems encountered in the synthesis of HePAN. The application in this study of literature-reported protocols for making HePAN⁶⁰, as well as literature-reported protocols for hydrolyzing PAN in solid state (not electrospun PAN)⁶⁴ have resulted in a high degree of irreproducibility. Some reaction runs resulted in products that, when subjected to ATR-IR analysis, are revealed to either be unreacted PAN or have a degree of conversion lower than the limit of detection of the ATR-IR instrument. To remedy this, it was decided to make the reaction conditions harsher: higher concentrations of NaOH, higher temperatures, and longer amounts of time. However, this resulted in the degradation of the mechanical properties of the electrospun fibers: swelling and dissolution of the fibers were observed, which rendered the fibers useless for further modification. Evidently, increasing the extent of conversion of the nitrile pendant groups into carboxylic acid groups increases the hydrophilicity of the fibers. This irreproducibility of results may be explained by differences in the electrospun substrates: substrates between runs may have different thicknesses and porosity and thus have differing surface areas available for reaction. This was the motivation for trying to react polymers with the necessary functionality first before electrospinning. Two approaches were explored: hydrolyzing PAN dissolved in DMF, and hydrolyzing PAN suspended in water. The result of the first experiment was the precipitation of an orange film-like substance; thus, this method was discarded as unviable. In the second setup, the PAN powder turned from white to orange, and was soluble in DMF. Unfortunately, as per section 2.3.1, this solution did not electrospin into fibers. However, since this method did yield usable PAN-co-PAA, it was decided that this also was to be used for the next steps in the modification of PAN, which is the actual grafting of the modified EDOT

monomers. Further studies to optimize the reproducibility of this reaction, as well as different combinations of reaction-electrospinning-grafting are currently underway in the laboratory.

A Fischer esterification between HePAN and EDOT-MeOH was attempted. A catalytic amount of H_2SO_4 , a non-nucleophilic acid, was used to reduce the possibility of the acid cleaving the ether in EDOT. This reaction resulted in the retention of the solid, nanofibrous structure of the electrospun substrate, although with enhanced brittleness. The proposed mechanism is shown in Scheme 8.



Scheme 8. Proposed mechanism for the reaction of PAA with EDOT-MeOH

The ATR-IR spectrum of this product is shown in Figure 69 below. Many of the peaks in the ATR-IR spectrum of PAN-co-PAA or HePAN have been either significantly attenuated because of the reaction or disappeared altogether. The carboxylic acid peak at 3368 cm^{-1} and the nitrile peak at 2244 cm^{-1} have completely disappeared. In addition, the attenuation of the amine N-H bend at 1561 cm^{-1} , the carboxylic acid O-H bends at 1454 cm^{-1} and 1377 cm^{-1} , the amine C-N stretch at 1221 cm^{-1} , and the carboxylic acid C-O stretch at 1091 cm^{-1} can be observed. Meanwhile, it can be observed that the carbonyl C=O stretch shifts from being at 1661 cm^{-1} in PAN-co-PAA to 1691 cm^{-1} . Taken with the appearance of a new peak at 1214 cm^{-1} , which can be attributed to the C-O stretching of an ester, it can be said that this may indicate the successful formation of PAN-co-PAA-graft-EDOT-MeOH. However, this is far from conclusive. Particularly suspect is the absence of a C-H stretch around 3000 cm^{-1} . Because this esterification was done with H_2SO_4 , it may be possible that the substrate was also heavily oxidized.

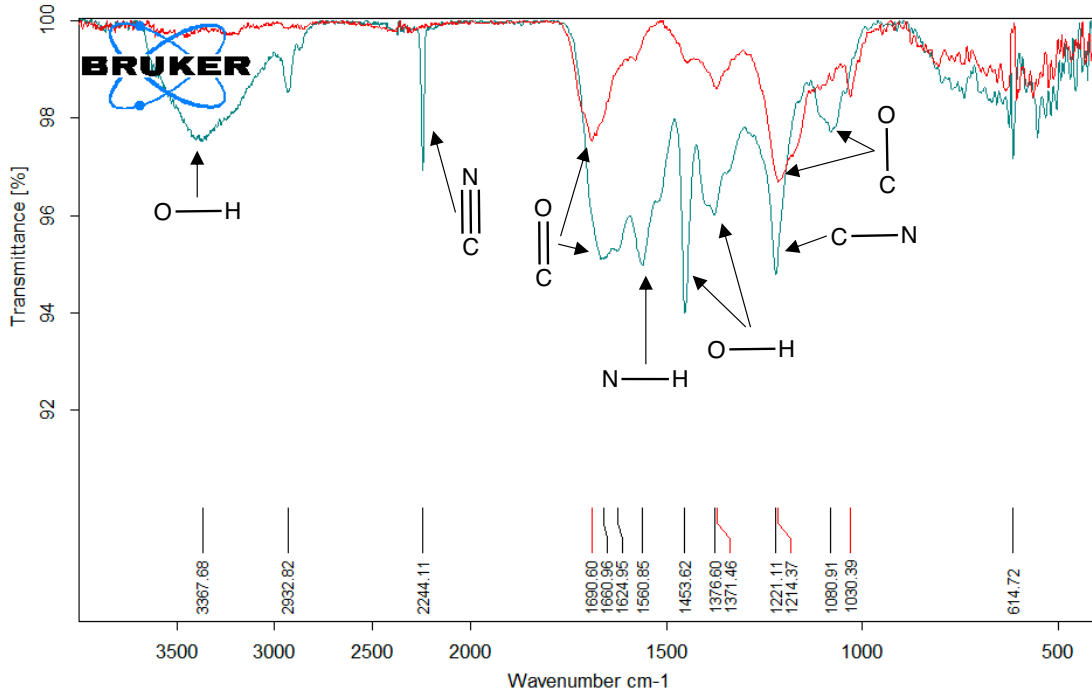
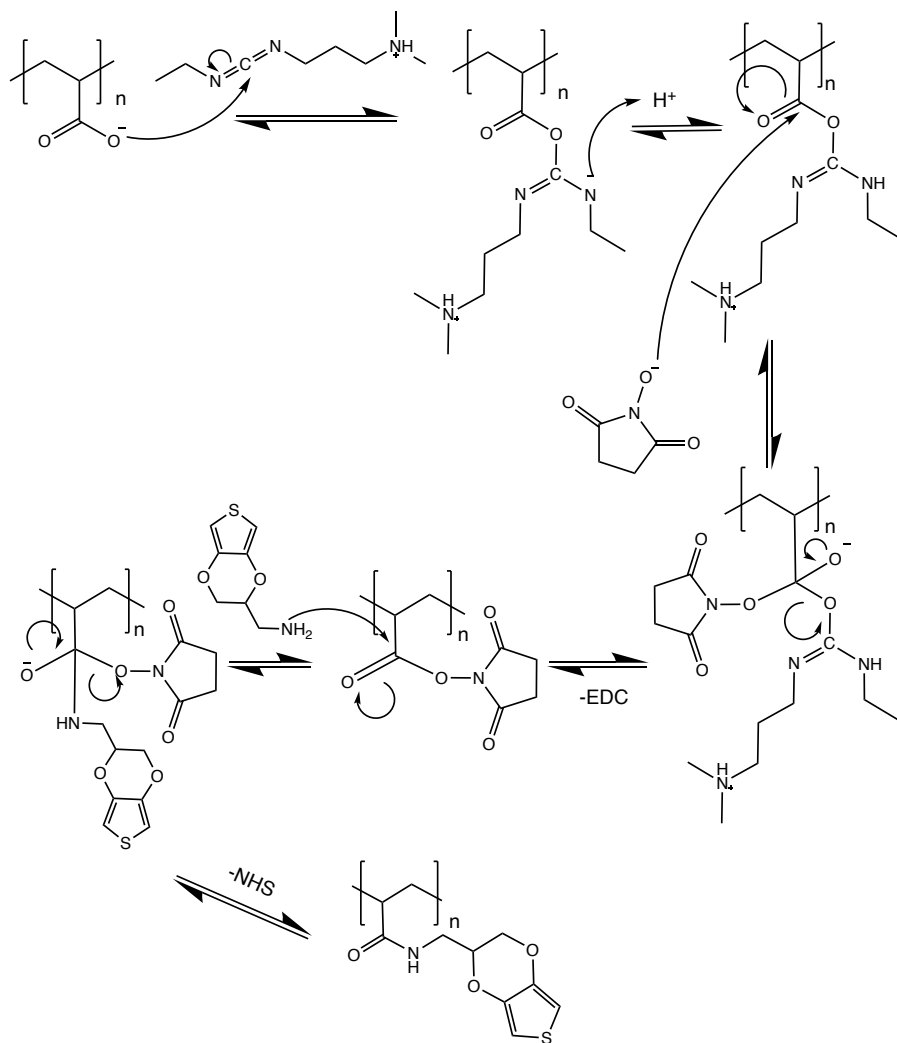


*Figure 69. ATR-IR spectra of (teal): PAN-co-PAA and (red): PAN-co-PAA-graft-EDOT-
MeOH*

Further studies should be done to elucidate the structure further, such as redissolution for NMR analysis, and even SEM-EDX analysis to look for the presence of S which can only come from EDOT. In addition, the black coloration of the product can come from PEDOT, which means that EDOT may have polymerized on the surface of these substrates already. As has been mentioned in section 5.3.1, the acidic conditions and the application of heat may be enough to induce the polymerization of EDOT. Further studies may be done which involves milder conditions for this esterification.

5.3.2.2 PAN modification via hydrolysis and amidation

To overcome the limitations outlined above for the esterification of PAN-co-PAA with EDOT-MeOH, it was decided to attempt the grafting of EDOT to PAN-co-PAA via EDC/NHS coupling between EDOT-MeNH₂ and PAN-co-PAA. The proposed mechanism is shown in Scheme 9 below. This is a well-known mechanism and coupling reaction that has been successfully used in coupling amino acids.



Scheme 9. Proposed mechanism for the reaction of EDOT-MeNH₂ and PAA via EDC/NHS coupling

To test the viability of this synthesis, this reaction was first attempted in solution. Figure 70 below shows the ^1H NMR spectrum of PAN in DMF-d₇. As expected, there are two signals corresponding to the two different types of hydrogens in PAN. There is also a significant water peak visible. Interestingly, there is not much literature reporting the ^1H NMR spectrum of PAN in DMF-d₇, nor is there a database of chemical shifts of common laboratory impurities in DMF-d₇. Literature-reported spectra only provide pictures of the spectra and do not report chemical shifts and look considerably different from what was obtained: Ha peaks were reported at 2.2 ppm and 3.0 ppm, and Hb peaks were reported at 3.2 and 4 ppm^{69,127}.

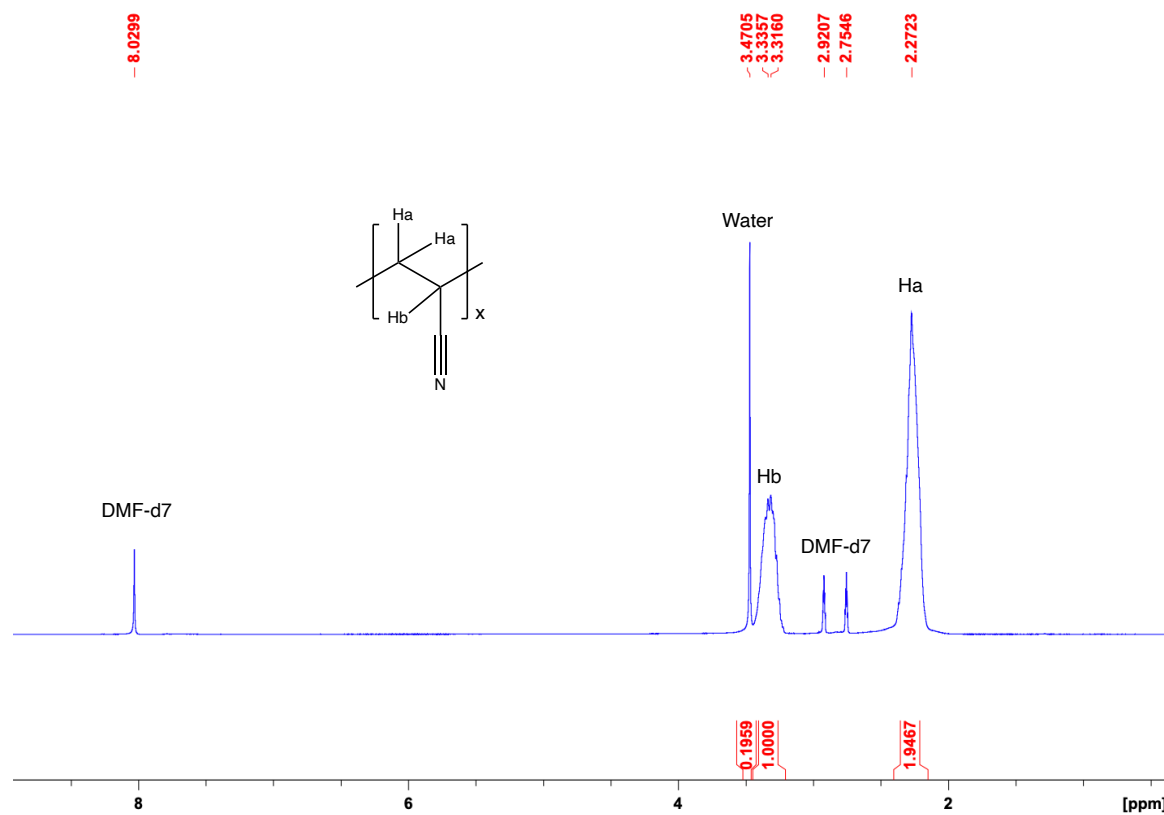


Figure 70. PAN ^1H NMR spectrum in DMF-d₇

Fortunately, the product of the EDC/NHS coupling was soluble in this solvent, which allows for better elucidation of the structure. The ^1H NMR spectrum of the product is shown in Figure 71 below. For comparison, the ^1H NMR spectrum of EDOT-MeNH₂ was also obtained in DMF-d₇, and this is shown in *Figure 72*. As can be observed in Figure 71, the ^1H NMR spectrum of the synthesized PAN-co-PAA-graft-EDOT-MeNH₂ contains a combination of the ^1H NMR spectra of PAN-co-PAA and EDOT-MeNH₂, as shown in *Figure 72*. The peaks in the EDOT-MeNH₂ ^1H NMR spectrum in DMF-d₇ were assigned based on their position in the ^1H NMR spectrum of EDOT-MeNH₂ in CDCl₃. The peaks corresponding to the acrylic acid monomer units have been assigned based on a previously-reported ^1H NMR spectrum of a PAA block-containing polymer in DMF-d₇¹²⁸. The remaining peaks in the PAN-co-PAA-graft-EDOT-MeNH₂ ^1H NMR spectrum were assigned based on their most probable identities and through the process of elimination.

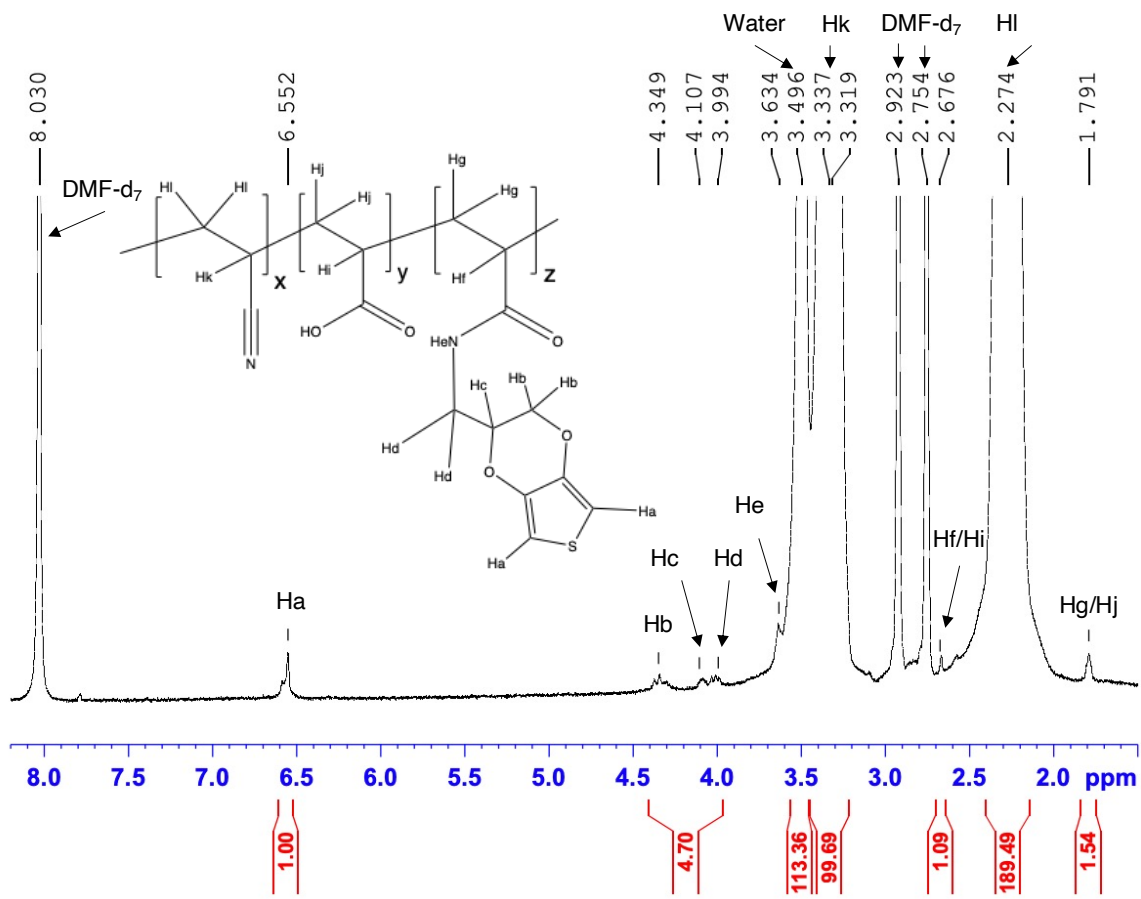


Figure 71. ^1H NMR of PAN-co-PAA-graft-EDOT-MeNH₂ in DMF-d₇

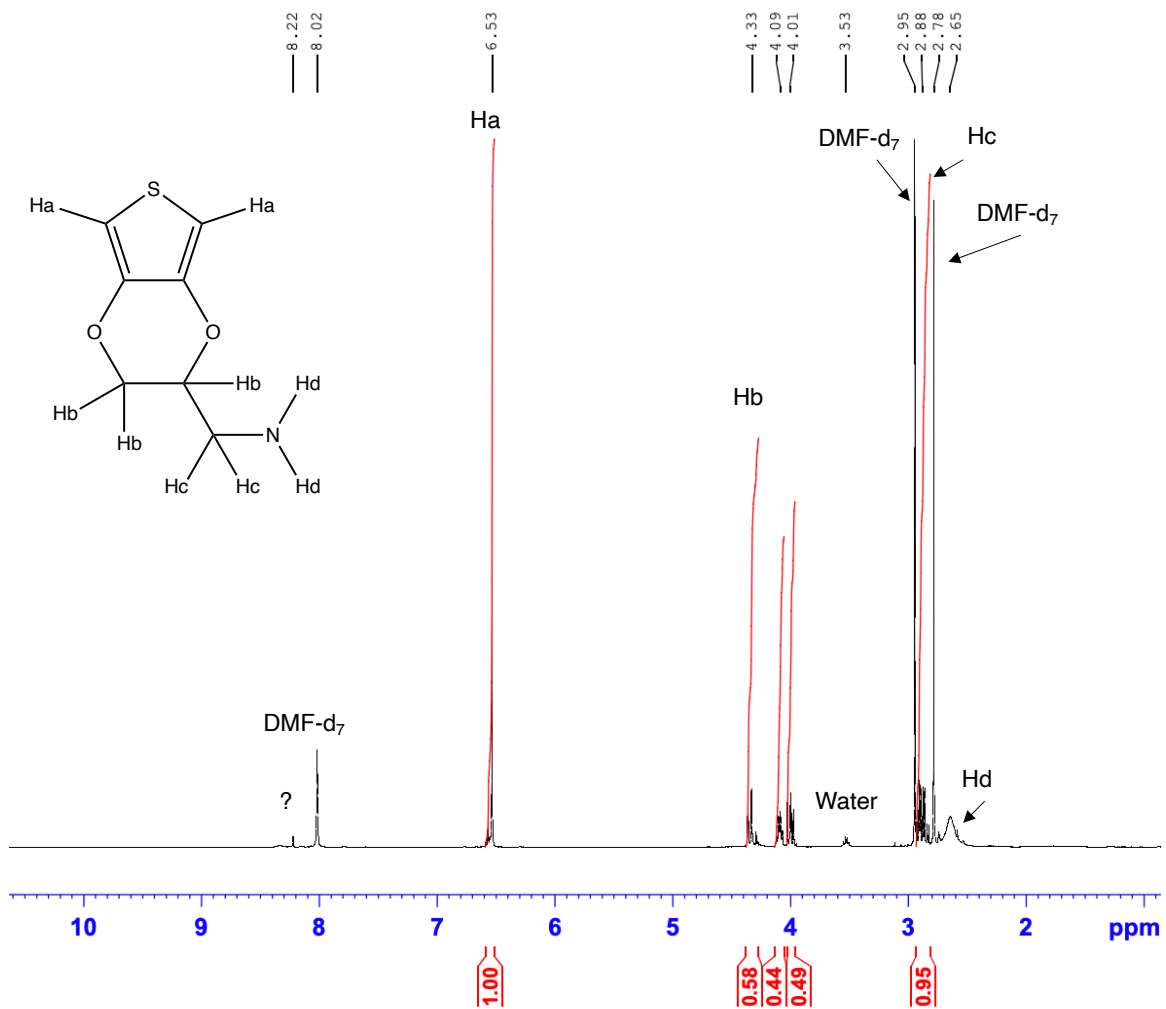
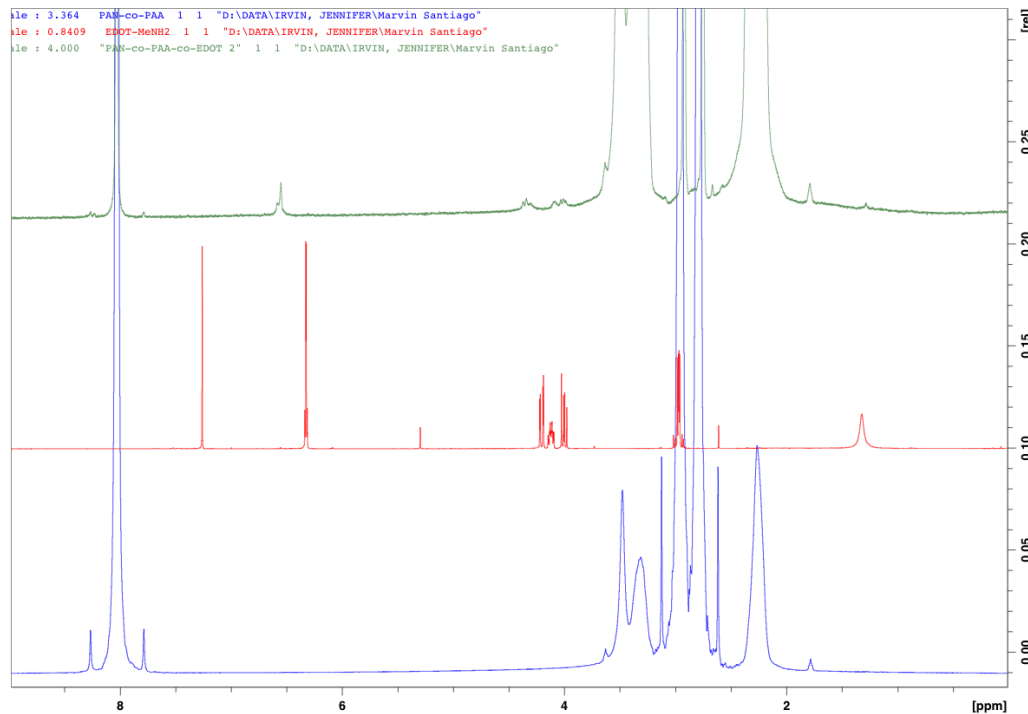


Figure 72. ^1H NMR spectrum of EDOT- MeNH_2 in DMF-d_7

This spectrum is stacked with the spectrum of PAN-co-PAA and EDOT- MeNH_2 in DMF-d_7 in Figure 73 below. Importantly, the signals for the hydrogens in the amine and neighboring methylene group of EDOT- MeNH_2 have been shifted, possibly indicating their attachment to PAN-co-PAA and the formation of an amide. The Hd amine hydrogens in EDOT- MeNH_2 have a chemical shift of 2.65 ppm, while the corresponding He amide hydrogen in PAN-co-PAA-graft-EDOT- MeNH_2 has a chemical shift of 3.63 ppm. The Hc methylene hydrogens in EDOT- MeNH_2 have a chemical shift of 2.88 ppm,

while there are no peaks in that region in the ^1H NMR of PAN-co-PAA-graft-EDOT-MeNH₂. It is possible that the shifted peaks are under the H_k peak, as is the remainder of the broad amide hydrogen peak.



*Figure 73. (Top) ^1H NMR of PAN-co-PAA-graft-EDOT-MeNH₂ in DMF-*d*₇; (middle) ^1H NMR of EDOT-MeNH₂ in DMF-*d*₇; (bottom) ^1H NMR of PAN-co-PAA*

The % conversion of nitrile pendant groups to carboxylic acid pendant groups could not be computed, because, as shown in Figure 71, many peaks of these units overlap. Instead, the % grafting of EDOT-MeNH₂ to PAN could be determined, which nevertheless gives a useful measure of the efficiency of the reaction, since this was the objective of the study in the first place. This can be done in two steps. First, the ^1H NMR spectrum of PAN-co-PAA has to be obtained, and then the ratio of the area under peak H_i to the area under peak H_k. This would determine the percent conversion of nitrile pendant groups to carboxylic acids. Afterwards, elemental analysis can be done to determine the percent content of S in the sample. Since S can only come from EDOT, this

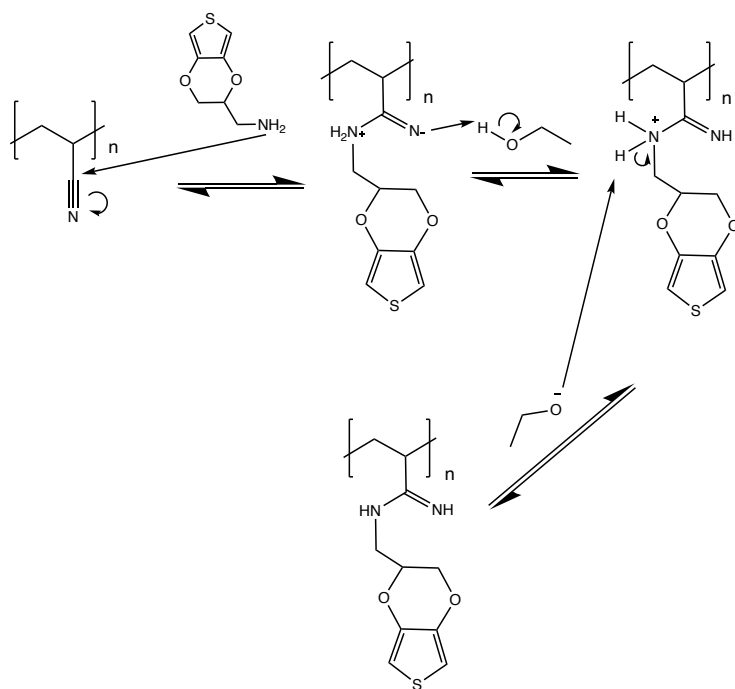
would provide an accurate measurement of the % grafting of EDOT-MeNH₂ to PAN.

This is left to future work.

This work preliminarily proves the possibility of grafting EDOT onto PAN via alkaline hydrolysis and then reaction via EDC/NHS coupling. To confirm this, future work should concentrate on getting IR spectra and SEM-EDX analysis. In addition, 2D NMR and mass spectrometry could also be done.

5.3.2.3 PAN modification via direct reaction with EDOT-MeNH₂

To overcome the limitations imposed by solubility differences in the modification of PAN via alkaline hydrolysis, it was decided to attempt the grafting of PAN with EDOT-MeNH₂ via direct reaction. The procedure was adapted from the direct reaction of electrospun PAN with ethylenediamine⁶⁹. The proposed mechanism of this reaction is shown in Scheme 10, which involves the direct nucleophilic attack of the N atom in EDOT-MeNH₂ to the electrophilic nitrile C and the formation of an imine. The formation of amidines by reactions of amines and nitriles has been reported elsewhere in literature, but with the help of rare earth metal catalysis, or by functionalizing the nitrile with electron withdrawing groups¹²⁹. Thus, it can be assumed that this reaction would be low yielding; however, the paper this procedure was adapted from has not reported the % conversion of nitriles to amidine group.



Scheme 10. Proposed mechanism for the direct grafting of EDOT-MeNH₂ on PAN

As can be observed in Figure 74 below, the ¹H NMR spectrum of the product of this reaction shows peaks consistent with the presence of PAN and EDOT-MeNH₂. These peaks were assigned in the same manner the peaks in Figure 71 were assigned. It can be observed that the water peak at around 3.47 ppm is much broadened and obscures the rest of the expected signals from Hb. As in the previous section, importantly, it can be observed that the peaks corresponding to Hc have been shifted from their expected shift at 2.88 ppm and may be under the broadened water peak, and the peak corresponding to the amine hydrogens in EDOT-MeNH₂ has shifted from 2.65 ppm to 1.28 ppm. There also is the appearance of a peak at 8.36 ppm, which may correspond to the imine H, as has been reported in literature for similar moieties¹³⁰. There also are impurities at 7.83 ppm, 7.57 ppm, and 7.37 ppm. If the peak at 8.36 ppm is not from the imine H, taken together with these, it may be possible that pyridine is present as a contaminant, although there was no pyridine reactant or solvent in the reaction mixture.

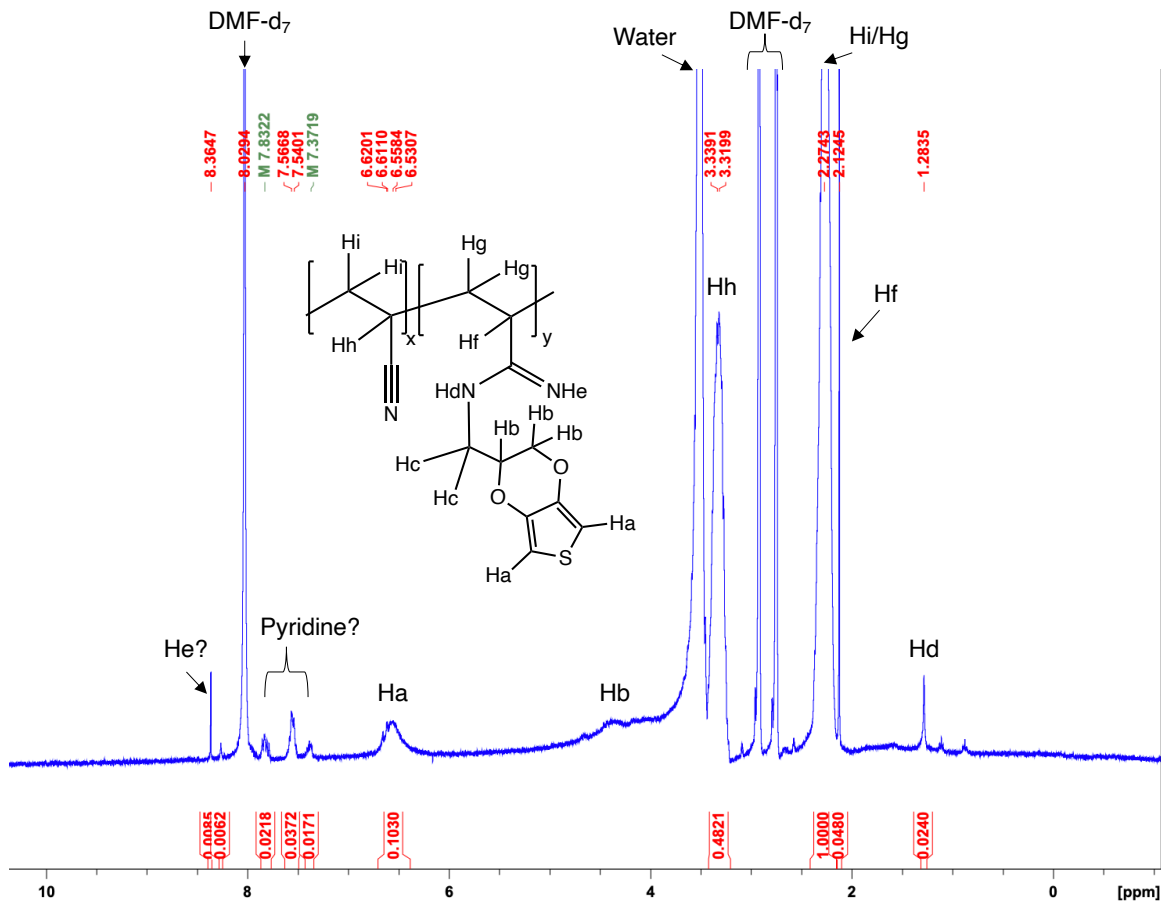


Figure 74. ^1H NMR of PAN-graft-EDOT- MeNH_2 in DMF-d_7

The shifting of the EDOT- MeNH_2 peaks is more clearly shown in Figure 75 below.

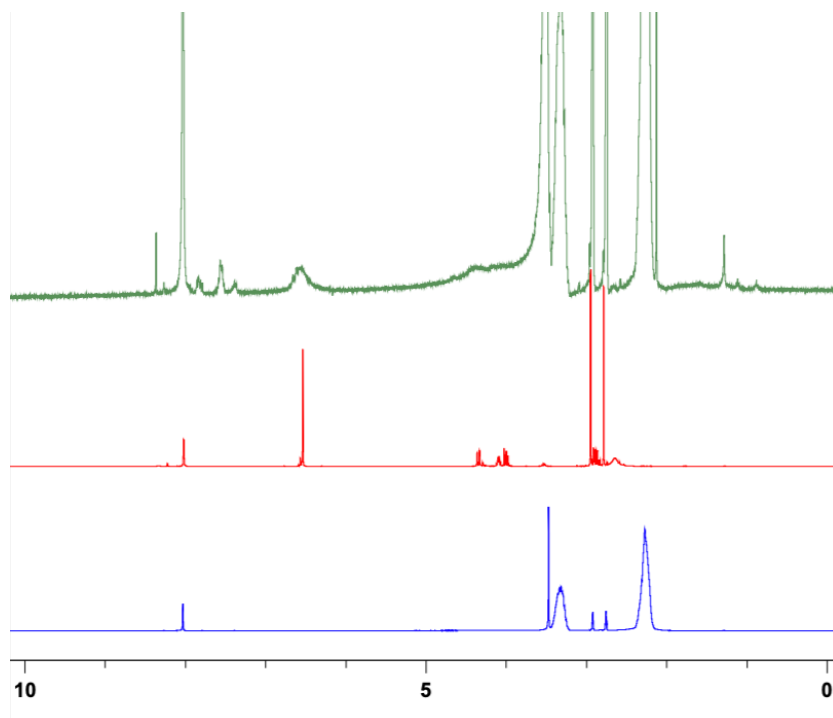
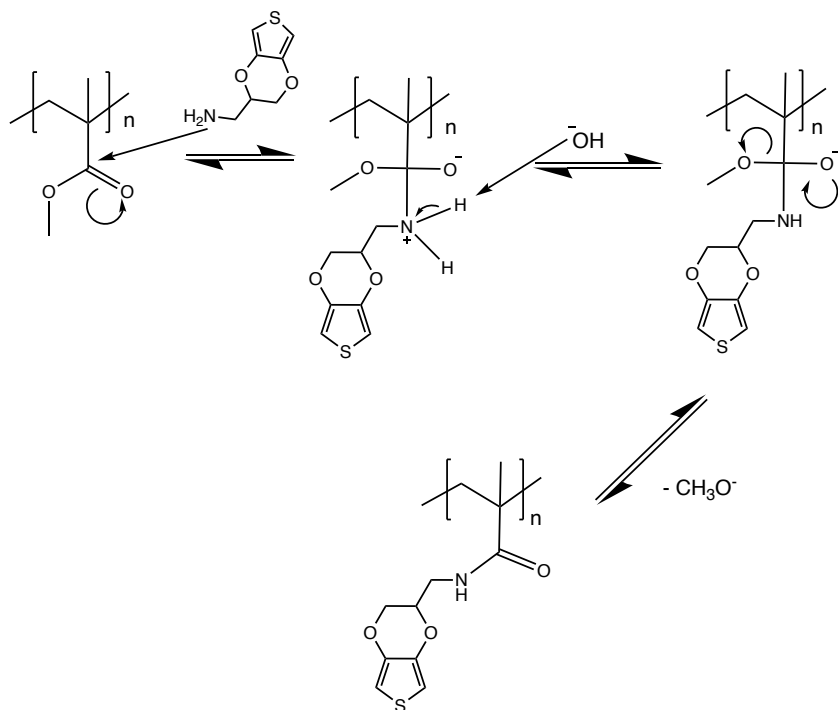


Figure 75. (Top) ^1H NMR of PAN-graft-EDOT- MeNH_2 in $\text{DMF}-d_7$; (middle) ^1H NMR of EDOT- MeNH_2 in $\text{DMF}-d_7$; (bottom) ^1H NMR of PAN in $\text{DMF}-d_7$

For this reaction, the % grafting of EDOT to PAN can be determined through elemental analysis and looking for S content and is left to future work. As with the EDC/NHS coupling reaction, it proves necessary for the future work in this field to include 2D NMR for a proper peak assignment, ATR-IR analysis to determine if the required amidine functionality is indeed present, and SEM-EDX to look for the presence of S. Future work should also focus on attempting the electrospinning of PAN-graft-EDOT- MeNH_2 and then analysis to determine if the required functionality survives the high voltages in electrospinning, and doing this same reaction on electrospun PAN to possibly increase % grafting as explained previously.

5.3.2.4 Surface PMMA modification

PMMA was also modified, adapting a literature-reported procedure on the modification of PMMA surfaces through amidolysis¹²⁶. The proposed mechanism for this reaction is shown in Scheme 11.



Scheme 11. PMMA amidolysis mechanism

This reaction was first done on electrospun PMMA substrates. However, after reaction, the electrospun PMMA substrates swelled and were unusable for further reaction. Nevertheless, these swelled fibers were subjected to ATR-IR analysis. The ATR-IR spectrum of the reacted PMMA is shown in Figure 76 below. As can be observed, the ATR-IR spectra of PMMA and PMMA grafted with EDOT-MeNH₂ are considerably different. PMMA has absorptions at 1726 cm⁻¹ and 1147 cm⁻¹, corresponding to the C=O and C-O stretches of the ester group, respectively. Meanwhile, PMMA-graft-EDOT-MeNH₂ has a possible N-H stretch at 3309 cm⁻¹, an sp² C-H stretch

at 3110 cm^{-1} , a C=O stretch at 1728 cm^{-1} , an absorption at 1578 cm^{-1} which can be attributed to either amine N-H bending or alkene C=C stretching, a strong absorption at 1483 cm^{-1} which can be attributed to alkane C-H bending, an absorption at 1373 cm^{-1} which can be attributed to alkane C-H bending, absorptions at 1186 cm^{-1} and 1080 cm^{-1} which can be attributed to amide C-N stretching, and absorptions at 917 cm^{-1} and 750 cm^{-1} which can be attributed to alkene C=C bending and alkane C-H bending, respectively.

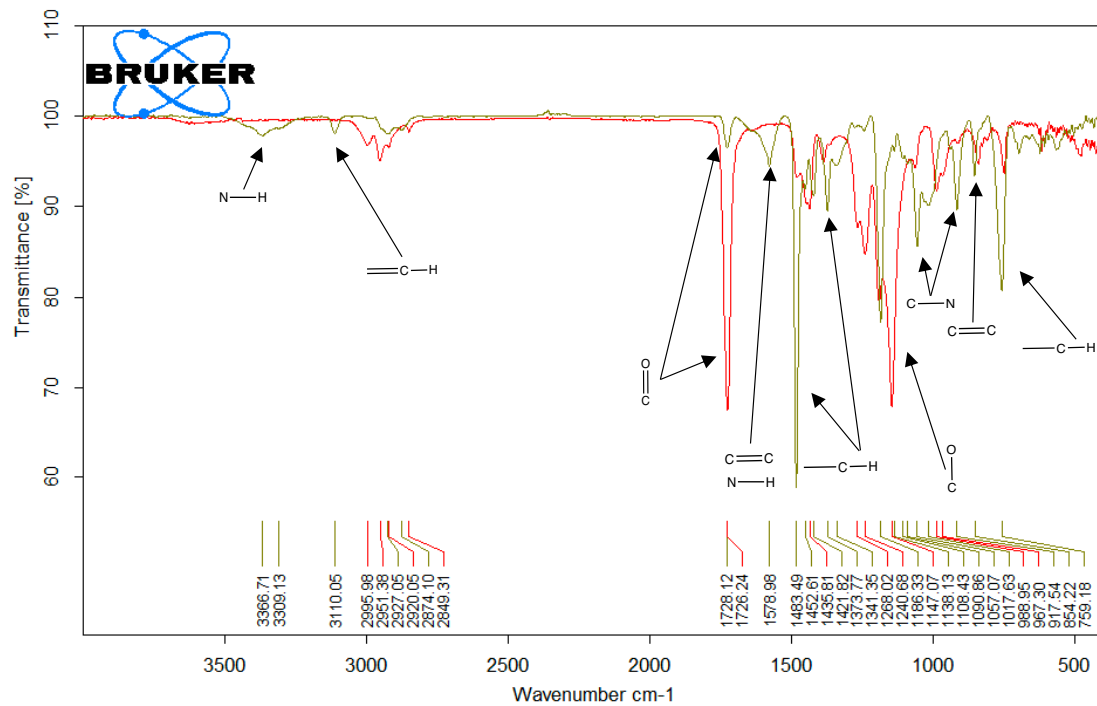


Figure 76. ATR-IR spectra of PMMA (red) and PMMA-graft-EDOT-MeNH₂ (gold)

Because of these observations, it is indeed possible that amidolysis of PMMA by EDOT-MeNH₂ has indeed occurred and an amide bond has been formed. To verify these observations, the reacted PMMA fibers were dissolved in CDCl₃ and their ¹H NMR spectrum taken, which is shown in Figure 78. For comparison, the ¹H NMR spectrum of PMMA is shown in Figure 77. Comparing Figure 78 with Figure 77 and the ¹H NMR spectrum of EDOT-MeNH₂ in CDCl₃ in Figure 67, it can be observed that the chemical

shifts of the hydrogens in PMMA are retained with peaks at 3.60 ppm, a cluster of peaks from 1.81-2.06 ppm, and peaks at 1.02 ppm and 0.85 ppm. The EDOT-MeNH₂ peaks also appear at 6.41 and 6.33 ppm and 4.38-3.93 ppm. The Hd peaks, however, corresponding to the CH₂-N hydrogens, have broadened at 2.97 ppm. The NH₂ peaks have also been shifted from 1.32 ppm to 1.75 ppm.

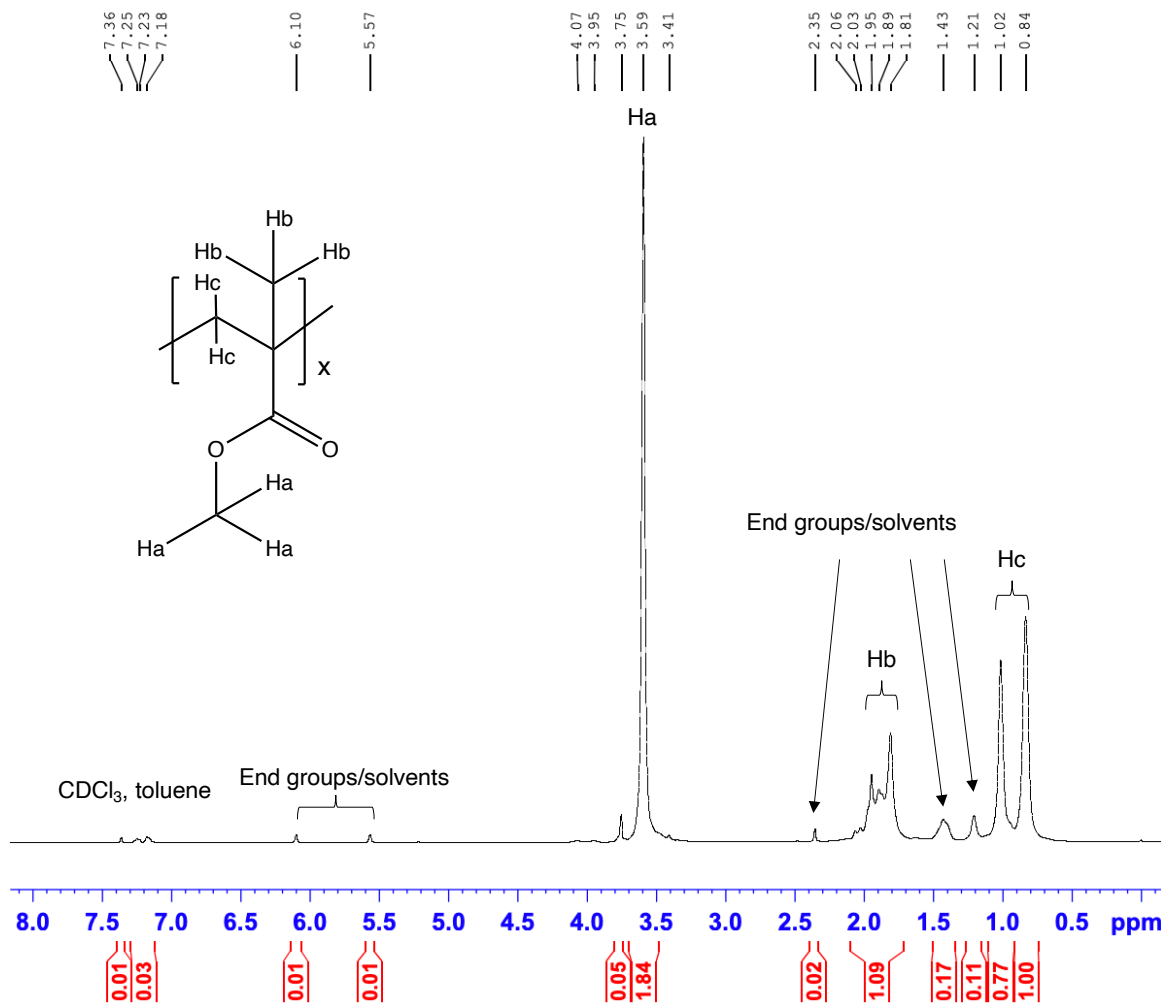


Figure 77. ¹H NMR spectrum of PMMA in CDCl_3

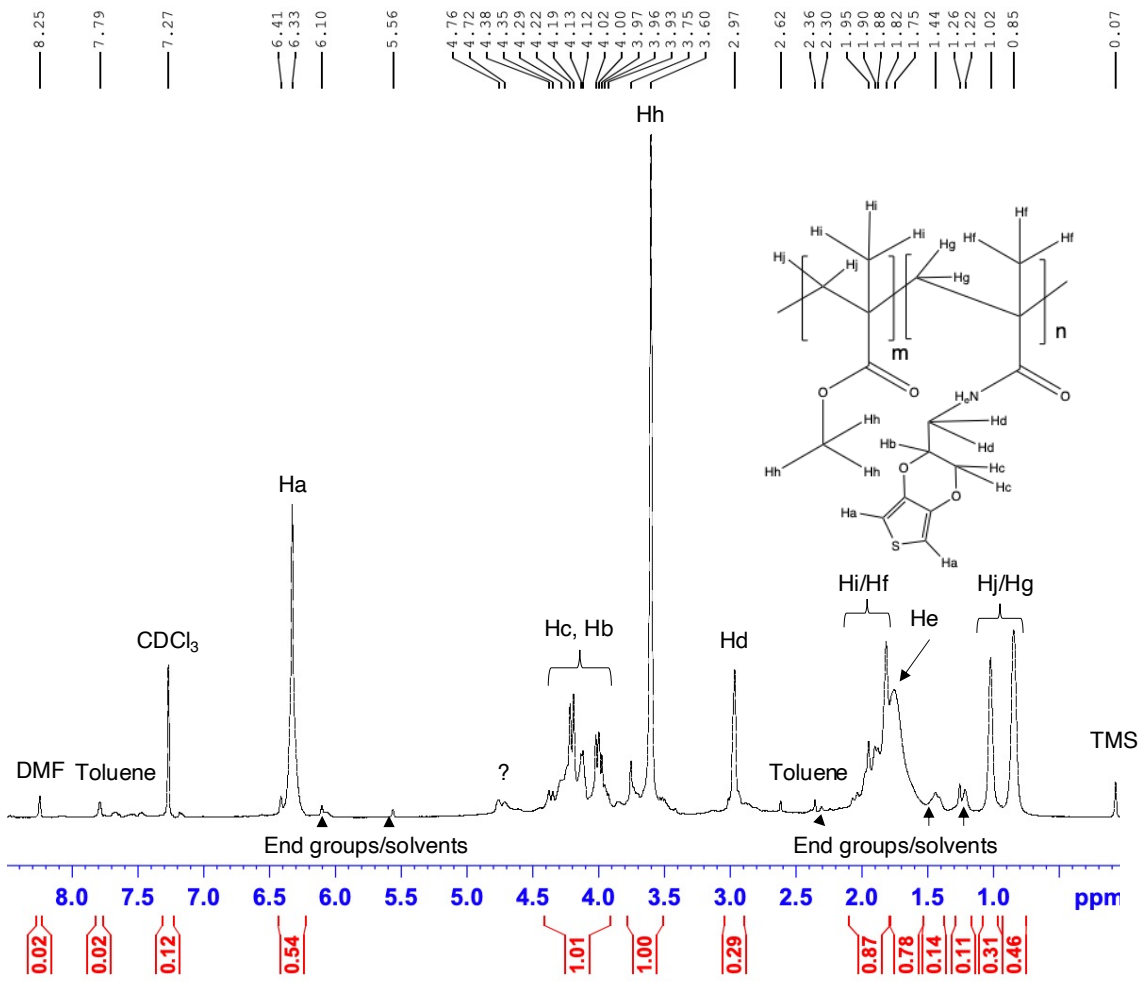


Figure 78. ^1H NMR spectrum of PMMA-graft-EDOT- MeNH_2 in CDCl_3

These differences can be more clearly seen in Figure 79 below.

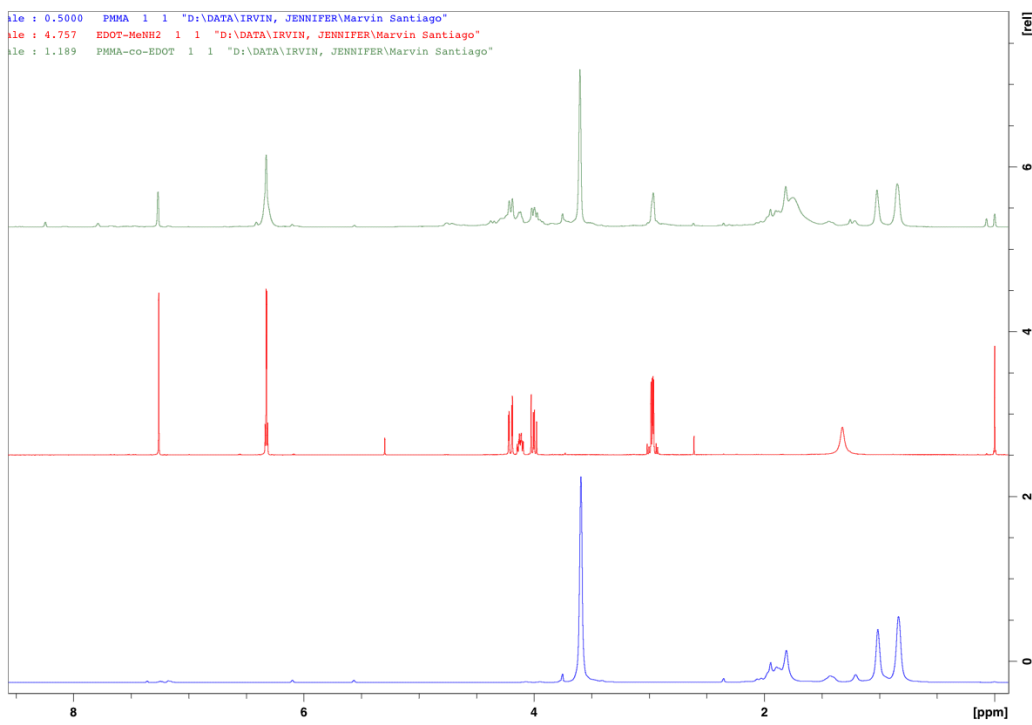


Figure 79. (Top) ^1H NMR of PMMA-graft-EDOT- MeNH_2 in CDCl_3 ; (middle) ^1H NMR of EDOT- MeNH_2 in CDCl_3 ; (bottom) ^1H NMR of PMMA in CDCl_3

Because of the shifting of these peaks, and with the information gleaned from Figure 76, it can be said that there is preliminary evidence that EDOT- MeNH_2 was successfully grafted onto PMMA via amidolysis. The % grafting of EDOT on PMMA can be determined through elemental analysis and looking for S content and is left to future work. More work may also be done to ensure the correct assignment of peaks via 2D NMR, and SEM-EDX to look for S on these samples.

5.4 Conclusions and Future Work

This chapter has demonstrated the attempts to graft of modified EDOTs to the electrospinnable polymers PAN and PMMA. These grafting reactions and their intermediate reactions also modify the hydrophilicity of the polymers, and combinations of reacting then electrospinning, or electrospinning then reacting were optimized, with the desired end goal of having a solid electrospun polymer with grafted EDOT for

subsequent chemical oxidative polymerization. Preliminary evidence in the form of possible indicators of the formation of esters and amide has been found to indicate successful grafting of EDOT-MeOH to PAN-co-PAA, EDOT-MeNH₂ to PAN, and EDOT-MeNH₂ to PMMA. Further spectroscopic studies are needed to completely verify the formation of these bonds, as well as optimization of reaction conditions to increase the % grafting without solubilizing the electrospun polymer substrate. Further work is also to be done in the next step of “grafting from”, which is the actual growth of the ICP EDOT. These electrospun polymer-ICP composites, which are held together by covalent bonding, are hypothesized to have stronger adhesion than the ICP coatings discussed in the previous chapters.

6 CONCLUSIONS AND FUTURE WORK

This thesis describes the fabrication of a novel composite which can be used as a neural tissue scaffold for improving nerve regeneration. Electrospinning was chosen as a process to electrospin the biocompatible, biodegradable polymer PCL into a nanofibrous, aligned structure. This structure mimics the native ECM of nervous systems in mammals. This property, compared with the large surface area and porosity of polymer nanofibers, was hypothesized to be conducive for the attachment of growing cells. PCL was successfully electrospun into nanofibers bearing the required ester functional groups for biodegradability. PAN, PVC, and PMMA were also successfully electrospun into nanofibers.

Next, it was hypothesized that coating these electrospun substrates with ICPs would add electrical conductivity to them, which have proven to be important in the growth and communication of nerves. The biocompatible ICP PPy was chosen in this regard. A method of coating PPy onto electrospun PCL using *in situ* chemical oxidative polymerization with previous pre-treatment with oxidant FeCl_3 was developed. This was proven to coat the electrospun substrates evenly and conformally.

Lastly, together with the group of Dr. Romero-Uribe at the University of Texas at San Antonio, it was hypothesized that the addition of MNPs into neural tissue scaffolds would add remote controllability, sites for cell attachment and mechanically induced stretch growth, hyperthermic regeneration of cell functions, and electromagnetic induction to the composite. To this end, MNPs were blended and successfully dispersed onto electrospun PCL, and this blend was successfully coated with PPy following the protocol that was developed for even, conformal coating. These composites were proven

to be conducive for the attachment of mouse myoblast C2C12 and mouse myoblast ND7/23 cells. On composites with high degrees of alignment of the electrospun PCL substrate, evidence was found of cellular differentiation leading to the development of organelles.

It was hypothesized that coating ICPs onto electrospun substrates through “grafting from” copolymerization would enhance their adhesion. EDOT-MeNH₂ may have been successfully grafted onto PMMA via amidation, onto PAN via amidine formation, and onto PAN via PAN alkaline hydrolysis and EDC/NHS coupling. EDOT-MeOH may also have been successfully grafted to base-hydrolyzed PAN.

Future work in these fields should concentrate on the optimization of the electrospinning conditions of PAN, PVC, and hydrolyzed PAN. Mechanical, thermal, and electrical property and function tests of both PCL-PPy and PCL-MNP-PPy should be conducted. Further growth and *in vivo* studies of nerve regeneration on PCL-MNP-PPy are needed, as are optimization of the reaction conditions for the grafting of modified EDOTs on PAN and PMMA.

Of particular interest is the processing of ICPs into nanofibrous form, whether through coating or grafting onto electrospun polymer substrates. This is because this would be an enabling technology not just for biomedical engineering but also for applications in sensors, energy storage and conversion, and wearable electronics, to name a few. Thus, it would prove interesting to probe the structure of ICP coatings onto electrospun substrates which aim to explain, for example, why PPY coatings on electrospun PCL take on the morphology of the substrate fibers, and PEDOT coatings on electrospun PAN take on the beads-on-a-string morphology. It would also be of interest

to attempt to graft other electrospinnable polymers with functional pendant groups as well, such as PVC. In this field, a collaboration with the group of Dr. Nathaniel Lynd at the University of Texas at Austin is possible involving the synthesis of an alkyne-functionalized poly(ethylene oxide) which would then be electrospun and grafted with EDOT in our laboratory.

REFERENCES

- (1) Rehfeld, A.; Nylander, M.; Karnov, K. *Compendium of Histology*; **2017**.
<https://doi.org/10.1007/978-3-319-41873-5>.
- (2) Dhp1080. Neuron description
<https://commons.wikimedia.org/wiki/File:Neuron.svg>.
- (3) Rotshenker, S. Wallerian Degeneration: The Innate-Immune Response to Traumatic Nerve Injury. *J. Neuroinflammation* **2011**, *8* (August).
<https://doi.org/10.1186/1742-2094-8-109>.
- (4) Ide, C. Peripheral Nerve Regeneration. *Neurosci. Res.* **1996**, *25* (2), 101–121.
[https://doi.org/10.1016/S0168-0102\(96\)01042-5](https://doi.org/10.1016/S0168-0102(96)01042-5).
- (5) Faroni, A.; Mobasseri, S. A.; Kingham, P. J.; Reid, A. J. Peripheral Nerve Regeneration: Experimental Strategies and Future Perspectives. *Adv. Drug Deliv. Rev.* **2015**, *82*, 160–167. <https://doi.org/10.1016/j.addr.2014.11.010>.
- (6) Raffa, V. *Chapter 7 - Engineering Magnetic Nanoparticles for Repairing Nerve Injuries*; Elsevier Inc., **2020**. <https://doi.org/10.1016/B978-0-12-816865-3.00007-X>.
- (7) Chen, R.; Romero, G.; Christiansen, M. G.; Mohr, A.; Anikeeva, P. Wireless Magnetothermal Deep Brain Stimulation. *Science (80-.).* **2015**, *347* (6229), 1477–1480. <https://doi.org/10.1126/science.1261821>.
- (8) Jiménez, G. L.; Thevi Guntnur, R.; Giuliani, J.; Romero, G. Enhancing Magnetic Hyperthermia in Ferrite Nanoparticles through Shape Anisotropy and Surface Hybridization. *AIChE J.* **2021**, *e17437*.
<https://doi.org/10.1002/aic.17437>.

- (9) Romero, G.; Christiansen, M. G.; Stocche Barbosa, L.; Garcia, F.; Anikeeva, P. Localized Excitation of Neural Activity via Rapid Magnetothermal Drug Release. *Adv. Funct. Mater.* **2016**, *26* (35), 6471–6478.
<https://doi.org/10.1002/adfm.201602189>.
- (10) Teo, W. E.; He, W.; Ramakrishna, S. Electrospun Scaffold Tailored for Tissue-Specific Extracellular Matrix. *Biotechnol. J.* **2006**, *1* (9), 918–929.
<https://doi.org/10.1002/biot.200600044>.
- (11) Gu, X.; Ding, F.; Yang, Y.; Liu, J. Construction of Tissue Engineered Nerve Grafts and Their Application in Peripheral Nerve Regeneration. *Prog. Neurobiol.* **2011**, *93* (2), 204–230.
<https://doi.org/10.1016/j.pneurobio.2010.11.002>.
- (12) Siddiqui, N.; Asawa, S.; Birru, B.; Baadhe, R.; Rao, S. PCL-Based Composite Scaffold Matrices for Tissue Engineering Applications. *Mol. Biotechnol.* **2018**, *60* (7), 506–532. <https://doi.org/10.1007/s12033-018-0084-5>.
- (13) Alvarez-Perez, M. A.; Guarino, V.; Cirillo, V.; Ambrosio, L. Influence of Gelatin Cues in PCL Electrospun Membranes on Nerve Outgrowth. *Biomacromolecules* **2010**, *11* (9), 2238–2246.
<https://doi.org/10.1021/bm100221h>.
- (14) Lee, B. K.; Ju, Y. M.; Cho, J. G.; Jackson, J. D.; Lee, S. J.; Atala, A.; Yoo, J. J. End-to-Side Neurorrhaphy Using an Electrospun PCL/Collagen Nerve Conduit for Complex Peripheral Motor Nerve Regeneration. *Biomaterials* **2012**, *33* (35), 9027–9036.
<https://doi.org/10.1016/j.biomaterials.2012.09.008>.

- (15) Potas, J. R.; Haque, F.; Maclean, F. L.; Nisbet, D. R. Interleukin-10 Conjugated Electrospun Polycaprolactone (PCL) Nanofibre Scaffolds for Promoting Alternatively Activated (M2) Macrophages around the Peripheral Nerve in Vivo. *J. Immunol. Methods* **2015**, *420*, 38–49.
<https://doi.org/10.1016/j.jim.2015.03.013>.
- (16) Saderi, N.; Rajabi, M.; Akbari, B.; Firouzi, M.; Hassannejad, Z. Fabrication and Characterization of Gold Nanoparticle-Doped Electrospun PCL/Chitosan Nanofibrous Scaffolds for Nerve Tissue Engineering. *J. Mater. Sci. Mater. Med.* **2018**, *29* (9). <https://doi.org/10.1007/s10856-018-6144-3>.
- (17) Kirillova, A.; Yeazel, T. R.; Asheghali, D.; Petersen, S. R.; Dort, S.; Gall, K.; Becker, M. L. Fabrication of Biomedical Scaffolds Using Biodegradable Polymers. *Chem. Rev.* **2021**, *121* (18), 11238–11304.
<https://doi.org/10.1021/acs.chemrev.0c01200>.
- (18) Pan, X.; Sun, B.; Mo, X. Electrospun Polypyrrole-Coated Polycaprolactone Nanoyarn Nerve Guidance Conduits for Nerve Tissue Engineering. *Front. Mater. Sci.* **2018**, *12* (4), 438–446. <https://doi.org/10.1007/s11706-018-0445-9>.
- (19) Zhang, Z.; Rouabchia, M.; Wang, Z.; Roberge, C.; Shi, G.; Roche, P.; Li, J.; Dao, L. H. Electrically Conductive Biodegradable Polymer Composite for Nerve Regeneration: Electricity-Stimulated Neurite Outgrowth and Axon Regeneration. *Artif. Organs* **2007**, *31* (1), 13–22.
<https://doi.org/10.1111/j.1525-1594.2007.00335.x>.

- (20) Shastri, V. R.; Schmidt, C. E.; Kim, T. H.; Vacanti, J. P.; Langer, R. Polypyrrole - a Potential Candidate for Stimulated Nerve Regeneration. *Mat. Res. Soc. Symp. Proc.* **1996**, *414*, 113–118.
- (21) Wong, J. Y.; Langer, R.; Ingber, D. E. Electrically Conducting Polymers Can Noninvasively Control the Shape and Growth of Mammalian Cells. *Proc. Natl. Acad. Sci. U. S. A.* **1994**, *91* (8), 3201–3204.
<https://doi.org/10.1073/pnas.91.8.3201>.
- (22) Jing, W.; Ao, Q.; Wang, L.; Huang, Z.; Cai, Q.; Chen, G.; Yang, X.; Zhong, W. Constructing Conductive Conduit with Conductive Fibrous Infilling for Peripheral Nerve Regeneration. *Chem. Eng. J.* **2018**, *345* (December 2017), 566–577. <https://doi.org/10.1016/j.cej.2018.04.044>.
- (23) Zarras, P.; Irvin, J. *Electrically Active Polymers*; **2003**.
<https://doi.org/10.1002/0471440264.pst107>.
- (24) Cantu, T.; Irvin, J. A.; Betancourt, T.; Walsh, K.; Pattani, V. P.; Moy, A. J.; Tunnell, J. W. Conductive Polymer-Based Nanoparticles for Laser-Mediated Photothermal Ablation of Cancer: Synthesis, Characterization, and in Vitro Evaluation. *Int. J. Nanomedicine* **2017**, *12*, 615–632.
- (25) Runsewe, D.; Betancourt, T.; Irvin, J. A. Polymers in Biomedical Applications of Electroactive Polymer Electrochemical Sensors : A Review. *Materials (Basel)*. **2019**, *12*, 2629.

- (26) Sierra-Padilla, A.; García-Guzmán, J. J.; López-Iglesias, D.; Palacios-Santander, J. M.; Cubillana-Aguilera, L. E-Tongues/Noses Based on Conducting Polymers and Composite Materials: Expanding the Possibilities in Complex Analytical Sensing. *Sensors* **2021**, *21* (15).
<https://doi.org/10.3390/s21154976>.
- (27) Wang, L.; Wu, Y.; Hu, T.; Guo, B.; Ma, P. X. Electrospun Conductive Nanofibrous Scaffolds for Engineering Cardiac Tissue and 3D Bioactuators. *Acta Biomater.* **2017**, *59*, 68–81.
<https://doi.org/10.1016/j.actbio.2017.06.036>.
- (28) Namsheer, K.; Sekhar Rout, C. Conducting Polymers: A Comprehensive Review on Recent Advances in Synthesis, Properties and Applications. *RSC Adv.* **2021**, *11* (10), 5659–5697. <https://doi.org/10.1039/d0ra07800j>.
- (29) Blachowicz, T.; Ehrmann, A. Most Recent Developments in Electrospun Magnetic Nanofibers: A Review. *J. Eng. Fiber. Fabr.* **2020**, *15*, 1–14.
<https://doi.org/10.1177/1558925019900843>.
- (30) Omastová, M.; Mičušík, M. Polypyrrole Coating of Inorganic and Organic Materials by Chemical Oxidative Polymerisation. *Chem. Pap.* **2012**, *66* (5), 392–414. <https://doi.org/10.2478/s11696-011-0120-4>.
- (31) Yussuf, A.; Al-Saleh, M.; Al-Enezi, S.; Abraham, G. Synthesis and Characterization of Conductive Polypyrrole: The Influence of the Oxidants and Monomer on the Electrical, Thermal, and Morphological Properties. *Int. J. Polym. Sci.* **2018**. <https://doi.org/10.1155/2018/4191747>.

- (32) Tang, X.; Saveh-Shemshaki, N.; Kan, H. M.; Khan, Y.; Laurencin, C. T. Biomimetic Electroconductive Nanofibrous Matrices for Skeletal Muscle Regenerative Engineering. *Regen. Eng. Transl. Med.* **2020**, *6* (2), 228–237. <https://doi.org/10.1007/s40883-019-00136-z>.
- (33) Mohd Abdah, M. A. A.; Zubair, N. A.; Azman, N. H. N.; Sulaiman, Y. Fabrication of PEDOT Coated PVA-GO Nanofiber for Supercapacitor. *Mater. Chem. Phys.* **2017**, *192*, 161–169. <https://doi.org/10.1016/j.matchemphys.2017.01.058>.
- (34) Choi, J.; Park, D. W.; Shim, S. E. Electrospun PEDOT:PSS/Carbon Nanotubes/PVP Nanofibers as Chemiresistors for Aromatic Volatile Organic Compounds. *Synth. Met.* **2012**, *162* (17–18), 1513–1518. <https://doi.org/10.1016/j.synthmet.2012.06.028>.
- (35) Kumar, S.; Rai, P.; Sharma, J. G.; Sharma, A.; Malhotra, B. D. PEDOT:PSS/PVA-Nanofibers-Decorated Conducting Paper for Cancer Diagnostics. *Adv. Mater. Technol.* **2016**, *1* (4). <https://doi.org/10.1002/admt.201600056>.
- (36) Verpoorten, E.; Massaglia, G.; Ciardelli, G.; Pirri, C. F.; Quaglio, M. Design and Optimization of Piezoresistive Peo/Pedot:Pss Electrospun Nanofibers for Wearable Flex Sensors. *Nanomaterials* **2020**, *10* (11), 1–13. <https://doi.org/10.3390/nano10112166>.

- (37) Liu, J.; McCarthy, D. L.; Tong, L.; Cowan, M. J.; Kinsley, J. M.; Sonnenberg, L.; Skorenko, K. H.; Boyer, S. M.; DeCoste, J. B.; Bernier, W. E.; Jones, W. E. Poly(3,4-Ethylenedioxythiophene) (PEDOT) Infused TiO₂ Nanofibers: The Role of Hole Transport Layer in Photocatalytic Degradation of Phenazopyridine as a Pharmaceutical Contaminant. *RSC Adv.* **2016**, *6* (115), 113884–113892. <https://doi.org/10.1039/c6ra22797j>.
- (38) Daugaard, A. E.; Hvilsted, S.; Hansen, T. S.; Larsen, N. B. Conductive Polymer Functionalization by Click Chemistry. *Macromolecules* **2008**, *41* (12), 4321–4327. <https://doi.org/10.1021/ma702731k>.
- (39) Ouyang, L.; Wei, B.; Kuo, C.; Pathak, S.; Farrell, B.; Martin, D. C. Enhanced PEDOT Adhesion on Solid Substrates With. *Sci. Adv.* **2017**, *3* (March), e1600448.
- (40) Wang, C.; Wang, J.; Zeng, L.; Qiao, Z.; Liu, X.; Liu, H.; Zhang, J.; Ding, J. Fabrication of Electrospun Polymer Nanofibers with Diverse Morphologies. *Molecules* **2019**, *24* (5). <https://doi.org/10.3390/molecules24050834>.
- (41) Xue, J.; Wu, T.; Dai, Y.; Xia, Y. Electrospinning and Electrospun Nanofibers: Methods, Materials, and Applications. *Chem. Rev.* **2019**, *119* (8), 5298–5415. <https://doi.org/10.1021/acs.chemrev.8b00593>.

- (42) Radacsi, N.; Nuansing, W. Fabrication of 3D and 4D Polymer Micro- and Nanostructures Based on Electrospinning. In *3D and 4D Printing of Polymer Nanocomposite Materials: Processes, Applications, and Challenges*; Elsevier, **2019**; pp 191–229. <https://doi.org/10.1016/B978-0-12-816805-9.00007-7>.
- (43) Yuan, H.; Zhou, Q.; Zhang, Y. *Improving Fiber Alignment during Electrospinning*; Elsevier Ltd., **2017**. <https://doi.org/10.1016/B978-0-08-100907-9.00006-4>.
- (44) Beachley, V.; Katsanevakis, E.; Zhang, N.; Wen, X. *Highly Aligned Polymer Nanofiber Structures: Fabrication and Applications in Tissue Engineering*; **2012**; Vol. 246. https://doi.org/10.1007/12_2011_141.
- (45) Razak, S. I. A.; Wahab, I. F.; Fadil, F.; Dahli, F. N.; Khudzari, A. Z. M.; Adeli, H. A Review of Electrospun Conductive Polyaniline Based Nanofiber Composites and Blends: Processing Features, Applications, and Future Directions. *Adv. Mater. Sci. Eng.* **2015**, 356286. <https://doi.org/10.1155/2015/356286>.
- (46) Xue, J.; Wu, T.; Dai, Y.; Xia, Y. Electrospinning and Electrospun Nanofibers: Methods, Materials, and Applications. *Chem. Rev.* **2019**, *119* (8), 5298–5415. <https://doi.org/10.1021/acs.chemrev.8b00593>.

- (47) Song, J.; Sun, B.; Liu, S.; Chen, W.; Zhang, Y.; Wang, C.; Mo, X.; Che, J.; Ouyang, Y.; Yuan, W.; Fan, C. Polymerizing Pyrrole Coated Poly (PLCL) Conductive Nanofibrous Conduit Combined with Electric Stimulation for Long-Range Peripheral Nerve Regeneration. *Front. Mol. Neurosci.* **2016**, *9* (November), 117. <https://doi.org/10.3389/fnmol.2016.00117>.
- (48) Zhang, H.; Dou, C.; Pal, L.; Hubbe, M. A. Review of Electrically Conductive Composites and Films Containing Cellulosic Fibers or Nanocellulose. *BioResources* **2019**, *14* (3), 7494–7542.
- (49) Kim, S.; Jang, L. K.; Park, H. S.; Lee, J. Y. Electrochemical Deposition of Conductive and Adhesive Polypyrrole-Dopamine Films. *Sci. Rep.* **2016**, *6* (July), 30475. <https://doi.org/10.1038/srep30475>.
- (50) Zheng, J.; Liu, K.; Reneker, D. H.; Becker, M. L. Post-Assembly Derivatization of Electrospun Nanofibers via Strain-Promoted Azide Alkyne Cycloaddition. *J. Am. Chem. Soc.* **2012**, *134* (41), 17274–17277.
<https://doi.org/10.1021/ja307647x>.
- (51) Kalaoglu-altan, O. I.; Kirac-aydin, A.; Bolu, B. S.; Sanyal, R.; Sanyal, A. Diels-Alder ‘ Clickable ’ Biodegradable Nanofibers : Benign Tailoring of Scaffolds for Biomolecular Immobilization and Cell Growth Diels-Alder ‘ Clickable ’ Biodegradable Nanofibers : Benign Tailoring of Scaffolds for Biomolecular Immobilization and Cell. *Bioconjug. Chem.* **2017**, *28* (9), 2420–2428. <https://doi.org/10.1021/acs.bioconjchem.7b00411>.

- (52) Kratochvil, M. J.; Carter, M. C. D.; Lynn, D. M. Amine-Reactive Azlactone-Containing Nanofibers For the Immobilization and Patterning of New Functionality on Nanofiber-Based Scaffolds. *ACS Appl. Mater. Interfaces* **2017**, *9* (11), 10243–10253. <https://doi.org/10.1021/acsami.7b00219>.
- (53) Bhushani, J. A.; Anandharamakrishnan, C. Electrospinning and Electrospraying Techniques : Potential Food Based Applications. *Trends Food Sci. Technol.* **2014**, *38* (1), 21–33. <https://doi.org/10.1016/j.tifs.2014.03.004>.
- (54) Kai, D.; Shy, S.; Jun, X. Biodegradable Polymers for Electrospinning : Towards Biomedical Applications. *Mater. Sci. Eng. C* **2014**, *45*, 659–670. <https://doi.org/10.1016/j.msec.2014.04.051>.
- (55) Ahmed, F. E.; Lalia, B. S.; Hashaikeh, R. A Review on Electrospinning for Membrane Fabrication: Challenges and Applications. *Desalination* **2015**, *356*, 15–30. <https://doi.org/https://doi.org/10.1016/j.desal.2014.09.033>.
- (56) IUPAC. *Compendium of Chemical Terminology (the “Gold Book”)*, 2nd ed.; McNaught, A. D., Wilkinson, A., Eds.; Blackwell Scientific Publications: Oxford, **1997**. <https://doi.org/10.1351/goldbook.m03706>.
- (57) Chanda, M. *Introduction to Polymer Science and Chemistry*; Taylor & Francis: Boca Raton, FL, **2006**.
- (58) Agarwal, S.; Greiner, A.; Wendorff, J. H. Functional Materials by Electrospinning of Polymers. *Prog. Polym. Sci.* **2013**, *38* (6), 963–991. <https://doi.org/10.1016/j.progpolymsci.2013.02.001>.

- (59) Shenoy, S. L.; Bates, W. D.; Frisch, H. L.; Wnek, G. E. Role of Chain Entanglements on Fiber Formation during Electrospinning of Polymer Solutions : Good Solvent, Non-Specific Polymer – Polymer Interaction Limit. *Polymer (Guildf)*. **2005**, *46* (10), 3372–3384.
<https://doi.org/10.1016/j.polymer.2005.03.011>.
- (60) Kampalanonwat, P.; Supaphol, P. Preparation of Hydrolyzed Electrospun Polyacrylonitrile Fiber Mats as Chelating Substrates: A Case Study on Copper(II) Ions. *Ind. Eng. Chem. Res.* **2011**, *50* (21), 11912–11921.
<https://doi.org/10.1021/ie200504c>.
- (61) Mohammad Khanlou, H.; Chin Ang, B.; Talebian, S.; Muhammad Afifi, A.; Andriyana, A. Electrospinning of Polymethyl Methacrylate Nanofibers: Optimization of Processing Parameters Using the Taguchi Design of Experiments. *Text. Res. J.* **2015**, *85* (4), 356–368.
<https://doi.org/10.1177/0040517514547208>.
- (62) Shafei, S.; Foroughi, J.; Stevens, L.; Wong, C. S.; Zabihi, O.; Naebe, M. Electroactive Nanostructured Scaffold Produced by Controlled Deposition of PPy on Electrospun PCL Fibres. *Res. Chem. Intermed.* **2017**, *43* (2), 1235–1251. <https://doi.org/10.1007/s11164-016-2695-4>.
- (63) Jiang, T.; Carbone, E. J.; Lo, K. W.; Laurencin, C. T. Electrospinning of Polymer Nanofibers for Tissue Regeneration. *Prog. Polym. Sci.* **2015**, *6* (July 2015), 1–24. <https://doi.org/10.1016/j.progpolymsci.2014.12.001>.

- (64) Pérez-Álvarez, L.; Ruiz-Rubio, L.; Moreno, I.; Vilas-Vilela, J. L. Characterization and Optimization of the Alkaline Hydrolysis of Polyacrylonitrile Membranes. *Polymers (Basel)*. **2019**, *11* (11), 1–11.
<https://doi.org/10.3390/polym11111843>.
- (65) Zhao, H.; Chi, H. Electrospun Bead-on-String Fibers: Useless or Something of Value? In *Novel Aspects of Nanofibers*; Lin, T., Ed.; IntechOpen: London, **2018**. <https://doi.org/10.5772/intechopen.74661>.
- (66) Korycka, P.; Mirek, A.; Kramek-Romanowska, K.; Grzeczkowicz, M.; Lewinska, D. Effect of Electrospinning Process Variables on the Size of Polymer Fibers and Bead-on-String Structures Established with a 2³ Factorial Design. *Beilstein J. Nanotechnol.* **2018**, *9* (1), 2466–2478.
<https://doi.org/10.3762/bjnano.9.231>.
- (67) Alabduljabbar, F. A.; Haider, S.; Alghyamah, A. A.; Haider, A.; Khan, R.; Almasry, W. A.; Patel, R.; Mujtaba, I. M.; Ali, F. A. A. Ethanol Amine Functionalized Electrospun Nanofibers Membrane for the Treatment of Dyes Polluted Wastewater. *Appl. Nanosci.* **2021**.
<https://doi.org/10.1007/s13204-021-01715-9>.
- (68) Patel, S.; Hota, G. Synthesis of Novel Surface Functionalized Electrospun PAN Nanofibers Matrix for Efficient Adsorption of Anionic CR Dye from Water. *J. Environ. Chem. Eng.* **2018**, *6* (4), 5301–5310.
<https://doi.org/10.1016/j.jece.2018.08.013>.

- (69) Workman, C. D.; Hopkins, S.; Pant, J.; Goudie, M.; Handa, H. Covalently Bound S-Nitroso- N-Acetylpenicillamine to Electrospun Polyacrylonitrile Nanofibers for Multifunctional Tissue Engineering Applications. *ACS Biomater. Sci. Eng.* **2021**, 7 (11), 5279–5287.
<https://doi.org/10.1021/acsbiomaterials.1c00907>.
- (70) Gerard, M.; Chaubey, A.; Malhotra, B. D. Application of Conducting Polymers to Biosensors. *Biosens. Bioelectron.* **2002**, 17 (5), 345–359.
- (71) Le, T.-H.; Kim, Y.; Yoon, H. Electrical and Electrochemical Properties of Conducting Polymers. *Polymers (Basel)*. **2017**, 9 (4), 150.
<https://doi.org/10.3390/polym9040150>.
- (72) Guimard, N. K.; Gomez, N.; Schmidt, C. E. Conducting Polymers in Biomedical Engineering. *Prog. Polym. Sci.* **2007**, 32 (8), 876–921.
<https://doi.org/https://doi.org/10.1016/j.progpolymsci.2007.05.012>.
- (73) Li, C.; Bai, H.; Shi, G. Conducting Polymer Nanomaterials : Electrosynthesis and Applications. *Chem. Soc. Rev.* **2009**, 38 (8), 2397–2409.
<https://doi.org/10.1039/b816681c>.
- (74) Jang, J. Conducting Polymer Nanomaterials and Their Applications. In *Emissive Materials Nanomaterials*; **2006**; pp 189–259.
- (75) Hebert, D. D. Oxidative and Non-Oxidative Approaches to High Molecular Weight Ether-Substituted Polythiophenes, Texas State University, **2020**.
- (76) Das, T. K.; Prusty, S. Review on Conducting Polymers and Their Applications. *Polym. - Plast. Technol. Eng.* **2012**, 51 (14), 1487–1500.
<https://doi.org/10.1080/03602559.2012.710697>.

- (77) Dubey, N.; Leclerc, M. Conducting Polymers : Efficient Thermoelectric Materials. *J. Polym. Sci. Part B Polym. Phys.* **2011**, *49* (7), 467–475.
<https://doi.org/10.1002/polb.22206>.
- (78) Runsewe, D.; Betancourt, T.; Irvin, J. A. Biomedical Application of Electroactive Polymers in Electrochemical Sensors: A Review. *Materials.* **2019**.
<https://doi.org/10.3390/ma12162629>.
- (79) Malhotra, B. D.; Chaubey, A.; Singh, S. P. Prospects of Conducting Polymers in Biosensors. *Anal. Chim. Acta* **2006**, *578* (1), 59–74.
<https://doi.org/10.1016/j.aca.2006.04.055>.
- (80) Wang, W.; Li, W.; Zhang, R. The Preparation of Conducting Polymer Micro- and Nanofibers by Electrospinning. *J. Polym. Mater.* **2010**, *27* (4), 303–312.
- (81) Hebert, D. D.; Naley, M. A.; Cunningham, C. C.; Sharp, D. J.; Murphy, E. E.; Stanton, V.; Irvin, J. A. Enabling Conducting Polymer Applications : Methods for Achieving High Molecular Weight in Chemical Oxidative Polymerization in Alkyl- and Ether- Substituted Thiophenes. *Materials (Basel).* **2021**, *14*, 6146.
- (82) Huang, Y.-C.; Lo, T.-Y.; Chen, C.-H.; Wu, K.-H.; Lin, C.-M.; Whang, W.-T. Electrospinning of Magnesium-Ion Linked Binder-Less PEDOT:PSS Nanofibers for Sensing Organic Gases. *Sensors Actuators B. Chem.* **2015**, *216* (September 2015), 603–607.
<https://doi.org/10.1016/j.snb.2015.03.081>.

- (83) Huang, J.; Virji, S.; Weiller, B. H.; Kaner, R. B. Polyaniline Nanofibers : Facile Synthesis and Chemical Sensors. *J. Am. Chem. Soc.* **2003**, *125*, 314–315.
- (84) Tang, J.; Wu, C.; Chen, S.; Qiao, Z.; Borovskikh, P.; Shchegolkov, A.; Chen, L.; Wei, D.; Sun, J.; Fan, H. Combining Electrospinning and Electrospraying to Prepare a Biomimetic Neural Scaffold with Synergistic Cues of Topography and Electrotransduction. *ACS Appl. Bio Mater.* **2020**, *3* (8), 5148–5159. <https://doi.org/10.1021/acsabm.0c00595>.
- (85) Han, D.; Steckl, A. J. Coaxial Electrospinning Formation of Complex Polymer Fibers and Their Applications. *Chempluschem* **2019**, *84* (10), 1453–1497. <https://doi.org/https://doi.org/10.1002/cplu.201900281>.
- (86) Zhang, Y.; Rutledge, G. C. Electrical Conductivity of Electrospun Polyaniline and Polyaniline-Blend Fibers and Mats. *Macromolecules* **2012**, *45* (10), 4238–4246. <https://doi.org/10.1021/ma3005982>.
- (87) Lee, S.; Moon, G. D.; Jeong, U. Continuous Production of Uniform Poly (3-Hexylthiophene) (P3HT) Nanofibers by Electrospinning and Their Electrical Properties. *J. Mater. Chem.* **2009**, *19* (6), 743–748. <https://doi.org/10.1039/b814833c>.
- (88) Ding, Y.; Xu, W.; Yang, W.; Fong, H.; Zhu, Z. Scalable and Facile Preparation of Highly Stretchable Electrospun PEDOT:PSS@PU Fibrous Nonwovens towards Wearable Conductive Textile Applications. *ACS Appl. Mater. Interfaces* **2017**, *9* (35), 30014–30023. <https://doi.org/10.1021/acsami.7b06726>.

- (89) Zha, F.; Chen, W.; Hao, L.; Wu, C.; Lu, M.; Zhang, L.; Yu, D. Electrospun Cellulose-Based Conductive Polymer Nanofibrous Mats: Composite Scaffolds and Their Influence on Cell Behavior with Electrical Stimulation for Nerve Tissue Engineering. *Soft Matter* **2020**, *16* (28), 6591–6598. <https://doi.org/10.1039/d0sm00593b>.
- (90) Jin, G.; Li, J.; Li, K. Photosensitive Semiconducting Polymer-Incorporated Nanofibers for Promoting the Regeneration of Skin Wound. *Mater. Sci. Eng. C* **2017**, *70*, 1176–1181. <https://doi.org/10.1016/j.msec.2016.04.107>.
- (91) Shim, H.; Na, S.; Nam, S. H.; Ahn, H.; Kim, H. J.; Kim, D.; Kim, W. B. Efficient Photovoltaic Device Fashioned of Highly Aligned Multilayers of Electrospun TiO₂ Nanowire Array with Conjugated Polymer. *Appl. Phys. Lett.* **2008**, *92* (18), 183107. <https://doi.org/10.1063/1.2919800>.
- (92) Ercan, E.; Lin, Y. C.; Hsieh, H. C.; Hsu, L. C.; Ho, J. C.; Chen, W. C. One-Dimensional Micro-Scale Patterned Conjugated Polymer Structures in Bilayer Architecture and Light Emitting Diode Application. *Org. Electron.* **2020**, *87* (September), 105965.
<https://doi.org/10.1016/j.orgel.2020.105965>.
- (93) Inderan, V.; Arafat, M. M.; Haseeb, A. S. M. A.; Sudesh, K.; Lee, H. L. Electrospun (Nickel and Palladium) Tin(IV) Oxide/Polyaniline/Polyhydroxy-3-Butyrate Biodegradable Nanocomposite Fibers for Low Temperature Ethanol Gas Sensing. *Nanotechnology* **2020**, *31* (42). <https://doi.org/10.1088/1361-6528/aba0f1>.

- (94) Maslakci, N. N. Electrospun Polyacrylonitrile/Polythiophene Fibers for Phosphate Anion Sensing. *Bilge Int. J. Sci. Technol. Res.* **2020**, *4*, 6–12.
<https://doi.org/10.30516/bilgesci.815271>.
- (95) Billany, M. R.; Khatib, K.; Gordon, M.; Sugden, J. K. Alcohols and Ethanolamines as Hydroxyl Radical Scavengers. *Int. J. Pharm.* **1996**, *137* (2), 143–147.
[https://doi.org/10.1016/0378-5173\(96\)04246-9](https://doi.org/10.1016/0378-5173(96)04246-9).
- (96) Wang, L.; Li, B.; Dionysiou, D. D.; Chen, B.; Yang, J.; Li, J. Overlooked Formation of H₂O₂ during the Hydroxyl Radical-Scavenging Process When Using Alcohols as Scavengers. *Environ. Sci. Technol.* **2022**, *56* (6), 3386–3396. <https://doi.org/10.1021/acs.est.1c03796>.
- (97) Huang, Y.; Huang, Y. Biomaterials and Strategies for Nerve Regeneration. *Artif. Organs* **2006**, *30* (7), 514–522.
- (98) Scheib, J.; Höke, A. Advances in Peripheral Nerve Regeneration. *Nat. Rev. Neurol.* **2013**, *9*, 668–676. <https://doi.org/10.1038/nrneurol.2013.227>.
- (99) Bellamkonda, R. V. Peripheral Nerve Regeneration: An Opinion on Channels, Scaffolds and Anisotropy. *Biomaterials* **2006**, *27* (19), 3515–3518.
<https://doi.org/10.1016/j.biomaterials.2006.02.030>.
- (100) Green, R. A.; Lovell, N. H.; Wallace, G. G.; Poole-Warren, L. A. Conducting Polymers for Neural Interfaces : Challenges in Developing an Effective Long-Term Implant. *Biomaterials* **2008**, *29* (24–25), 3393–3399.
<https://doi.org/10.1016/j.biomaterials.2008.04.047>.

- (101) Ateh, D. D.; Navsaria, H. A.; Vadgama, P. Polypyrrole-Based Conducting Polymers and Interactions with Biological Tissues. *J. R. Soc. Interface* **2006**, *3* (11), 741–752. <https://doi.org/10.1098/rsif.2006.0141>.
- (102) Xiong, G. M.; Yuan, S.; Wang, J. K.; Do, A. T.; Tan, N. S.; Yeo, K. S.; Choong, C. Imparting Electroactivity to Polycaprolactone Fibers with Heparin-Doped Polypyrrole: Modulation of Hemocompatibility and Inflammatory Responses. *Acta Biomater.* **2015**, *23*, 240–249. <https://doi.org/10.1016/j.actbio.2015.05.003>.
- (103) Falconieri, A.; De Vincentiis, S.; Raffa, V. Recent Advances in the Use of Magnetic Nanoparticles to Promote Neuroregeneration. *Nanomedicine* **2019**, *14* (9), 1073–1076. <https://doi.org/10.2217/nmm-2019-0103>.
- (104) Young, H. D.; Freedman, R. A.; Ford, A. L. *Sears and Zemansky's University Physics*, 14th ed.; Pearson Education: USA, **2016**.
- (105) Noori, M.; Ravari, F.; Ehsani, M. Preparation of PVA Nanofibers Reinforced with Magnetic Graphene by Electrospinning Method and Investigation of Their Degradation Kinetics Using Master Plot Analyses on Solid State. *J. Therm. Anal. Calorim.* **2018**, *132* (1), 397–406. <https://doi.org/10.1007/s10973-017-6927-7>.
- (106) Chen, X.; Ge, X.; Qian, Y.; Tang, H.; Song, J.; Qu, X.; Yue, B.; Yuan, W. E. Electrospinning Multilayered Scaffolds Loaded with Melatonin and Fe₃O₄ Magnetic Nanoparticles for Peripheral Nerve Regeneration. *Adv. Funct. Mater.* **2020**, *2004537*, 1–12. <https://doi.org/10.1002/adfm.202004537>.

- (107) Hu, H.; Jiang, W.; Lan, F.; Zeng, X.; Ma, S.; Wu, Y.; Gu, Z. Synergic Effect of Magnetic Nanoparticles on the Electrospun Aligned Superparamagnetic Nanofibers as a Potential Tissue Engineering Scaffold. *RSC Adv.* **2013**, *3* (3), 879–886. <https://doi.org/10.1039/c2ra22726f>.
- (108) Hoffman-Kim, D.; Mitchel, J. A.; Bellamkonda, R. V. Topography, Cell Response, and Nerve Regeneration. *Annu. Rev. Biomed. Eng.* **2010**, *12*, 2013–2231. <https://doi.org/10.1146/annurev-bioeng-070909-105351>.
- (109) Hallab, N. J.; Bundy, K. J.; O'Connor, K.; Moses, R. L.; Jacobs, J. J. Evaluation of Metallic and Polymeric Biomaterial Surface Energy and Surface Roughness Characteristics for Directed Cell Adhesion. *Tissue Eng.* **2001**, *7* (1), 55–70. <https://doi.org/10.1089/107632700300003297>.
- (110) Metwally, S.; Ferraris, S.; Spriano, S.; Krysiak, Z. J.; Kaniuk, Ł.; Marzec, M. M.; Kim, S. K.; Szewczyk, P. K.; Gruszczyński, A.; Wytrwal-Sarna, M.; Karbowniczek, J. E.; Bernasik, A.; Kar-Narayan, S.; Stachewicz, U. Surface Potential and Roughness Controlled Cell Adhesion and Collagen Formation in Electrospun PCL Fibers for Bone Regeneration. *Mater. Des.* **2020**, *194* (108915). <https://doi.org/10.1016/j.matdes.2020.108915>.
- (111) Terpilowska, S.; Siwicki, A. K. Interactions between Chromium(III) and Iron(III), Molybdenum(III) or Nickel(II): Cytotoxicity, Genotoxicity and Mutagenicity Studies. *Chemosphere* **2018**, *201*, 780–789. <https://doi.org/10.1016/j.chemosphere.2018.03.062>.

- (112) Wang, Z.; Sahadevan, R.; Yeh, C.; Menkhaus, T. J.; Huang, J.; Fong, H. Hot-Pressed Polymer Nanofiber Supported Graphene Membrane for High-Performance Nanofiltration. *Nanotechnology* **2017**, *28*, 31LT02.
- (113) Tallman, D. E.; Vang, C.; Wallace, G. G.; Bierwagen, G. P. Direct Electrodeposition of Polypyrrole on Aluminum and Aluminum Alloy by Electron Transfer Mediation. *J. Electrochem. Soc.* **2002**, *149* (3), C173.
<https://doi.org/10.1149/1.1448820>.
- (114) Tessier, D.; Dao, L.; Zhang, Z.; King, M. W.; Guidoin, R. Polymerization and Surface Analysis of Electrically-Conductive Polypyrrole on Surface-Activated Polyester Fabrics for Biomedical Applications. *J. Biomater. Sci. Polym. Ed.* **2000**, *11* (1), 87–99.
<https://doi.org/10.1163/156856200743517>.
- (115) Gopal, R.; Zuwei, M.; Kaur, S.; Ramakrishna, S. Surface Modification and Application of Functionalized Polymer Nanofibers. In *Molecular Building Blocks for Nanotechnology: From diamondoids to nanoscale materials and applications*; Mansoori, G. A., George, T. F., Assoufid, L., Zhang, G., Eds.; Springer Science+Business: New York, NY, **2007**; pp 72–92.
<https://doi.org/10.1007/978-0-387-39938-6>.
- (116) Kang, E. T.; Neoh, K. G.; Tan, K. L.; Liaw, D.-J. Surface Graft Copolymerization and Grafting of Polymers for Adhesion Improvement. In *Adhesion Promotion Techniques: Technological applications*; Mittal, K. L., Pizzi, A., Eds.; Marcel Dekker: New York, NY, **2002**; pp 289–317.

- (117) Maity, N.; Dawn, A. Conducting Polymer Grafting: Recent and Key Developments. *Polymers (Basel)*. **2020**, *12* (3).
<https://doi.org/10.3390/polym12030709>.
- (118) Currie, E. P. K.; Norde, W.; Cohen Stuart, M. A. C. *Tethered Polymer Chains: Surface Chemistry and Their Impact on Colloidal and Surface Properties*; **2003**; Vol. 100–102. [https://doi.org/10.1016/S0001-8686\(02\)00061-1](https://doi.org/10.1016/S0001-8686(02)00061-1).
- (119) Higaki, Y.; Kobayashi, M.; Hirai, T.; Takahara, A. Direct Polymer Brush Grafting to Polymer Fibers and Films by Surface-Initiated Polymerization. *Polym. J.* **2018**, *50* (1), 101–108. <https://doi.org/10.1038/pj.2017.61>.
- (120) Bhattacharya, A.; Misra, B. N. Grafting: A Versatile Means to Modify Polymers: Techniques, Factors and Applications. *Prog. Polym. Sci.* **2004**, *29* (8), 767–814. <https://doi.org/10.1016/j.progpolymsci.2004.05.002>.
- (121) Molina, B. G.; Cianga, L.; Bendrea, A. D.; Cianga, I.; Del Valle, L. J.; Estrany, F.; Alemán, C.; Armelin, E. Amphiphilic Polypyrrole-Poly(Schiff Base) Copolymers with Poly(Ethylene Glycol) Side Chains: Synthesis, Properties and Applications. *Polym. Chem.* **2018**, *9* (31), 4218–4232.
<https://doi.org/10.1039/c8py00762d>.
- (122) Pandey, S.; Ramontja, J. Rapid, Facile Microwave-Assisted Synthesis of Xanthan Gum Grafted Polyaniline for Chemical Sensor. *Int. J. Biol. Macromol.* **2016**, *89*, 89–98. <https://doi.org/10.1016/j.ijbiomac.2016.04.055>.

- (123) Lu, Y.; Wen, Y. P.; Lu, B. Y.; Duan, X. M.; Xu, J. K.; Zhang, L.; Huang, Y. Electrosynthesis and Characterization of Poly(Hydroxy-Methylated- 3,4-Ethylenedioxythiophene) Film in Aqueous Micellar Solution and Its Biosensing Application. *Chinese J. Polym. Sci. (English Ed.)* **2012**, *30* (6), 824–836. <https://doi.org/10.1007/s10118-012-1195-2>.
- (124) Scavetta, E.; Mazzoni, R.; Mariani, F.; Margutta, R. G.; Bonfiglio, A.; Demelas, M.; Fiorilli, S.; Marzocchi, M.; Fraboni, B. Dopamine Amperometric Detection at a PEDOT:PSS Clicked Ferrocene Coated Electrode *E. J. Mater. Chem. B* **2014**, *2* (19), 2861–2867.
- (125) Wang, C.; Yan, Q.; Liu, H. B.; Zhou, X. H.; Xiao, S. J. Different EDC/NHS Activation Mechanisms between PAA and PMAA Brushes and the Following Amidation Reactions. *Langmuir* **2011**, *27* (19), 12058–12068. <https://doi.org/10.1021/la202267p>.
- (126) Fixe, F.; Dufva, M.; Telleman, P.; Christensen, C. B. Functionalization of Poly(Methyl Methacrylate) (PMMA) as a Substrate for DNA Microarrays. *Nucleic Acids Res.* **2004**, *32* (1), 1–8. <https://doi.org/10.1093/nar/gng157>.
- (127) Lazzari, M.; Chiantore, O.; Mendichi, R.; Arturo López-Quintela, M. Synthesis of Polyacrylonitrile-Block-Polystyrene Copolymers by Atom Transfer Radical Polymerization. *Macromol. Chem. Phys.* **2005**, *206* (14), 1382–1388. <https://doi.org/10.1002/macp.200500159>.

- (128) Imran, M.; Mai, B. T.; Goldoni, L.; Cirignano, M.; Jalali, H. B.; Di Stasio, F.; Pellegrino, T.; Manna, L. Switchable Anion Exchange in Polymer-Encapsulated APbX₃Nanocrystals Delivers Stable All-Perovskite White Emitters. *ACS Energy Lett.* **2021**, *6* (8), 2844–2853.
<https://doi.org/10.1021/acsenergylett.1c01232>.
- (129) Wang, J.; Xu, F.; Cai, T.; Shen, Q. Addition of Amines to Nitriles Catalyzed by Ytterbium Amides: An Efficient One-Step Synthesis of Monosubstituted N-Arylamidines. *Org. Lett.* **2008**, *10* (3), 445–448.
<https://doi.org/10.1021/ol702739c>.
- (130) Silverstein, R. M.; Webster, F. X.; Kiemle, D. J.; Bryce, D. L. *Spectrometric Identification of Organic Compounds*, 8th ed.; John Wiley & Sons: Singapore, **2015**.